Aus dem Institut für Schlaganfall- und Demenzforschung (ISD)
der Ludwig-Maximilians-Universität München
Vorstand: Prof. Dr. med. Martin Dichgans

Deletion of a conserved *cis*-regulatory element exacerbates atherosclerosis via upregulation of *Hdac9* in myeloid cells

Dissertation
zum Erwerb des Doktorgrades der Naturwissenschaften
an der Medizinischen Fakultät der
Ludwig-Maximilians-Universität zu München
vorgelegt von

Guangyao Yan

aus

Yangzhou, Jiangsu, China

2020

Mit Genehmigung der Medizinischen Fakultät
der Universität München

Betreuer:	Prof. Dr. rer. nat. Jürgen Bernhagen
Zweitgutachter:	Prof. Dr. rer. nat. Alexander Fauner
Mitbetreuung durch den promovierten Mitarbeiter:	Dr. rer. nat. Matthias Prestel
Dekan:	Prof. Dr. med. dent. Reinhard Hickel
Tag der mündlichen Prüfung:	31.08.2020

Eidesstattliche Versicherung

Guangyao Yan
Name, Vorname

Ich erkläre hiermit an Eides statt,
dass ich die vorliegende Dissertation mit dem Thema

Deletion of a conserved *cis*-regulatory element exacerbates atherosclerosis via upregulation of *Hdac9* in myeloid cells

selbständig verfasst, mich außer der angegebenen keiner weiteren Hilfsmittel bedient und alle Erkenntnisse, die aus dem Schrifttum ganz oder annähernd übernommen sind, als solche kenntlich gemacht und nach ihrer Herkunft unter Bezeichnung der Fundstelle einzeln nachgewiesen habe.

Ich erkläre des Weiteren, dass die hier vorgelegte Dissertation nicht in gleicher oder in ähnlicher Form bei einer anderen Stelle zur Erlangung eines akademischen Grades eingereicht wurde.

München 17.02.2020
Ort, Datum

Guangyao Yan
Unterschrift, Doktorand

Contributions to other projects during doctoral study

1. Compartment-resolved Proteomic Analysis of Mouse Aorta during Atherosclerotic Plaque Formation Reveals Osteoclast-specific Protein Expression

In this project, I sacrificed around 30 mice and dissected the aortas and hearts. Afterwards, I embedded the aorta in paraffin and produced more than 600 paraffin sections. In addition, I established paraffin IHC protocols for several antibodies (e.g. Mamdc2) and acquired confocal microscopy images.

2. Histone deacetylase 9 promotes vascular inflammation by activating IKK

In this project, I dissected aortas from more than 50 mice and contributed to generating figures (e.g. heat maps) using R programming.

3. An engineered soluble chemokine receptor that blocks atherogenic inflammation by agonist-specific targeting

In this project, I dissected aortas and hearts. Corresponding sections, images and quantifications were partially done by me. Moreover, I taught new colleagues techniques to characterize atherosclerotic plaques.

4. Exploring the potential atherogenic effect of TSPAN2

In this project, I sacrificed more than 30 mice. Afterwards, I dissected aortas and hearts and generated corresponding sections and quantification of atherosclerotic plaques.

List of publications

1. Yaw Asare, (…), **Guangyao Yan**, (…), Jürgen Bernhagen, Martin Dichgans. Histone deacetylase 9 activates IKK to activate atherosclerotic plaque vulnerability. ***Circulation Research***. 2020 June 17. doi.org/10.1161/CIRCRESAHA.120.316743

2. Michael Wierer, (…), **Guangyao Yan**, (…), Martin Dichgans, and Matthias Mann. Compartment-resolved Proteomic Analysis of Mouse Aorta during Atherosclerotic Plaque Formation Reveals Osteoclast-specific Protein Expression. ***Mol Cell Proteomics***. 2017 Dec 4. doi: 10.1074/mcp.RA117.000315

3. Christos Kontos, (…), **Guangyao Yan**, (…), Aphrodite Kapurniotu, Jürgen Bernhagen. An engineered soluble chemokine receptor that blocks atherogenic inflammation by agonist-specific. ***Nature Communications***. **Accepted**.

4. **Guangyao Yan**, (…), Jürgen Bernhagen, Martin Dichgans. Deletion of a conserved *cis*-regulatory element exacerbates atherosclerosis via upregulation of HDAC9 in myeloid cells. In preparation.

5. **Yan G**, Fan Y, Li P, Zhang Y, Wang F. Ectopic expression of DAZL gene in goat bone marrow-derived mesenchymal stem cells enhances the trans-differentiation to putative germ cells compared to the exogenous treatment of retinoic acid or bone morphogenetic protein 4 signalling molecules. *Cell Bio Int.* 2015 Jan;39(1):74-83. doi: 10.1002/cbin.10348. Epub 2014 Sep 1.

6. Li PZ, **Yan GY**, Han L, Pang J, Zhong BS, Zhang GM, Wang F, Zhang YL. Overexpression of STRA8, BOULE, and DAZL Genes Promotes Goat Bone Marrow-Derived Mesenchymal Stem Cells In Vitro Transdifferentiation Toward Putative Male Germ Cells. *Reprod Sci*. 2017 Feb;24(2):300-312. doi: 10.1177/1933719116654990. Epub 2016 Sep 27.

7. **Yan G**, Li P, Ren C, Wang F, Zhang Y. Construction of goat germ cell specific reporting system p*VASA*-EGFP. *Sheng Wu Gong Cheng Xue Bao*. 2015 Sep;31(9):1313-24.

8. Zhang GM, Lan S, Jia RX, **Yan GY**, Wang LZ, Nie HT, Lei ZH, Wang F. Age-associated and tissue-specific expression of osteopontin in male Hu sheep reproductive tract. *Tissue Cell*. 2016 Oct;48(5):496-502. doi: 10.1016/j.tice.2016.07.003. Epub 2016 Jul 21

TABLE OF CONTENTS

LIST OF FIGURES

LIST OF TABLES

1. Summary:

Previous results from genome-wide association studies (GWAS) showed that the strongest risk locus rs2107595 was associated with atherosclerotic stroke. This single nucleotide polymorphism (SNP) was shown to regulate *HDAC9* in a gene-dosage effect. Furthermore, *Hdac9* knockout attenuated atherogenesis in both *Apoe*$^{-/-}$ and *Ldlr*$^{-/-}$ mouse models, underscoring the atherogenic effect of HDAC9. However, the direct causative role of the risk locus rs2107595 in atherogenesis was not established. Since rs2107595 is not conserved in the mouse genome, the highly conserved intergenic region encompassing the SNP was exploited to study the role of rs2107595 during atherogenesis. Therefore, this is the first study to show a direct causative role of the *cis*-regulatory element (CRE) containing rs2107595 in atherosclerotic development.

In this study, a novel mouse model, the *Hdac9*$^{\Delta Cis-/-}$ mouse, was generated via deleting the highly conserved CRE (around 1.1 kb) encompassing the SNP. Interestingly, *Hdac9*$^{\Delta Cis-/-}$ mice displayed an upregulation of HDAC9 in myeloid cells, especially in pro-inflammatory macrophages, representing an expression pattern mimicking human risk allele A carriers. After cross-breeding *Hdac9*$^{\Delta Cis-/-}$ mice into the atheroprone *Apoe*$^{-/-}$ mouse model, *Apoe*$^{-/-}$ *Hdac9*$^{\Delta Cis-/-}$ were generated, which developed significantly larger atherosclerotic plaques. Chemokine and cytokine profiles showed that *Apoe*$^{-/-}$ *Hdac9*$^{\Delta Cis-/-}$ mice developed a pro-inflammatory milieu with a prominent upregulation of IL-1β, IL-6 and IL-18 in the plasma, indicating an enhanced NLRP3 inflammasome activation. Flow cytometric analysis revealed the enrichment of pro-inflammatory cell types (i.e. neutrophils, classical monocytes), further confirming the pro-inflammatory contribution of myeloid cells from *Apoe*$^{-/-}$ *Hdac9*$^{\Delta Cis-/-}$ mice. Bone marrow transplantation (BMT) experiments further confirmed the atherogenic role of

Summary

Apoe$^{-/-}$ *Hdac9*$^{\Delta Cis-/-}$ myeloid cells. To explore the potential role of HDAC9 in NLRP3 inflammasome activation, *Apoe*$^{-/-}$ *Hdac9*$^{\Delta Cis-/-}$ bone marrow-derived macrophages (BMDMs) were studied and showed elevated cleavage of pro-caspase-1 compared to *Apoe*$^{-/-}$ BMDMs. Loss-of-function experiments in BMDMs further confirmed the role of HDAC9 in Pro-caspase-1 cleavage. Furthermore, co-immunoprecipitation results revealed a potential physical interaction between HDAC9 and NLRP3. Taken together, knocking out the highly conserved *cis*-regulatory element of *Hdac9* exacerbated atherosclerosis via an upregulation of HDAC9 specifically in myeloid cells. Moreover, preliminary results indicated a potential role of HDAC9 in NLRP3 inflammasome activation.

2. Zusammenfassung:

Frühere Ergebnisse aus genomweiten Assoziationsstudien (GWAS) zeigten, dass der stärkste Risikolokus rs2107595 mit dem atherosklerotischen Schlaganfall assoziiert ist. Dieser Einzelnukleotid-Polymorphismus (engl. Single Nucleotide Polymorphism: SNP) reguliert nachweislich HDAC9 in einer Gen-Dosis-abhängigen Weise. Darüber hinaus kommt es durch den *Hdac9*-Knockout zu einer verminderten Atherogenese; sowohl in *Apoe*$^{-/-}$ als auch in *Ldlr*$^{-/-}$ Mausmodellen, was die atherogene Wirkung von HDAC9 unterstreicht. Die direkte ursächliche Rolle des Risikolokus rs2107595 in der Atherogenese konnte jedoch nicht festgestellt werden. Da rs2107595 im Mausgenom nicht konserviert ist, wurde die hochkonservierte intergenische Region, die den SNP umfasst, ausgenutzt, um die Rolle von rs2107595 während der Atherogenese zu untersuchen. Daher ist dies die erste Studie, die eine direkte ursächliche Rolle des *cis*-regulierenden Elements (CRE), welches rs2107595 beinhaltet, bei der atherosklerotischen Pathogenese zeigt.

In dieser Studie wurde ein neuartiges Mausmodell, die *Hdac9*$^{\Delta Cis-/-}$ Maus, durch die Deletion des hochkonservierten CRE (ca. 1,1 kb), welches den SNP umfasst, generiert. Interessanterweise zeigten *Hdac9*$^{\Delta Cis-/-}$ Mäuse eine Hochregulation von HDAC9 in myeloischen Zellen, insbesondere in pro-inflammatorischen Makrophagen, welche ein Expressionsmuster darstellten, das das der menschlichen Risiko-Allel-Träger nachahmt. Durch die Einkreuzung von *Hdac9*$^{\Delta Cis-/-}$ Mäusen in das atheroprone *Apoe*$^{-/-}$ Mausmodell wurden *Apoe*$^{-/-}$ *Hdac9*$^{\Delta Cis-/-}$ Mäuse generiert, die dadurch signifikant größere atherosklerotische Plaques entwickelten. Eine Untersuchung der Chemokin- und Zytokinprofile zeigte, dass die *Apoe*$^{-/-}$ *Hdac9*$^{\Delta Cis-/-}$ Mäuse ein pro-inflammatorisches Milieu mit einer prominenten Hochregulierung von IL-1β, IL-6 und

Zusammenfassung

IL-18 im Plasma entwickelten, was auf eine verstärkte Aktivierung des NLRP3-Inflammasoms hinweist. Durchflusszytometrische Analysen ergaben eine Anreicherung pro-inflammatorischer Zelltypen (d.h. Neutrophile, klassische Monozyten), was die pro-inflammatorische Beteiligung der myeloischen Zellen von *Apoe*$^{-/-}$ *Hdac9*$^{\Delta Cis-/-}$ Mäusen weiter bekräftigte. Knochenmark-Transplantationsexperimente (engl. bone marrow transplantation: BMT) bestätigten des Weiteren die atherogene Rolle der myeloischen Zellen in *Apoe*$^{-/-}$ *Hdac9*$^{\Delta Cis-/-}$ Mäusen. Zur Untersuchung der potenziellen Rolle von HDAC9 bei der Aktivierung des NLRP3-Inflammasoms wurden isolierte Makrophagen aus dem Knochenmark von *Apoe*$^{-/-}$ *Hdac9*$^{\Delta Cis-/-}$ Mäusen untersucht (engl. bone marrow-derived macrophages: BMDMs), die im Vergleich zu BMDMs von *Apoe*$^{-/-}$ Mäusen eine erhöhte Spaltung von Pro-Caspase-1 zeigten. Funktionsverlust-Experimente in BMDMs bestätigten zudem die Rolle von HDAC9 bei der Spaltung von Pro-Caspase-1. Darüber hinaus konnte mit Hilfe von Koimmunpräzipitationsexperimenten eine mögliche physikalische Interaktion zwischen HDAC9 und NLRP3 nachgewiesen werden. Zusammenfassend lässt sich daraus schließen, dass die Ausschaltung des hochkonservierten *cis*-Regulationselements von *Hdac9* die Atherosklerose durch eine Hochregulierung von HDAC9 speziell in myeloischen Zellen verstärkt. Darüber hinaus weisen erste Ergebnisse auf eine mögliche direkte Rolle von HDAC9 bei der Aktivierung des NLRP3-Inflammasoms hin.

3. Introduction

3.1 Ischemic stroke

Stroke is a leading cause of worldwide mortality and long-term disability, inflicting an enormous burden (DALYs and Collaborators, 2018; Gorelick, 2019). Stroke is categorized into two major categories: ischemic stroke and hemorrhagic stroke (Brainin and Heiss, 2019). Given the scope of this work, this introduction focuses on ischemic stroke, especially large artery atherosclerotic stroke (LAS).

Ischemic stroke, the most common etiology of stroke, is often initiated by the rupture of vulnerable atheromatous plaques, which later develop into thrombi adhered by platelets resulting in obstruction of blood flow (Brainin and Heiss, 2019). Among different subtypes of ischemic stroke, LAS patients represent 20,9 % of all ischemic stroke incidences and show the highest rate of stroke recurrence (Adams et al., 1993). Diagnostic criteria for LAS include large cerebral arterial stenosis (>50%) or complete blockage of a main or branch artery, where the occlusion is presumably due to atherosclerotic plaque rupture. Owning to the heterogeneous nature of ischemic stroke, a multitude of modifiable and non-modifiable risk factors are identified (Boehme et al., 2017). Traditionally, non-modifiable risk factors refer to age (Abbott et al., 2003), sex (Wyller, 1999) and ethnicity (Fustinoni and Biller, 2000), whereas modifiable factors include smoking (Wolf et al., 1988), diet (Fung et al., 2009), physical activity (Lee et al., 2003), hyperlipidemia (Meyer et al., 1987) and other aspects of lifestyle (Gill et al., 1986). Besides the abovementioned risk factors, cumulative evidence has shown that genetics are key contributors to stroke incidence.

3.2 Genetics of ischemic stroke

The role of genetics in stroke was originally evidenced by a classic twin study in which a concordance rate higher than 65% was reported in monozygotic compared to dizygotic twins (Brass et al., 1992). In accord with these twin studies, data from family history studies consistently showed that genetics play a role in ischemic stroke (Flossmann et al., 2004; Jerrard-Dunne et al., 2003). Notably, the genetic heritability for all ischemic stroke subtypes was estimated at around 37.9%, with 40.3% for large vessel disease (LVD) (Bevan et al., 2012). Thus, exploring the causative risk locus may provide insights into understanding and preventing ischemic stroke especially for LVD.

Stroke is a syndrome with multiple etiologies rather than one single disease (Malik and Dichgans, 2018; Markus, 2011), different genetic variants may contribute differently to stroke development and progression. Identifying new genetic variants will provide a better understanding of the disease and its underlying mechanisms. Genome-wide association studies (GWAS) involve inspection of the whole genome and associate single nucleotide polymorphisms (SNPs) with different stroke outcomes or subtypes, without making any assumptions like candidate-gene-analysis approach which is based on previous limited knowledge (Patnala et al., 2013). Moreover, combined with a large sample size and stringent statistical methods (e.g. Bonferroni-corrected thresholds), GWAS significantly reduce the type I errors (false positive), so that the identified risk variants are more reliable and reproducible (Falcone et al., 2014; Hardy and Singleton, 2009).

Recently, more than 500,000 human samples from different ethnic backgrounds were analyzed by the MEGASTROKE consortium, and *TSPAN2, EDNRA, HDAC9-TWIST1* and *MMP12* were identified in association with large artery stroke with *HDAC9-*

TWIST1 being the strongest risk locus to date (Malik et al., 2018). In conclusion, GWAS allows us to identify new stroke risk variants (e.g. *HDAC9-TWIST1)*, thereby offering new perspectives to investigate stroke pathology.

3.2.1 *Cis*-regulatory elements

Interestingly, around 90% of GWAS hits locate in genomic non-coding regions especially *cis*-regulatory elements (CREs) (Giral et al., 2018). Mechanistically, most variants located in CREs (e.g. enhancer element) regulate target gene transcription by disrupting or creating novel binding sites for certain transcription factors (Shlyueva et al., 2014). This regulatory function of CREs is concurrent with enrichment of several epigenetic markers, such as DNase I hypersensitive sites (DHSs) and histone modifications.

The compact structure of DNA wrapping around histones – the basic building block of chromatin – often hinders the site-specific binding of transcription factors to DNA. DHSs refer to less condensed genomic regions that are sensitive to digestion by DNase I enzyme. Most importantly, DHSs are more amenable for transcription factors binding (Boyle et al., 2008), explaining the regulatory function of DHSs.

Histone modifications are also indicative for the function of CREs. Histone tail modifications such as acetylation and methylation remodel chromatin structure by changing chemical properties of histones, thereby changing the compactness of chromatin. For instance, histone H3 lysine 27 acetylation (H3K27ac) neutralizes the positive charge at lysine 27, thereby weakening the interaction between histones and DNA (Bannister and Kouzarides, 2011). Besides H3K27ac, there are also other histone markers for open chromatin, such as H3K4me1 at enhancers and H3K4me3 at promoters (Heintzman et al., 2007; Santos-Rosa et al., 2002).

In addition, the 3-dimensional structure of DNA facilitates the long-range interactions between CREs. For example, enhancers are shown to physically interact with promoters to regulate transcription of a gene located far away from the enhancer (Gupta et al., 2017).

Since the above-mentioned epigenetic markers are manifested in a cell-type-specific manner, the regulatory function of CREs is accordingly cell-type-dependent. For instance, enhancers are divided into different status: poised state without regulating the gene expression (enriched with H3K4me1 and H3K27me3) and active state regulating the transcription (enriched with H3K4me1 and H3K27ac).

In conclusion, SNPs located in CREs contain information regarding gene-specificity and cell-type-specificity, which might provide insights into further understanding ischemic stroke especially LAS.

3.2.2 Strongest risk locus in association with LAS: the rs2107595 locus

So far, rs2107595 is the strongest risk variant in association with LAS (Malik et al., 2018). This SNP is also considered to be a major risk locus for coronary artery disease (Wang et al., 2016), myocardial infarction (Nelson et al., 2017) and peripheral artery disease (Matsukura et al., 2015) thus indicating a central role in cardiovascular diseases. Interestingly, rs2107595 is located in an intergenic region between *HDAC9* and *TWIST1* (Azghandi et al., 2015). According to Roadmap epigenetics (Roadmap Epigenomics et al., 2015) and ENCODE (Davis et al., 2018), rs2107595 resides in a region that colocalizes with DHS, H3K27ac and H3K4me1, suggesting a regulatory function of rs2197595.

To confirm the regulatory role of rs2107595, our group showed that rs2107595 risk allele A was associated with *HDAC9* gene expression level in human peripheral blood mononuclear cells (PBMCs) in a gene-dosage-dependent manner, whereas no

alteration of expression of the neighboring genes *TWIST1* or *FERD3L* was observed, suggesting that rs2107595 specifically regulated *HDAC9* gene transcription (Azghandi et al., 2015). To explore the mechanism underlying the regulatory function of rs2107595, potential binding molecules to common allele G and risk allele A were screened by performing proteome-wide analysis of disease-associated SNPs (PWAS) and identified the E2F3/TFDP1/Rb1-complex as a G allele-specific binder (Prestel et al., 2019). Chromatin immunoprecipitation (ChIP) experiments confirmed that E2F3 and Rb1 proteins were enriched at the common allele G and dissociation of the E2F3/TFDP1/Rb1-complex at risk allele A was associated with transcriptional upregulation of *HDAC9* (Fig. 1) (Prestel et al., 2019). In conclusion, our group has shown the regulatory function of rs2107595 in *HDAC9* transcription.

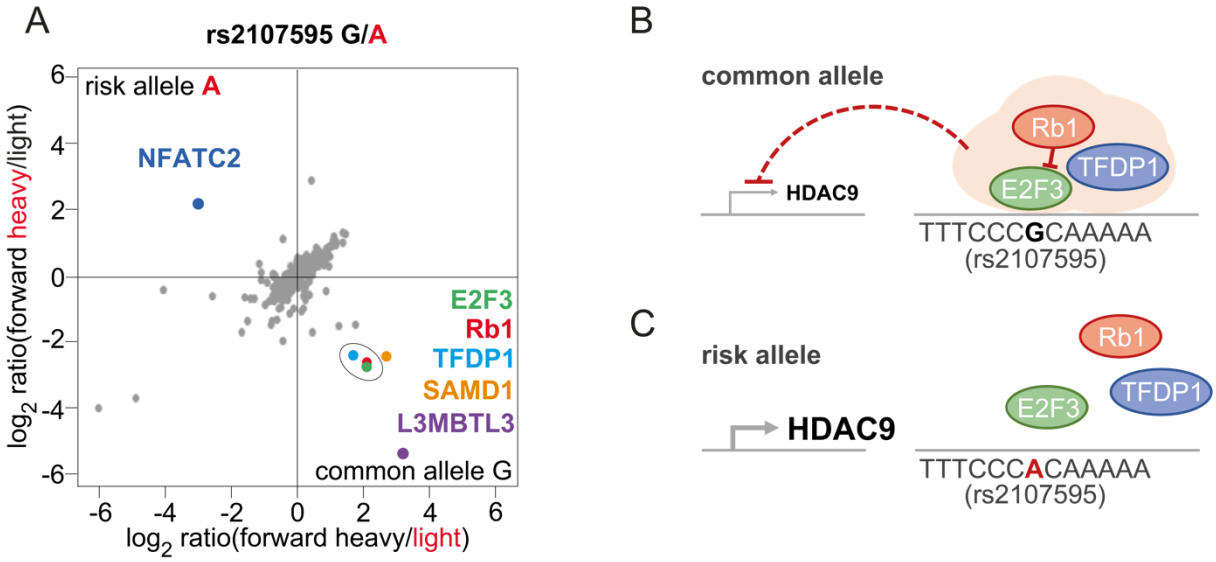

Figure 1. The rs2107595 risk variant interferes with E2F3/Rb1 binding.

(A) Identification of common and risk allele-specific binding molecules of rs2107595 using PWAS. E2F3, Rb1, TFDP1 were enriched at the common allele G whereas NFATC2 at the risk allele A. (B, C) Illustrations show that E2F3/Rb1 complex loses binding affinity at risk allele A and results in upregulation of *HDAC9*. (Adapted from Prestel M*, Prell-Schicker C* et al, *Stroke*, 2019 (Prestel et al., 2019)).

A recent study from LAS patients has explored the downstream gene expression and biological function of rs2107595 in circulating leukocytes using human transcriptome microarrays (Shroff et al., 2019). The comparative transcriptome profiles showed that risk allele A was associated with cholesterol efflux, IL-6 signaling and platelet aggregation, indicating the association of the risk allele with chronic inflammation and platelet aggregation. However, *HDAC9* was not detected as one of the significantly regulated genes correlated with rs2107595 risk allele A, which is probably due to the limited sample numbers (43 risk allele subjects and 112 common allele subjects) and the relatively low expression of *HDAC9* in circulating leukocytes. Another study showed that rs2107595 is associated with Moyamoya disease, which is characterized by stenosis in both carotid arteries (Duan et al., 2018), further underscoring the role of this risk locus during atherosclerotic development.

3.3. Atherosclerosis

Atherosclerosis is one of the major etiologies for LAS. It is a lipid triggered chronic inflammatory disorder. When Felix Marchand first introduced “atherosclerosis” in 1904 (Konstantinov et al., 2006), the pathological understanding of this disease was limited to hyperlipidemia. Not until the 1980s, immune cells - especially macrophages and T cells - were found inside human atherosclerotic plaques (Jonasson et al., 1986), establishing the concept that atherosclerosis is a chronic inflammation disorder. Once infiltrated into the intima, different immune responses take place between the leukocytes. They secret a wide array of chemokines and cytokines, recruiting more leukocytes and building up the atherosclerotic plaque (Libby et al., 2011).

3.3.1 Anatomical structure of the aorta

The human vessel wall has three major layers: intima, media and adventitia (Geer et al., 1961). The intima is inner most layer facing the lumen of the vessel. It is composed of a single layer of endothelial cells, which are sensitive to the shear stress (Malek et al., 1999) and modified lipids (e.g. oxLDL) (Szmitko et al., 2003). The media, the middle layer of the aorta, is built up by smooth muscle cells (SMCs) contributing to the constriction, dilation and extra cellular matrix production of the vessel (Nikkari et al., 1994). The most external layer of the vessel is called adventitia, which contains fibroblasts, nerves and some immune cells to form the lately discovered arterial tertiary lymphoid organs (ATLOs) (Mohanta et al., 2014). For mouse models, histological analyses are normally focused on aortic root and bifurcations at the arch (Anderson, 2000; VanderLaan et al., 2004).

3.3.2 Pathologies underlying different stages during atherogenesis

Dysfunction of endothelial cells plays a key role in the initiation of atherogenesis. Triggers for endothelial dysfunction include mechanical injury (Orford et al., 2000), high blood pressure (Schiffrin, 2002), pro-inflammatory cytokines (Libby et al., 2006), damage-associated molecular patterns (DAMPs) (Schiopu and Cotoi, 2013) or the retention of modified lipoproteins in the sub-endothelium (Gimbrone and Garcia-Cardena, 2016; Pober and Cotran, 1990), which can ensue downstream pro-inflammatory cascades. An important mediator of inflammation is the transcription factor Nuclear factor-kappa-B (NFκB) (Hajra et al., 2000). Upon activation, NFκB translocates to the nucleus and drives the expression of inflammatory genes, such as vascular cell adhesion molecules (VCAM-1) and intercellular adhesion molecules (ICAMs) (Davies et al., 1993). VCAM-1 and ICAMs then recruit leukocytes to the

vascular beds (Davies et al., 1993), causing intima thickening (Cybulsky et al., 1999). This early-stage atheroma is also called fatty streaks, mostly attributed to macrophage-derived lipid-enriched foam cells. During atheroprogression, the local inflammation is unabated, characterized by increasing infiltration and proliferation of leukocytes (Galkina and Ley, 2009). Leukocytes release pro-inflammatory cytokines (e.g. IL-1β), chemokines (e.g. CCL2) and growth factors (e.g. platelet derived growth factor (PDGF)). The released growth factors promote smooth muscle cells migration from the media to the intima (Tsai et al., 1994). Upon migration, smooth muscle cells proliferate within the plaque and secret extracellular matrix (ECM) (Rudijanto, 2007). Gradually, a fibrous cap is formed above the lipid core and necrotic tissue (Schwartz et al., 2000b). Degradation or erosion of the fibrous cap by macrophage-secreted metalloproteinases (MMPs) may lead to plaque rupture (Newby, 2007). Once the plaque is ruptured, a thrombus can be formed to obstruct blood flow, causing ischemic stroke or myocardial infarction (Libby et al., 2011) (Fig.2). A wide range of different cell types are involved in atherosclerotic progression, but due to the aim of this project, I will focus on introducing the role of monocytes/macrophages in atherosclerosis.

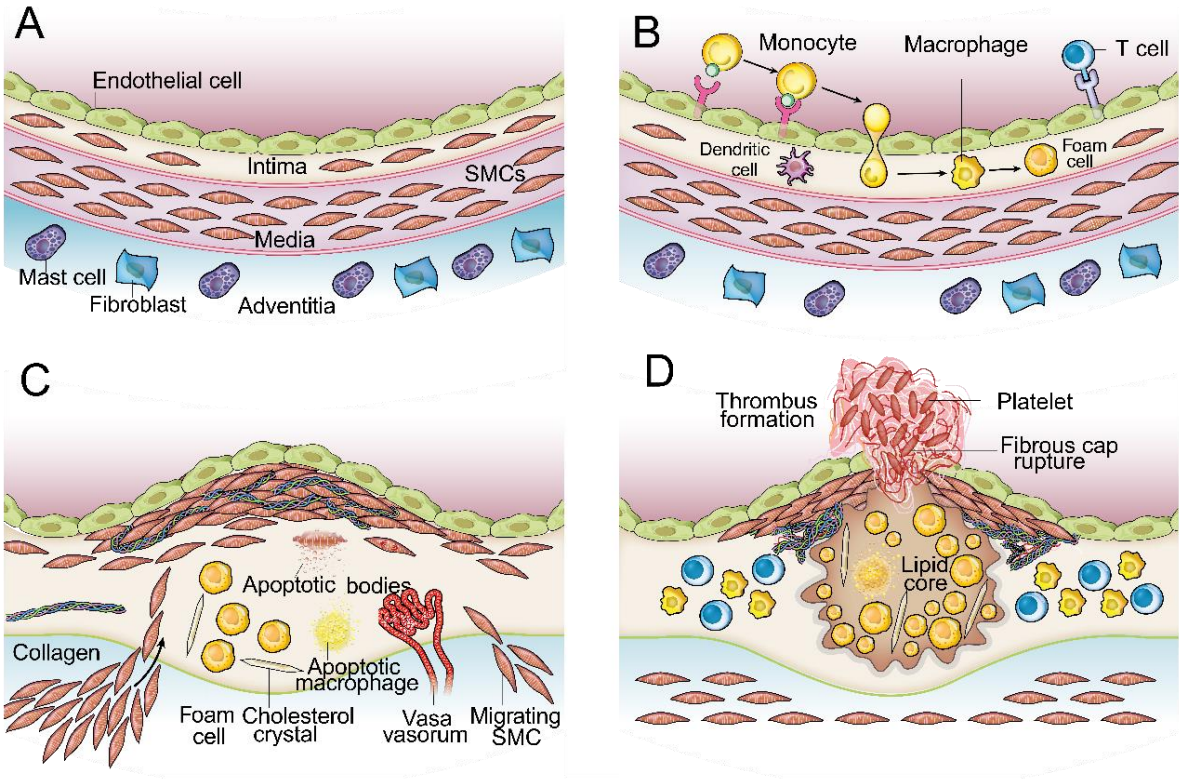

Figure 2. Different stages during atherogenesis.

(A) The normal human artery is made of three layers. Intima, the most inner layer, is formed of a single layer of endothelial cells that are in direct contact with blood flow. Healthy human intima, different from other species, contains resident smooth muscle cells (SMCs). Media, the middle layer, contains only SMCs. The outer layer of arteries, adventitia, contains different cell types including mast cells, nerve endings and other micro vessels. (B) The early stage of atherosclerosis is initiated with adhesion of leukocytes (especially monocytes and T cells) recruited via different cytokines and chemokines secreted upon endothelial activation. Once the monocytes infiltrate into the sub-endothelial layer, they become macrophages which engulfed lipid and differentiate into foam cells. (C) Unresolved inflammation gradually promotes plaque into advanced stage which is characterized by increase of the plaque size, necrotic cores and migration of SMCs. SMCs produce collagen which can stabilize the plaque. (D) The fibrous cap can be digested by MMPs which are majorly produced from macrophages. Plaque rupture leads to formation of blood clots resulting in different complications such as ischemic stroke. (Adapted from Libby et al, Nature, 2011 (Libby et al., 2011))

3.3.3 The role of monocytes/macrophages in atherosclerosis

3.3.3.1 Adhesion of monocytes/macrophages

Much attention has been paid to the monocyte adhesion, rolling and infiltrating in the initial stage of atherogenesis (Ross, 1999). Monocytes originate from hematopoietic stem and progenitor cells (HSPCs) resided in bone marrow (Sata et al., 2002). HSPCs tend to proliferate especially when mice are fed with western diet (Feng et al., 2012) or carry an *Apoe* deficiency (Murphy et al., 2011). For example, several groups found that hyperlipidemia led to monocytosis in different animal models including mice (Averill et al., 1989; Tacke et al., 2007). One study showed that *Apoe*$^{-/-}$ mouse model had around 50% more pro-inflammatory circulating Ly-6C^{hi} pro-inflammatory monocytes compared to wild-type mice, whereas the number of Ly-6C^{low} anti-inflammatory monocytes was not changed (Swirski et al., 2007). Besides monocytosis, a key step in monocyte extravasation is the capturing and rolling of monocytes, which is regulated by the five major chemokine axes: CCR2–CCL2, CX3CR1–CX3CRL1, CCR5-CCL5, CXCR2/CXCL1 and CXCR2/MIF (Combadiere et al., 2008; Schober et al., 2008; Tacke et al., 2007; van der Vorst et al., 2015). CCR2, CCR5, CX3CR1 are essential for Ly-6C^{hi} monocytes recruitment (Combadiere et al., 2008; Tacke et al., 2007). After entering the sub-endothelium, macrophages were previously thought to differentiate into different subtypes, such as M1, M2, Mox, M4 and other phenotypes (Chinetti-Gbaguidi et al., 2015). However, recent single-cell RNA sequencing technologies offered new insights into the monocytes heterogeneity inside atherosclerotic plaques (Cochain et al., 2018; Kim et al., 2018; Lin et al., 2019). Cochain and others have identified new populations of macrophages exclusively in atherosclerotic plaques, such as *TREM2*^{high} macrophages enriched in *Trem2* expression (Cochain et al., 2018). These *TREM2*^{high} macrophages entail an expression

profile similar to osteoclasts, indicating a role of plaque calcification. This finding proves the wide range of functions of macrophages in atherosclerotic plaques.

3.3.3.2 Lipid metabolism in macrophages

Macrophages engulf lipids especially oxLDL in plaques, differentiating into foam cells. The uptake process is mediated by scavenger receptors such as CD36, scavenger receptor A1 (SR-A1) and lectin-like oxidized LDL receptor 1 (LOX1) (Suzuki et al., 1997). Engulfed lipoproteins are degraded into free cholesterol and accumulated at the endoplasmic reticulum (ER) membrane (Febbraio et al., 2001). Cholesterol is esterified in the ER and stored in cytosolic lipid droplets, thereby activating transcription factors such as liver X receptor (LXR) regulating cholesterol metabolism (Erbay et al., 2009). LXR for example upregulates lipid exporters such as the ATP-binding cassette subfamily A member 1 (ABCA1) and ATP-binding cassette subfamily G member 1 (ABCG1). ABCA1 and ABCG1 export the cholesterol metabolites into the peripheral circulation (Wang et al., 2007). Impaired cholesterol efflux results in aberrant lipid hemostasis, leading to damage of the lysosomal pathway and activation of inflammasome pathway mediated by the NOD-, LRR- and pyrin domain-containing protein 3 (NLRP3) (Duewell et al., 2010). However, recent single-cell RNA sequencing technology revealed that the foam cells entail a less pro-inflammatory profile compared with non-foamy cells (Kim et al., 2018). Specifically, they found that non-foamy cells harbor more transcripts of pro-inflammatory genes, such as *Nlrp3* and *IL1-beta,* indicating an undetermined function of foam cells in atherosclerosis.

3.3.3.3 NLRP3 inflammasome in macrophages

The inflammasome is an intracellular multiprotein complex, which functions as an immune sensor to pathogen-associated molecular patterns (PAMPs) and damage-

associated molecular patterns (DAMPs) (Jo et al., 2016). Inflammasomes cleave Pro-caspase-1 into Caspase-1. Caspase-1 then further cleaves the pro-inflammatory cytokines pro-IL1-β and pro-IL-18 into IL1-β and IL-18, resulting in an inflammatory milieu. Inflammasomes have been identified majorly in myeloid cells especially in macrophages during atheroprogression (Duewell et al., 2010; Tschopp and Schroder, 2010). There are several different inflammasome protein complexes, among which NLRP3 inflammasome is one of the most extensively studied. Given the nature of this work, I will focus on introducing the NLRP3 inflammasome.

3.3.3.3.1 Components of NLRP3 inflammasome

The NLRP3 inflammasome is comprised of NLRP3, adaptor Apoptosis-Associated Speck-Like Protein Containing A CARD (ASC), pro-caspase-1 and a newly identified component NEK7 (He et al., 2016). Inflammasome induction is broadly divided into two major steps: priming and activation. During the priming event, the NF-κB signaling pathway is activated and upregulates the transcription of inflammasome components and downstream effectors (e.g. pro-IL1-β and pro-IL-18) (Jin and Flavell, 2010). During the activation phase, a wide range of stimuli (e.g. oxLDL, ATP, pore-forming toxins) can induce inflammasome assembly (Fig. 3). Upon assembly, pro-caspase-1 is cleaved into caspase-1.

The NLRP3 protein contains three domains: an N-terminal effector domain PYD, a central NACHT domain and C-terminal leucine-rich repeats (LRRs). ASC harbors an N-terminal PYD and a C-terminal caspase recruitment domain (CARD). Caspase-1 has a CARD and catalytic domains (composed of p10 and p20). Upon stimulation of DAMPs and PAMPs, NACHT domains of NLRP3 form a homotypic scaffold to facilitate the interaction between NLRP3 and ASC via their PYD domains. Then, the CARD from

the ACS recruits pro-capase-1 and cleaves it to exert proteolytic function. Besides cleaving pro-IL1-β and pro-IL-18, proteolytic capsapse-1 also induces pyroptosis by cleaving Gasdermin D (GSDMD). The resulting membrane permeability facilitates the release of IL1-β and IL-18 into circulation and further functions to prime the NLRP3 inflammasome (Zhou et al., 2011). One report identified NEK7 as a new component of the NLRP3 inflammasome (He et al., 2016).

3.3.3.3.2. The priming step of NLRP3 inflammasome

Priming upregulates the transcriptional level of NLRP3 inflammasome components, pro-IL1-β and pro-IL-18 via NF-κB pathway. A wide range of PAMPs and DAMPs can activate Toll like receptor (TLR), TNF-α receptor (TNFR) and IL1-β receptor (IL-1R1), leading to NF-κB activation. However, priming serves more than increasing the mRNA abundance of the inflammasome components. There is accumulative evidence showing that NLRP3 is post translationally modified (i.e. deubiquitination, phosphorylation) during the priming phase, which is required to facilitate inflammasome assembly. For example, inhibition of NF-κB did not inhibit NLRP3 inflammasome activation, indicating a transcriptional independent role for priming (Gong et al., 2010). Moreover, NLRP3 was reported to be phosphorylated at S194 mediated by c-Jun N-terminal kinase1 (JNK1) during the priming step, which is essential for NLRP3 oligomerization (Song et al., 2017). Therefore, the priming not only regulates transcription but also confers post-translational modifications (PTMs) to components such as NLRP3.

3.3.3.3.3. Activation phase of NLRP3 inflammasome

Multiple upstream activation stimuli have been identified, such as K^+ efflux, Ca^{2+} mobilization, Cl^- efflux, lysosome damage, mitochondrial dysfunction and reactive

oxygen species (ROS) production (Duewell et al., 2010; Green et al., 2018; Menu et al., 2011; Murakami et al., 2012; Tschopp and Schroder, 2010). The inflammasome sensor NLRP3 is activated in an environment with low concentration of K^+, while inhibited at high concentration (Muñoz-Planillo et al., 2013; Petrilli et al., 2007). Based on these findings, K^+ efflux has been commonly applied in *in vitro* models to activate NLRP3 inflammasome by the potassium ionophore Nigericin. Additionally, K^+ efflux was shown to intertwine with other ion fluxes, such as Ca^{2+} and Cl^-. K^+ efflux was reported to open Ca^{2+} channels, thereby releasing Ca^{2+} from the ER and activating the inflammasome (Lee et al., 2012; Murakami et al., 2012; Yaron et al., 2015). Blocking the Cl^- channel and increasing the concentration of Cl^- in extracellular environment was shown to inhibit inflammasome activation (Domingo-Fernández et al., 2017; Tang et al., 2017) by interfering with ASC polymerization (Green et al., 2018). Extracellular ATP changes are also widely used *in vitro* to activate the NLRP3 inflammasome (Mariathasan et al., 2006). A recent study showed that cell stress in PBMCs from NLRP3 mutation patients had an enhanced ATP externalization and pro-inflammatory cytokines IL-18 expression, suggesting the potential role of ATP in inflammasome activation (Carta et al., 2015). The disruption of the lipid metabolism is also associated with regulation and activation of the NLRP3 inflammasome. The dietary intake of saturated fatty acids was reported to induce NLRP3 inflammasome activation (Wen et al., 2011). Metabolism is associated with reactive oxygen species (ROS) production. Therefore, another generally accepted proposal is that ROS production triggers the activation. Some ROS triggers (e.g. nicotinamide adenine) were shown to increase inflammasome activation (Agarwal et al., 2011; Bauernfeind et al., 2011; Brown and Griendling, 2009; Paletta-Silva et al., 2013). Recently, mitochondrial DNA, the product from mitochondrial dysfunction, was reported to result in NLRP3 inflammasome

activation via interacting with NLRP3 (Shimada et al., 2012). The role of Golgi has been underappreciated until one study showed that disassembly of the transGolgi network (dTGN) was induced under inflammasome stimuli (Boucher et al., 2018). The so called dTGN was shown to serve as a scaffold for NLRP3 aggregation and later assembly with ASC.

In conclusion, multiple stimuli have been identified for inflammasome activation. However, there appears to be a role for different stimuli, which do not function mutually exclusive. Some identified signaling pathways overlap with each other. Moreover, some stimuli can cause energy metabolism changes and organelle damage at the same time. Thus, it is hard to determine and disentangle the molecular pathway that drive NLRP3 inflammasome. Furthermore, there might be unknown molecules contributing to inflammasome activation.

3.3.3.3.4. The role of NLRP3 inflammasome in macrophages during atherogenesis

Already during early stages of atherosclerosis, cholesterol crystals were identified as a primary trigger for NLRP3 inflammasome activation and were detected in macrophages in atherosclerotic plaques (Duewell et al., 2010). Moreover, *in vitro* experiments showed that cholesterol crystals induced cleavage of pro-caspase-1 and IL1-β release in wild-type macrophages, which was not observed in macrophages deficient for NLRP3 or ASC. Mechanistically, cholesterol crystals damage lysosomes, thereby activating the NLRP3 inflammasome (Duewell et al., 2010). However, one year later, a contradictory study using *Nlrp3* deficiency in an *Apoe*$^{-/-}$ background failed to show attenuation of atherosclerosis (Menu et al., 2011). The discrepancy between those two studies may lie in the use of different atheroprone models. The more

aggressive *Apoe*$^{-/-}$ model develops spontaneous plaques under chow diet, whereas the milder *Ldlr*$^{-/-}$ model develops atherosclerosis only under western diet.

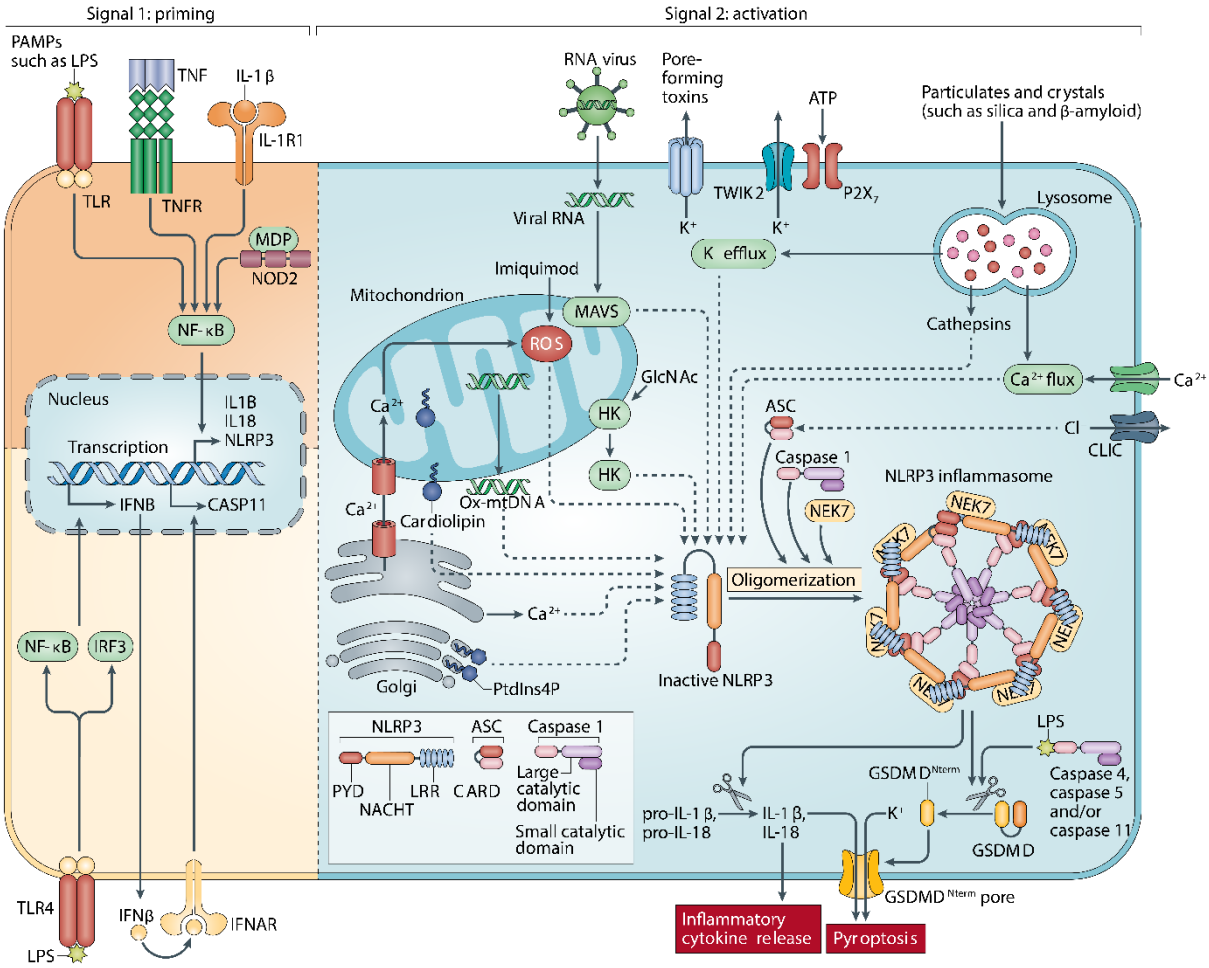

Figure 3. NLRP3 inflammasome priming and activation.

Priming step is induced by DAMPs and PAMPs, leading to the transcriptional upregulation of NLRP3 inflammasome components and downstream effectors. Activation step is achieved via a wide range of signals, such as pore-forming toxins, ATPs, particulates and mitochondrial dysfunction. Most of the activation phase stimuli result in fluxes of ions, especially K^+, Ca^+ and Cl^-. Moreover, the ROS production from mitochondria, relocation of cardiolipin and release of oxidized mitochondria DNA (Ox-mtDNA) have demonstrated the activating role of mitochondria. Upon activation, NLRP3 oligomerize via NACHT-NACHT interaction and then further recruit ASC and others. Once the NLRP3 inflammasome is assembled, caspase-1 cleaves pro-IL-1β and pro-IL-18 and Gasdermin D (GSDMD), thereby causing inflammatory cytokine release and cell pyroptosis. Alternative pathway for cell pyroptosis is that LPS-induced caspase4,5 and 11 may also cleave GSDMD. (From Karen V. Swanson, 2019, Nat Rev Immunol (Swanson et al., 2019)).

3.4. The HDAC class IIa family and its biological functions

Acetylation of lysines at the N-terminal tail of histones plays a key role in modulating the epigenetic landscape (Dang et al., 2009; Masumoto et al., 2005; Paauw et al., 2018). Similar to other PTMs, lysine acetylation does not only occur on histone tails, but also in non-histone proteins (Choudhary et al., 2009). Lysine acetylation marks are set by a protein family called histone acetyl transferases (HATs) (Legube and Trouche, 2003). The removal of lysine acetylation marks is performed by a diverse family of histone deacetylases (HDACs) (Yang and Seto, 2008). HDAC9 belongs to the class IIa which also contains HDAC4, HDAC5 and HDAC7 and MEF2 interacting transcriptional repressor (MITR) (Fig. 4).

HDAC class IIa members share some common molecular and biological traits: HDAC9 and other class IIa members are known to shuttle between cytoplasm and nucleus. This subcellular relocation ability is dependent on the phosphorylation status of the two conserved serine residues, namely Ser223 and Ser253 in HDAC9. When retained in the nucleus, HDAC class IIa members interact with transcriptional co-repressor complex (SMART, N-COR) and regulates genes expression (Di Giorgio et al., 2017; Fischle et al., 2002; Haberland et al., 2007). Upon phosphorylation, HDAC class IIa members bind to chaperone protein 14-3-3 and are exported into cytoplasm, thereby derepressing target gene expression (Alchini et al., 2017; Fischer et al., 2010; Grozinger and Schreiber, 2000; Parra and Verdin, 2010).

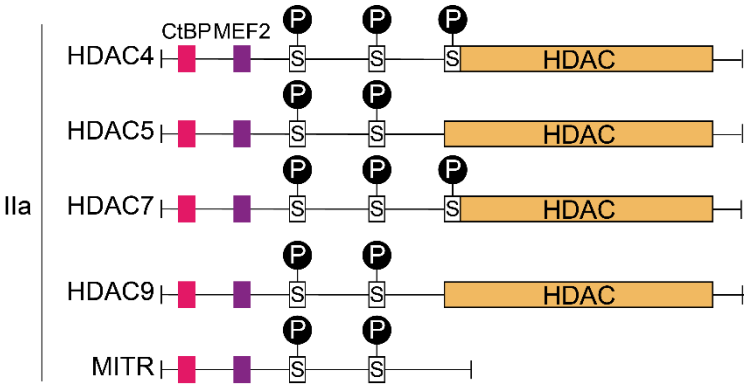

Figure 4. Structures of different HDAC class IIa members. HDAC4, HDAC5, HDAC7, HDAC9 and MITR belong to HDAC subclass IIa. They share similar N-terminal domain which is around 450-600 amino acids, which tend to interact with transcriptional repressor CtBP and transcription factor MEF2. HDAC class IIa members can shuttle between cytoplasm and nucleus. The shuttling is controlled by the phosphorylation status of the conserved serine residues. (Adapted from Eric Verdin, TRENDS in genetics, 2003)

The phosphorylation of the serine residues is regulated by multiple kinases. One of the well-studied kinases is the Ca^{2+}/calmodulin-dependent protein kinase II (CaMKII), which is known to phosphorylate the serine residues of HDAC4 and HDAC5 in cardiomyocytes and induce the relocation of HDAC4 and HDAC5 from the nucleus to the cytoplasm (Backs et al., 2008; Backs et al., 2006; Little et al., 2007). Besides CaMKII, protein kinase D (PKD1) has also been discovered to phosphorylate serine residues and induce the translocation of HDAC4 (Vega et al., 2004). However, much attention has been paid to cardiomyocyte and skeleton muscle cells, little is known about HDAC class IIa regulating kinases in immune cells.

Most class I HDACs are expressed ubiquitously in different cells and tissue, whereas class IIa HDACs are only expressed in certain cell types. HDAC4, 5 and 9 have been reported to be highly expressed in different muscles (heart and skeleton), brain and immune cells. The biological functions of class IIa HDACs is to some extent redundant since knocking out class IIa HDACs together did not result in additive phenotypic effect. (Fischle et al., 1999; Grozinger et al., 1999; Verdel and Khochbin, 1999; Wang et al., 1999; Zhou et al., 2001; Zhou et al., 2000).

Introduction

One of the most interesting traits of HDAC class IIa members is that they exert their biological functions via different interaction partners (Fig. 5). For example, HDAC class IIa members interact with other class I HDACs (e.g. HDAC3) to obtain the deacetylase capacity within the protein complex (Fischle et al., 2002). Besides HDAC3, the C-terminal-binding protein (CtBP) interacts with HDAC4, HDAC5 and MITR via a PXDLS motif, functioning as a transcriptional repressor (Chinnadurai, 2002). Like introduced before, phosphorylation of class IIa HDACs facilitates the binding of the chaperone protein 14-3-3, thereby blocking the interaction with MEF2 (Zhang et al., 2002).

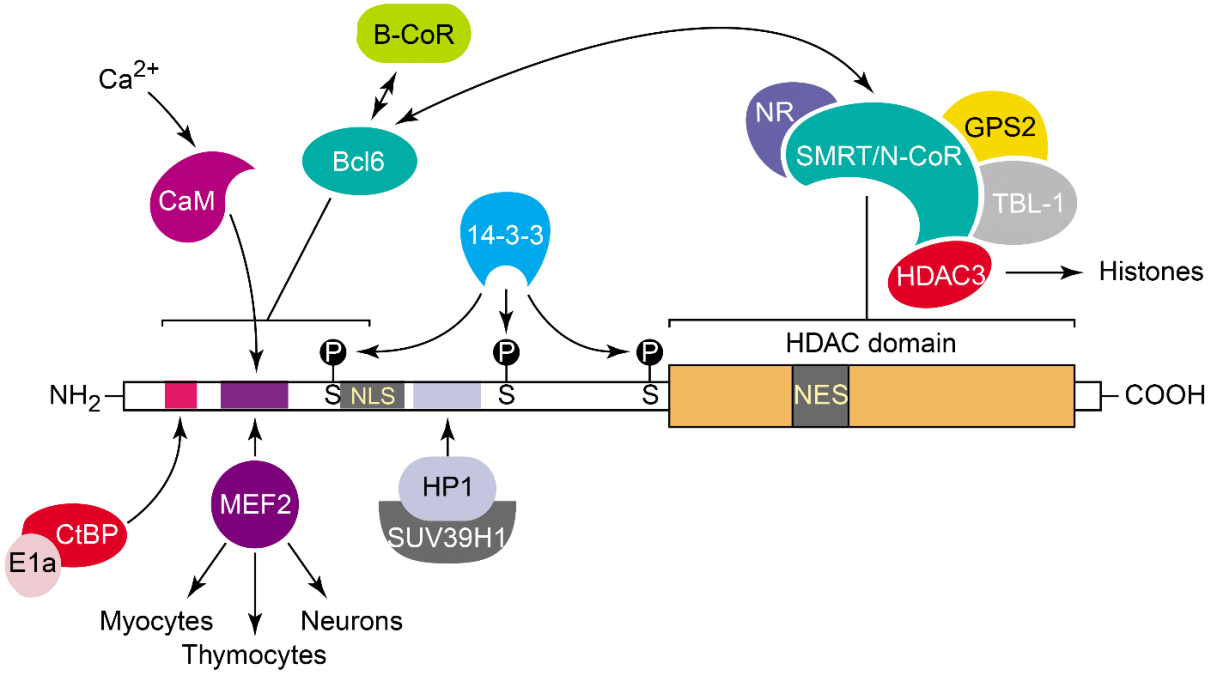

Figure 5. Different interaction partners of HDAC class IIa members.

Class IIa HDACs interact with different partners via different domains. The N-terminal domain primarily interacts with CtBP and MEF2, which can be disrupted by phosphorylation of the conserved serine residues (Verdin et al., 2003).

In conclusion, class IIa members have several shared traits: 1. they shuttle between the nucleus and the cytoplasm; 2. they are expressed in a cell-type-specific manner;

3. they interact with different partners to exert biological functions, such as repressing MEF2 downstream targets.

3.5 The biological function of HDAC9

Based on GWAS and other quantitative technologies, HDAC9 was recently reported to be associated with a wide range of diseases and phenotypes, such as intracranial aneurysm (Lansdell et al., 2019; Li et al., 2019), high circulating level of adiponectin (Spracklen et al., 2019), breast cancer (Huang et al., 2018), neuropathological characteristics to Alzheimer's disease (AD) (Chung et al., 2018), Saethre-Chotzen syndrome (Shimbo et al., 2018), small vessel disease in western Africans (Akinyemi et al., 2018), peripheral arterial disease (Matsukura et al., 2015) and most importantly atherosclerosis and large artery stroke (Azghandi et al., 2015; Malik et al., 2018). Abovementioned evidence suggests the pivotal role of HDAC9 in regulating different biological functions and the importance to study HDAC9.

3.5.1 The complexity of HDAC9 gene locus

HDAC9 locus is larger than 600 kb in human genome, and more than 40 isoforms have been identified. The long isoform of human HDAC9 has 23 exons and is translated into a 1011 amino acid protein (Petrie et al., 2003; Thierry-Mieg and Thierry-Mieg, 2006). A shorter isoform of HDAC9 is MITR (593 amino acid), which is devoid of the deacetylase domain (Zhang et al., 2001). In mouse, the *Hdac9* locus is around 500 kb and is alternatively spliced into 9 different isoforms suggesting an equal complexity of HDAC9 in mouse.

3.5.2 Recently identified interaction partners of HDAC9

Recently, several novel interaction partners of HDAC9 have been identified. In vascular smooth muscle cells (VSMCs), HDAC9 was found to form a ternary complex including epigenetics regulator BRG1 and a long non-coding RNA called MALAT1 (Lino Cardenas et al., 2018). This newly discovered complex modulated the chromatin landscape, thereby silencing SMCs contractile gene expression and leading to aortic aneurysm. Moreover, the disruption of MALAT1 and HDAC9 interaction rescued the aortic aneurysm phenotype. Of note, this complex did not regulate epigenetic landscape directly, but via recruiting the polycomb repressor complex 2 (PRC2) to set the repressive H3K27me3 mark (Lino Cardenas et al., 2019). Another novel interaction partner of HDAC9 is HDAC6. HDAC9 directly interacted with the second deacetylase domain of HDAC6, thereby regulating BAX/BCL2 pathway and promoting neuronal cell survival (Salian-Mehta et al., 2015).

3.5.3 The role of HDAC9 in cell proliferation

Many studies have shown that HDAC9 plays a role in cell proliferation, especially in different cancer cells. For example, in non-small cell lung cancer (NSCLC), low *HDAC9* expression increased cell apoptosis and decreased cell proliferation both *in vitro* and *in vivo* (Ma et al., 2019). Among gastric cancer patients, high expression of *HDAC9* was observed in cancer tissue samples and associated with poor prognosis (Xu et al., 2019). In the hepatocellular carcinoma, *HDAC9* expression was positively correlated with the proliferation marker Ki67 (Hu et al., 2019). Moreover, in trophoblast cells, *HDAC9* was shown to deacetylate the histone tails in TIMP3 promoter region, thereby downregulating the expression of TIMP3 and consequently changing cell migration behavior (Xie et al., 2019). In addition, HDAC9 has been reported to promote invasion

and angiogenesis via elevating the expression of *VEGF* and *MAPK3* level in breast cancer background (Salgado et al., 2018). Moreover, HDAC9 was reported to putatively regulate the transcriptional level of *P53* in human osteosarcoma cells by modulating the *P53* promoter chromatin landscape (Zhao et al., 2015). Recently, our group showed that in HeLa cells, *HDAC9* expression was increased at the G1/S boundary and during S phase, further indicating the role of HDAC9 in cell proliferation (Prestel et al., 2019).

3.5.4. HDAC9 deacetylates non-histone proteins

HDAC9 is thought to play a role in epigenetic reprogramming, but recent evidence suggests that it also deacetylases non-histone proteins. For example, HDAC9 was shown to deacetylate FoxO1, which leads to modulating the epigenetic landscape and regulating glucocorticoid receptor (GR) and cyclic AMP-responsive element-binding protein (CREB) gene expression (Chen et al., 2017). HDAC9 was also shown to directly interact with a kinase called TBK1 via the deacetylase domain, thereby deacetylating TBK1 and compromising its kinase activity in macrophages (Liu et al., 2016). However, both studies did not address whether the deacetylation is due to HDAC9 alone or its interaction partners such as HDAC3.

3.5.5. HDAC9 regulates the pro-inflammatory response

A large body of evidence showed that HDAC9 plays a role in regulating pro-inflammatory response. HDAC9 together with HDAC8 were shown to regulate the pro-inflammatory response via toll like receptor (TLR) 2, thereby changing the pro-inflammatory cytokine production in sebocytes when ingesting short chain fatty acid (SCFAc) (Sanford et al., 2019). Moreover, in ischemic stroke brains, HDAC9 was shown to be elevated (Lu et al., 2018). Specifically, HDAC9 deficiency decreased the

infarct volume and attenuated stroke outcome compared to the sham control. Most interestingly, in this study, *Hdac9* knockout mice showed lower level of pro-inflammatory cytokines such as interleukin-6 (IL-6), IL-1β, and IL-18 in the brain after ischemic injury. Mechanistically, phosphorylated IκBα and NF-κB activation was decreased in an *Hdac9* knockout model, which indicated the role of HDAC9 in NF-κB pathway activation (Lu et al., 2018).

3.5.6. The role of HDAC9 in atherosclerosis

The expression of *HDAC9* was shown to be associated with M4 (CXCL4-induced macrophages) but not smooth muscle cells in human advanced carotid plaque, indicating that HDAC9 might regulate plaque stability in a macrophage-specific-manner (Oksala et al., 2017). To directly show the role of HDAC9 in atherogenesis, the global *Hdac9* knockout in female *Ldlr*$^{-/-}$ mice reduced the atherosclerotic plaque formation (Cao et al., 2014). This study also showed that *Hdac9* deficient bone marrows cells alone were able to attenuate atherogenesis via bone marrow transplantation experiments, indicating the atherogenic role of HDAC9 majorly in hematopoietic stem cells. Mechanistically, ChIP experiments demonstrated that HDAC9 decreased the histone acetylation level in the promoter region of *Abca1* and *Abcg1* in macrophages, thereby decreasing cholesterol efflux. In accord with these findings, our group showed that *Hdac9* deficiency in *Apoe*$^{-/-}$ mice also attenuated atherogenesis at the age of 18 and 26 weeks under chow diet (Azghandi et al., 2015), further confirming the role of HDAC9 in atherogenesis. Translating to humans, the expression of HDAC9 in human peripheral monocytes was upregulated in risk allele A carriers in a gene dosage effect, indicating that rs2107595 might exacerbate atherosclerotic development via upregulating *HDAC9*. The neighboring genes *FER3DL* and *TWIST1* did not show risk-allele-dependent pattern of expression, which

further confirms the causative relationship between rs2107595 and atherosclerosis mediated by HDAC9. Taken together, HDAC9 was shown to promote atherosclerotic development in different atheroprone mouse models. In human samples, rs2107595 was shown to be correlated with *HDAC9* expression in PBMCs. All the evidence indicates that rs2107595 harbors an atherogenic effect.

Aim of this study

First, since the *cis*-regulatory element (CRE) encompassing rs2107595 is highly conserved, I was motivated to explore the atherogenic effect of the CRE via generating a novel mouse model devoid of this CRE. To test if this mouse model mimics the human risk allele A carriers, the atherosclerotic phenotype was characterized. Second, via exploiting the cell-type-specific and gene-expression-specific trait of the CRE, I was prompted to analyze the gene expression (e.g. *Hdac9*) in different cell types to narrow down candidate cell types driving atherosclerotic development mediated by the CRE. Finally, after narrowing down to the cell types, I planned to address the molecular role of target genes in this cell type during the progression of atherosclerosis. Overall, it was therefore the aim of this thesis to systematically characterize atherosclerotic development and gene expression in a novel mouse model. Guided by this information, I tend to explore the function of HDAC9 during atherosclerotic development.

4. MATERIALS AND METHODS:

4.1. Materials

4.1.1 Chemicals and reagents

Table 1 Chemicals and reagents

CHEMICALS/ REAGETNS	COMPANY
1 KB PLUS DNA LADDER	Bioline, Germany
2-PROPANOL	Sigma-Aldrich Chemie GmbH, Germany
AGAROSE	Sigma-Aldrich Chemie GmbH, Germany
AMPICILLIN	Sigma-Aldrich Chemie GmbH, Germany
CITRIC ACID	Merck KGaA, Germany
COLLENASE TYPE 2	Worthington, USA
DMEM	Thermo Fisher Scientific, USA
DMSO	Thermo Fisher Scientific, USA
EDTA	Sigma-Aldrich Chemie GmbH, Germany
ETHANOL 99%	Sigma-Aldrich Chemie GmbH, Germany
FBS	Thermo Fisher Scientific, USA
FERD3L TAQMAN PROBE	Thermo Fisher Scientific, USA
HCL	Merck KGaA, , Germany
HDAC9 HUMAN TAQMAN PROBE	Thermo Fisher Scientific, USA
HDAC9 MOUSE TAQMAN PROBE 1	Thermo Fisher Scientific, USA
HDAC9 MOUSE TAQMAN PROBE 2	Thermo Fisher Scientific, USA
HEMATOXYLIN SOLUTION	Sigma-Aldrich Chemie GmbH, Germany
LIPOPOLYSACCHARIDES	Sigma-Aldrich Chemie GmbH, Germany
NIGERICIN SODIUM SALT	Sigma-Aldrich Chemie GmbH, Germany
OIL RED O	Sigma-Aldrich Chemie GmbH, Germany
PARAFORMALDEHYDE (PFA) 4%	MORPHISTO, Germany
PBS	Sigma-Aldrich Chemie GmbH, Germany
PENICILLIN-STREPTOMYCIN	Sigma-Aldrich Chemie GmbH, Germany
PHOSSTOP™	Sigma-Aldrich Chemie GmbH, Germany
COMPLETE™ PROTEASE INHIBITOR COCKTAIL	Sigma-Aldrich Chemie GmbH, Germany
RESTORE™ WESTERN BLOT STRIPPING BUFFER	Thermo Fisher Scientific, USA

ROTI-HISTO	CARL ROTH, Germany
RPMI-1640	Thermo Fisher Scientific, USA
SKIM MILK POWDER	Sigma-Aldrich Chemie GmbH, Germany
TISSUE-TEK O.C.T	Sakura, Europe
TRIZMA® BASE	Sigma-Aldrich Chemie GmbH, Germany
TWEEN 20	Sigma-Aldrich Chemie GmbH, Germany
TWIST1 MOUSE TAQMAN PROBE	Thermo Fisher Scientific, USA
TAQMAN™ UNIVERSAL PCR MASTER MIX	Thermo Fisher Scientific, USA
UNIVERSAL-AGAROSE, PEQGOLD	VWR life science , Germany
IMMOBILON WESTERN HRP SUBSTRAT	Millipore, Germany
SUPERSIGNAL™ WEST PICO PLUS CHEMILUMINESCENT SUBSTRATE	Thermo Fisher Scientific, USA
TAQ DNA POLYMERASE, RECOMBINANT	Thermo Fisher Scientific, USA

4.1.2 Kits

Table 2 Kits

KITS	COMPANY
MONOCYTE ISOLATION KIT	Miltenyi Biotec GmbH, Germany
PAN B CELL ISOLATION KIT	Miltenyi Biotec GmbH, Germany
PAN T CELL ISOLATION KIT	Miltenyi Biotec GmbH, Germany
OMNISCRIPT RT KIT	QIAGEN, Germany
RNEASY MICRO KIT	QIAGEN, Germany
RNEASY MINI KIT	QIAGEN, Germany
QUANTINOVA SYBR GREEN PCR KIT	QIAGEN, Germany
PIERCE™ BCA PROTEIN ASSAY KIT	Thermo Fisher Scientific, USA
TRICHROME STAIN (MASSON) KIT	Sigma-Aldrich Chemie GmbH, Germany
WEIGERT'S IRON HEMATOXYLIN SOLUTION	Sigma-Aldrich Chemie GmbH, Germany
CHOLESTEROL FLUOROMETRIC ASSAY KIT	Cayman Chemical, USA
TRIGLYCERIDE COLORIMETRIC ASSAY KIT	Cayman Chemical, USA
CASPASE-GLO® 1 INFLAMMASOME ASSAY	Promega, Germany

4.1.3 Materials

Table 3 Materials

MATERIALS	COMPANY
QIAGEN TISSUELYSER STEEL BEADS	QIAGEN, Germany
SAFETY SCALPEL	Corning, Germany
6-WELL PLATES	Sigma-Aldrich Chemie GmbH, Germany
12-WELL PLATES	Sigma-Aldrich Chemie GmbH, Germany
96-WELL PLATES	Sigma-Aldrich Chemie GmbH, Germany
384-WELL PLATES FOR QPCR	Thermo Fisher Scientific, USA
15 ML FALCON TUBES	Corning, Germany
50 ML FALCON TUBES	Corning, Germany
CELL SCRAPERS	Corning, Germany
SUPERFROST PLUS™ SLIDES	Thermo Fisher Scientific, USA
TISSUE-TEK® O.C.T.™ COMPOUND	SAKURA, Japan
40UM CELL TRAINERS	Corning, Germany

4.1.4 Instruments

Table 4 Machines

MACHINES AND EQUIPMENT	COMPANY
LIGHTCYCLER® 480 INSTRUMENT	Roche, Switzerland
AUTOMACS PRO SEPARATOR	Miltenyi Biotech, Germany
WESTERN BLOT SYSTEM	Bio-rad, Germany
PARAFFIN EMBEDDING MACHINE	Thermo Fischer, Germany
CELL CULTURE INCUBATOR	Thermo Fischer, Germany
HEATING OVENS	Salvislab, Switzerland
THERMOSHAKER	Cell Media, Germany
NANODROP™1000 SPECTROPHOTOMETER	Thermo Fischer, Germany
2100 BIOANALYZER INSTRUMENT	Agilent, Germany
WATER BATH	GFL, Europe
4°C FRIDGE	Siemens, Germany
-20°C FRIDGE	Siemens, Germany
-80°C FRIDGE	Thermo Fischer, Germany

CENTRIFUGE	Thermo Fischer, Germany
TC20™ AUTOMATED CELL COUNTER	Bio-rad, Germany

4.1.5 Primers

Table 5 Genotyping primers

GENOTYPING PRIMERS		5`-3` PRIMERS SEQUENCE
HDAC9$^{\Delta CIS-/-}$	FORWARD	GATATGAATTTGTGGATCACTCACTTGTC
HDAC9$^{\Delta CIS-/-}$	WT REVERSE	TTCCAGCTACCTCCTTCTCAGAAC
HDAC9$^{\Delta CIS-/-}$	KO REVERSE	CTTAGTCAATAGGTTTATCATCAGCAAAGC
APOE	FORWARD	GCCTAGCCGAGGGAGAGCCG
APOE	WT REVERSE	TGTGACTTGGGAGCTCTGCAGC
APOE	KO REVERSE	GCCGCCCCGACTGCATCT

Table 6 Gene expression primers

GENE EXPRESSION PRIMERS	5`-3` PRIMERS SEQUENCE
ARGINASE-1_FOR	GAACCCAACTCTTGGGAAGAC
ARGINASE-1_REV	GGAGAAGGCGTTTGCTTAGTT
ß-ACTIN_FOR	GGATGCAGAAGGAGATTACTGC
ß-ACTIN_REV	CCACCGATCCACACAGAGTA
CCL2_FOR	CTTCTGGGCCTGCTGTTCA
CCL2_REV	CCAGCCTACTCATTGGGATC
CD36_FOR	CCGAGGACCACACTGTGTC
CD36_REV	AACCCCACAAGAGTTCTTTCAAA
MIF_FOR	TTTAGCGGCACGAACGATCC
MIF_REV	CGTTGGCAGCGTTCATGTC
ACTIN_FOR	AGTGTGACGTTGACATCCGT
ACTIN_REV	GCAGCTCAGTAACAGTCCGC
MIL6_FOR	TAGTCCTTCCTACCCCAATTTCC
MIL6_REV	TTGGTCCTTAGCCACTCCTTC
MTNFA_FOR	GACGTGGAACTGGCAGAAGAG
MTNFA_REV	TTGGTGGTTTGTGAGTGTGAG

VCAM-1_FOR	TGCCGAGCTAAATTACACATT
VCAM-1_REV	CCTTGTGGAGGGATGTACAGA
ICAM-1_FOR	GCCTTGGTAGAGGTGACTGAG
ICAM-1_REV	GACCGGAGCTGAAAAGTTGTA
IL-1ß_FOR	AGAGCATCCAGCTTCAAATCTC
IL-1ß_REV	CAGTTGTCTAATGGGAACGTC
IL-4_FOR	AAACTCCATGCTTGAAGAAGAACT
IL-4_REV	CTACGAGTAATCCATTTGCATGAT
IL-6 V2_FOR	ATGGATGCTACCAAACTGGAT
IL-6 V2_REV	TGAAGGACTCTGGCTTTGTCT
IL-10_FOR	TGAATTCCCTGGGTGAGAAG
IL-10_REV	GCTCCACTGCCTTGCTCTTA
INOS_FOR	CTCTACAACATCCTGGAGCAAGTG
INOS_REV	ACTATGGAGCACAGCCACATTGA
MIF_FOR	TTTAGCGGCACGAACGATCC
MIF_REV	CGTTGGCAGCGTTCATGTC
KLF2_FOR	TCTGCGTACACACACAGGTGAGAA
KLF2_REV	ACATGTGTCGCTTCATGTGCAAGG
NLRP3_FOR	TGCTCTTCACTGCTATCAAGCCCT
NLRP3_REV	ACAAGCCTTTGCTCCAGACCCTAT
IL-18_FOR	TGGTTCCATGCTTTCTGGACTCCT
IL-18_REV	TTCCTGGGCCAAGAGGAAGTGATT
HPRT_FOR	CACAGGACTAGAACACCTGC
HPRT_REV	GCTGGTGAAAAGGACCTCT

4.1.6 Software

Table 7 Software

SOFTWARES	COMPANY
FLOWJO V10.3	Tree Star, Inc., OR, USA
GRAPHPAD PRISM 7.00	GRAPHPAD SOFTWARE INC, USA
IMAGE J	National Institutes of Health, USA
R	R CORE TEAM, USA
ADOBE ILLUSTRATOR	Adobe, USA
ZEN	ZEISS, GERMANY

4.2 Methods

4.2.1 Mouse model

4.2.1.1 Generation of *Hdac9*$^{\Delta Cis-/-}$ and *Apoe*$^{-/-}$ *Hdac9*$^{\Delta Cis-/-}$ mouse line

Hdac9$^{\Delta Cis-/-}$ mouse model was generated by Dr. Benidikt Wefers from the German Center for Neurodegenerative Diseases (DZNE). To generate *Hdac9*$^{\Delta Cis-/-}$ mice, the CRISPR-Cas9 technology was used (Wefers et al., 2017). First, guided RNA (gRNA) specific to target the CRE were designed. Then gRNA and Cas9 were directly injected into murine zygotes via electroporation. After injection, zygotes were cultured *in vitro* and then transferred to surrogate females. F0 founder mice were weaned at the age of 3 weeks old and biopsies were taken for genotyping. Progenies were bred according the founder mice genotyping results (Wefers et al., 2017). The deletion size for *Hdac9*$^{\Delta Cis-/-}$ is 1.1 kb.

To facilitate the spontaneous atherosclerotic plaque development, *Hdac9*$^{\Delta Cis-/-}$ was bred with atheroprone model *Apoe*$^{-/-}$. For the first batch of analysis, mice were fed with normal chow diet for 28 weeks before sacrifice. For the second batch, HFD was used

to feed the mice (Nakashima et al., 1994). Only littermates were used for all the experimental analysis and comparison in a blinded fashion. All the breeding and husbandry of the mice are executed according to the laws and regulations by the government of upper Bavaria.

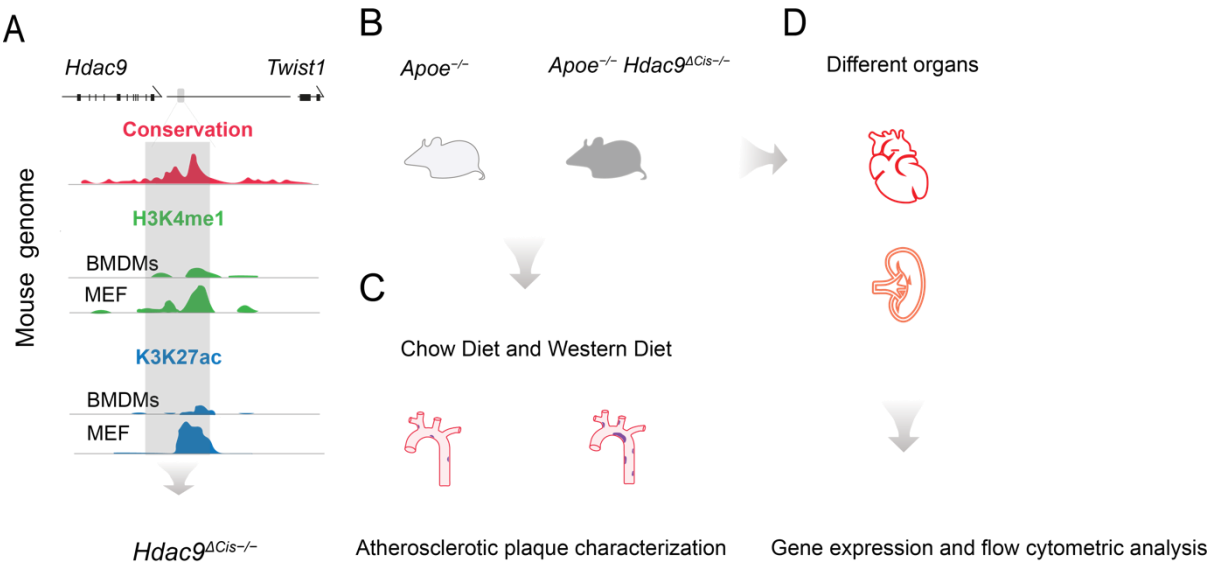

Figure 6. Illustration of *in vivo* experimental flow.

(A) The targeted *cis*-regulatory element is highly conserved among different species and contains enrichment of histone markers in a cell-type-specific manner. Deletion was mediated by CRISPR-Cas9 system and 1,1 kb was knocked out. (B) *Hdac9*$^{\Delta Cis-/-}$ was bred with *Apoe*$^{-/-}$ mice to facilitate the spontaneous plaque formation. Littermates were used for downstream analysis. (C) Mice were fed with chow diet for 28 weeks or HFD for 8 weeks starting from the 8th week. Aortas and other tissues were dissected for plaque and other analysis. (D) Spleen and other organs were used for gene expression analysis.

4.2.1.2 Bone marrow transplantation

Bone marrow transplantation was performed by Dr. Emiel Van der Vorst from the Institute for Cardiovascular Prevention (IPEK), LMU Munich. We provided donor littermate mice: *Apoe*$^{-/-}$ *Hdac9*$^{\Delta Cis-/-}$ and *Apoe*$^{-/-}$. Prior to bone marrow transplantation, recipient *Apoe*$^{-/-}$ mice were subject to radiation to deplete their endogenous bone marrow cells. Afterwards, bone marrows from donor mice were flushed and injected into recipient mice. After surgery, recipient mice were treated with antibiotics for 3

weeks, and then fed with HFD to develop atherosclerotic plaque. Aorta, hearts and other organs were collected for analysis.

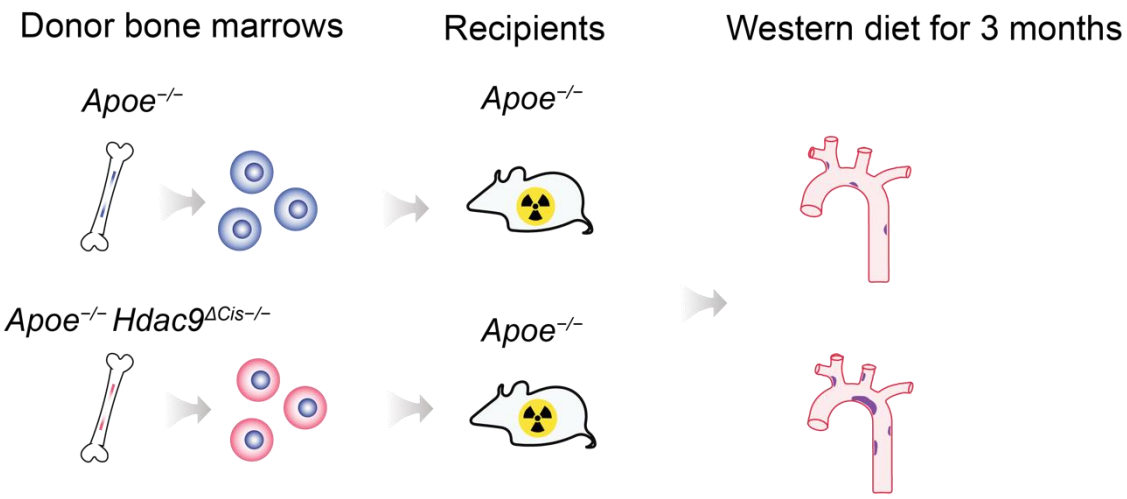

Figure 7. Illustration of bone marrow transplantation.

4.2.1.3 Genotyping of the mice

To genotype each mouse, biopsies were harvested from newly weaned mice. To further validate the genotype, a second-time genotyping was performed from a different person. For this purpose, tail biopsies were cut after sacrificing the mice. All the biopsies were digested with 100 µl NaOH (5mM) at 95°C for 30 minutes in 1.5 ml tubes. Centrifugation was performed to collect the evaporation. 30 µl Tris-HCL was added to neutralize the PH value from the lysate. The lysate DNA was kept in 4°C and applied for polymerase chain reaction (PCR). *Hdac9*$^{\Delta Cis-/-}$ genoyping PCR products were validated with 1% agarose gel run by 100 voltage for 1 hour. WT PCR product size is 662 bp and KO is 1020 bp. *Apoe*$^{-/-}$ genotyping PCR products were validated with 2% agarose gel run by 100 voltage for 1 hour. WT PCR product size is 155 bp and KO is 245bp.

Table 8 Genotyping PCR reaction mix

Reagents	Amount
Taq polymerase	0. 6 µl
Forward primer	1 µl
Reverse primer	1 µl
dNTP	1 µl
MgCl2	5 µl
H2O	35.4 µl
Genotyping material	1 µl
PCR buffer	5 µl

Table 9 Genotyping PCR program

Cycle	Temperature	Time
1	95°C	3 min
35	95°C	30 sec
	53°C/63°C	30 sec
	72°C	1 min
1	72°C	10 min
1	4°C	∞

4.2.1.4. Sacrifice and dissection of mice

All animal experiments were executed according to the laws and regulations of the government of upper Bavaria. Before sacrificing, all mice were anesthetized with isoflurane. Reflexes from the mice were tested before euthanizing with Ketamine/Xylazine. Blood was obtained via cardiac punch. 0.9% sodium chloride solution was used to perfuse the mice via the left ventricle into the arterial tree, different organs (e.g. aorta, heart and spleen) were harvested. For histological analysis, aorta and its main branches were fixed in 1% PFA solution, then embedded in paraffin and cut into consecutive 4µm sections using microtome. Heart was dissected and later fixed with tissue tek in a plastic box on dry ice. 8µm consecutive sections of aortic root were obtained from the heat. Aortic root sections were stored at -80°C and paraffin sections at room temperature.

4.2.2 Cell culture

4.2.2.1 Primary culture of aortic smooth muscle cells

Aorta was dissected carefully to avoid contamination and later cut into small pieces. Collagenase II was added for digestion at 37°C for around 5 hours until major pieces were digested. Cell clumps were pelleted by centrifugation and resuspended in smooth muscle cell culture media with 10% FCS and 1% antibiotics. After 12 hours, cell culture media was replaced with fresh medium to avoid contamination from other cell types. Cell between 2^{nd} and 4^{th} passages were used for gene expression analysis.

4.2.2.2. Primary culture of Bone Marrow Derived Macrophages (BMDMs)

Mice were sacrificed by cervical dislocation. The abdomen and hind legs were sterilized with 70% ethanol. Along the midline of the abdomen, an incision was made, and hind legs were expose by clipping the tissues outward. Afterwards the knee joint was cut and femur was separated followed by removal of connecting tissues from the bones. To attain the bone marrow, both ends from the bones were cut and bone marrow was flushed out using RPMI 1640 medium (1% penicillin-streptomycin and 10% FCS) using 5 ml syringe and 25-gauge needle. Bone marrows were pipetted up and down to achieve single cell suspension followed by sieving through a 40 µM cell strainer. Centrifugation was performed at 500g for 10 min and cell pellets were counted and incubated in BMDM specific medium containing 15% L929 conditioned medium (LCM) for differentiation for 5-7 days. Mature and fully differentiated macrophages adhered to petri dished. Mature BMDMs were detached by scraping with a cell scraper. After washing the cells with PBS, around 1-3 $x10^6$ cell were plated into each well of a 6-well plate. Before treatment, BMDMs were starved by replacing the medium with serum-free RPMI 1640 medium for 12 hours to synchronize cell cycle. To polarize the

BMDMs into pro-inflammatory or anti-inflammatory phenotype, LPS (100ng/ml) or/ IL4 (20 ng/ml) was administered for 24 hours, respectively. Subsequently, cells were washed with warm PBS and BMDMs lysed with different buffers dependent on later analysis.

4.2.3 Histological analysis

4.2.3.1 Oil Red O staining

8 μm serial sections are collected from the onset of two aortic valves until all the valves diminish. Oil Red O was used to stain the lipid composition accumulated in atherosclerotic plaque from the aortic valves. Aortic root sections were equilibrated to room temperature from -80°C and then re-hydrated with PBS for 5 minutes at room temperature. Oil Red O solution was poured into the sections container jars and submerged all the aortic root sections. Sections were incubated at 37 °C incubator for 45 minutes. Slides were rinsed with tap water at the back side to avoid loss of sections. Nuclear counterstaining was achieved with hematoxylin for 1 min followed with rinsing with tap water for 5 minutes. Slides were dried in the hood before mounting. In terms of the quantification of Oil Red O staining, 10 sections were selected with interval of 64 μm between each two sequential sections. Image J was used to delineate and quantify the red areas inside the aortic valves. Mean value from the 10 sections was used for statistics.

4.2.3.2 Trichrome staining

To quantify the content of collagen, necrotic cores and fibrous cap thickness, trichrome staining was applied. Aortic root sections were equilibrated to room temperature and then re-hydrated with PBS for 5 minutes at room temperature. To re-fix the sections,

Bouin’s solution was applied at 56°C for 1 hour followed by gentle wash with tap water for 10 minutes to remove the yellow residual color. Next, Nuclear counterstaining was performed with Weigert's iron hematoxylin working solution for 10 minutes and then washed with warm tap water for 10 minutes. Afterwards, the Biebrich scarlet-acid fuchsin solution was applied for 10 minutes and followed by washing with tap water for 10 minutes. To develop the collagen staining sections were incubated in phosphomolybdic-phosphotungstic acid solution followed by directly staining with aniline blue solution for 10 minutes to further visualize the collagen. After washing with tap water for 10 minutes, quickly dehydrate the sections by dipping through 95% and 100% ethanol. Successful staining visualizes the collagen as blue, nuclei as black and cytoplasm as red.

In terms of quantification of the percentage of collagen, image J was applied to quantify the blue area inside the aortic valves. The value was then divided by the total size of atherosclerotic plaque. Regarding necrotic cores quantification, the acellular areas devoid of nuclei were measured and divided by the lesion size. The thickness measurement for fibrous cap is based on the necrotic cores.

4.2.3.3 MAC2 staining

Aortic root sections are equilibrated to room temperature from -80°C freezers and then re-hydrated with PBS for 5 min at room temperature. Slides were quickly dried with tissue papers before circling around the sections with pap pen. First, sections were blocked with blocking buffer (0.05% Tween 20, 3% BSA and 1% goat serum) to avoid unspecific binding. Sections are quickly dried to get rid of the blocking buffer and then incubated with Mac2 antibody (1:100) in PBS at 4°C overnight with gentle shaking. Next day morning, sections were washed with PBS 3 times for 5 min each followed by

secondary antibody (goat anti rat 1:500) CY5 conjugated and 4′,6-diamidino-2-phenylindole (DAPI) (1:5000) for 1 hour at room temperature. Sections then were washed before being mounted with aqua medium. In terms of the quantification of the $Mac2^+$ area, the red areas were selected and quantified by image J.

4.2.3.4 En face staining

Aortas from bone marrow transplantation mice were collected and fixed in 1%PFA for 24 hours and then used for en face staining. Dissection and cutting of the aorta was based on a published guideline (Ko et al., 2017). Oil Red O staining was applied to visualize the lipid composition inside the aorta. Red areas were quantified by Image J.

4.2.4 Flow cytometric analysis

After dissection, spleens were placed on ice for later analysis. Afterwards, spleens were meshed via 70μm cell strainers to obtain single cell suspension. Cells were centrifuged in 50 ml falcon tubes at the speed of 500g for 5 minutes. Pellets were pipetted resuspended and sifted through a 70μm cell strainers to exclude cell clumps. Cell pellets were washed again. 3×10^5 splenic cells were used for each panel of flow cytometric analysis. Before staining the splenic cells, red blood cell lysis buffer (RBC lysis buffer) was applied by adding 5 ml pre-warmed RBC lysis buffer for 1 minutes and followed by 10 ml cold PBS wash. Different panels of antibody cocktails were prepared to stain the cells. After incubating cells at 4°C for 30 minutes, 2X washes were applied with PBS. Cells were then resuspended with flow cytometry buffer.

Table 10 Red blood cell lysis buffer (1L):

Reagents	Amount
NH4Cl	8.26 g
KHCO3	1 g
EDTA	0.037 g
Millipore water	Fill up to 1 L

Table 11 Myeloid cell panel:

Antibody	Dilution	Company	Clone	Host
CD45 eFluo450	1:800	eBioscience	30-F11	Rat
CD11c PE-Cy7	1:1000	eBioscience	N418	Armenian Hamster
Ly6G PE	1:400	BD Bioscience	1A8	Rat
CD11b PerCp-Cy5.5	1:600	eBioscience	M1/70	Rat
Ly6C APC	1:10	Miltenyl	N.A.	Rat

Table 12 T cell panel:

Antibody	Dilution	Company	Clone	Host
CD3 FITC	1:200	eBioscience	145-2C11	Armenian Hamster
CD4-APC-H7	1:200	BD Bioscience	GK1.5	Rat
CD8 eFluor450	1:400	eBioscience	53-6.7	Rat
CD44 APC	1:1500	eBioscience	IM7	Rat
CD62L PE-Cy7	1:800	eBioscience	Mel-14	Rat

4.2.5 Magnetic activated cell sorting (MACS)

Same protocol was applied for making single cell suspension from spleens. After re-suspending the cell pellets with MACS running buffer, total cell number was determined. MACS antibodies were added according to kit-specific instructions. After incubation at 4°C for 30 minutes (incubation time depends on different kits), cell suspension was washed 2 times with MACS running buffer at 4°C at 500g for 5 minutes. Cell pellet was re-suspended with 500 µl MACS running buffer and sorted by Auto

MACS machine. Kit-specific selection program was chosen. After sorting, cell were pelleted by centrifugation and washed 2 times with PBS. Afterwards, the cell pellets were directly lysed by QIAzol and immediately snap frozen for later RNA isolation.

4.2.6 RNA isolation

Different tissues were dissected and preserved for later RNA isolation. For tissue RNA isolation, tissues were placed into 50 ml falcon tubes and submerged by 2ml Trizol. Tissue lysis into a single cell suspension was supported by mechanical disruption using an electronic drill. The single cell suspension was placed at room temperature for 30 minutes and 0.2 ml chloroform (per ml Trizol) was added followed by shaking the mixed solution violently for 10 seconds. Afterwards, centrifugation was performed at 16,000 g for 30 minutes and the upper aqueous layer was transferred into a new tube. 0.5 ml isopropanol was added into new tubes followed by incubation at room temperature for 10 minutes and RNA precipitate was pelleted by centrifugation at 16,000 g. Pellet was washed with 75% ethanol. Pellet was washed once more before being dissolved in RNase-free water. Pellet was dissolved at 55-60°C for 10 minutes before determining the concentration.

For isolating the RNA from cells, RNA isolation kits were used and performed according to the protocol from the manufacturer.

4.2.7. Quantitative real-time PCR (qPCR)

To relatively quantify transcriptional levels of different genes, Taqman or Sybr green quantitative real-time PCR were applied. To detect genes of interest, gene-specific primers or probes were used. For HDAC9 detection, two taqman probes were selected to detect the expression of short isoform MITR and long isoform HDAC9.

Table 13 Sybr Green qPCR

Reagents	Amount
Primer Forward	1 µl
Primer Reverse	1 µl
Master mix	6 µl
cDNA	2 µl
Nuclease-free H_2O	2 µl

Table 14 Taqman qPCR

Reagents	Amount
Taqman probes	0,6 µl
Master mix	6 µl
cDNA	2 µl
Nuclease-free H_2O	3,4 µl

The housekeeping genes Hypoxanthine Guanine Phosphoribosyltransferase (HPRT), Beta (β)-actin (ACTB) and Glyceraldehyde 3-phosphate dehydrogenase (GAPDH) were used for normalization. The relative fold change was calculated based on following equations:

dCt=Ct (gene of interest)-Ct (normalizer)

ddCt=dCt (Genotype A)-average dCt (Genotype B)

Fold change=2^{-ddCt}

4.2.7.1. Reverse transcription

Isolated RNA was reverse transcribed into cDNA according to the manufacturer's instruction (Qiagen): After mixing the reagents on ice, reaction was placed in 37 °C for 90 minutes. Afterwards, the solution was diluted 1:10 for downstream qPCR analysis.

4.2.8. Cell transfection

BMDMs were seeded into12-well plates to reach 10^6 cells per well. Different plasmids (total amount is 1.6 µg), siRNAs (50 nmol) and lipofectamine 2000 (4 µl) were dissolved in 50 µl Opti-MEM and placed in room temperature. After 5 minutes, plasmids or siRNA was pipetted into lipofectamine and incubated for 30 minutes before adding to cells. Cell medium was replaced after 24 hours with normal medium deprived of antibiotics.

Two different isoforms of *Hdac9* were used for transfection. Plasmids were provided by Dr. Matthias Prestel from our lab.

4.2.9. Western blot analysis

Cell lysate and corresponding supernatant were collected. Protease and phosphatase inhibitors were added to prevent protein degradation. Cell lysate were treated with 1µl benzonase (250 units/µL) to digest the chromatin and avoid the protein and chromatin clumps. Protein concentration was measured by BCA protein assay kit. After adjusting the total protein weight, samples were diluted and boiled with Laemmli buffer at 95°C for 5 minutes. 7.5% sodium dodecyl sulphate (SDS) gel was used to separate proteins at 100V for 90 minutes. Nitrocellulose membrane was used for transferring proteins at 100 V for 70 minutes. Once the transfer was done, membranes were collected and washed with TBST and blocked with 5% fat free milk for 40 min at RT. Primary antibody was diluted also in 5% fat free milk, and incubated at 4°C overnight and then washed with TBST for 3 times and 5 min each in RT. Then secondary antibody was applied and incubated in RT for 1 hour.

Table 15 NP40 buffer

Reagents	Concentration
Tris pH 7.5	50 mM
NaCl	150 mM
EDTA	1 mM
MgCl2	1.5 mM
DTT	1 mM
Glycerol	10%
NP40	1%

Table 16 Urea buffer

Reagents	Amount
9M Urea	27 g
1% SDS	0.5 g
25mM Tris PH 6,8	1.25 ml (1 M stock)
1mM EDTA	0.1 ml (0.5 M stock)
0,02% Bromophenol blue	1 ml (0,2% stock)
DTT	1 mM
H2O	Fill up to 50 ml

4.2.10 Co-IP experiment

To show protein-protein interaction, co-IP experiments were performed. After transfection, cell lysates were collected. Afterwards, the lysate was subject to chromatin digestion by benzonase nuclease and centrifugation was applied before supernatant was collected. Meanwhile, dynabeads were washed and conjugated with corresponding IP antibodies. Once the conjugation is done, dynabeads were pipetted into cell lysate which was rotated at 4 °C overnight. Cell lysate then was discarded and dynabeads were then collected using a magnetic rack and washed using low salt and high slat buffer for 15 minutes. Finally, the beads were again collected and enriched using a magnetic rack. Beads were boiled using laemmili buffer at 95 °C for 5 minutes. Centrifugation was applied to detach denatured proteins from the beads. Supernatant was applied for later western blot analysis.

4.2.11 Inflammasome activation

BMDMs were cultured and differentiated according to protocols mentioned above. 10^6 BMDMs were seeded into one well in 6-well plates. Cells were primed with 300 ng/ml LPS (*Escherichia coli* O111:B4) for 3 hours and then replace with serum-free medium containing nigericin at the concentration of 5 mM for 45 minutes. Cell lysates and corresponding supernatant were harvested for later analysis.

4.2.12 Statistical analysis

Statistical analysis was performed with R studio and GraphPad Prism version 7 and 8. Data were represented as means ± standard deviation (SD). When comparing two groups, data was tested for normality and then analysed by unpaired Student's t-test or Mann-Whitney U as appropriate. When comparing three or more groups with only

one variant (i.e. genotype), one-way ANOVA was used for statistical analysis. When comparing three or more groups with two variants (i.e. genotype and different tissues or treatments), two-way ANOVA was used for statistical analysis. $P<0.05$ was considered statistically significant.

5. Results

5.1 *Apoe*$^{-/-}$ *Hdac9*$^{\Delta Cis-/-}$ male mice show exacerbation of atherogenesis compared with *Apoe*$^{-/-}$ littermates

In mice, *Hdac9* deficiency was shown to attenuate atherosclerotic plaque development in both *Apoe*$^{-/-}$ and *Ldlr*$^{-/-}$ models (Azghandi et al., 2015; Cao et al., 2014). However, the direct atherogenic impact of the risk SNP rs2107595 has not been addressed. This SNP is not conserved in mice, but the region encompassing rs2107595 is highly conserved across different species, with enrichment of active histone markers (e.g. H3K4me1 and H3K27ac), indicating the regulatory role of the CRE (Prestel et al., 2019). To explore the potential atherogenic function of the highly conserved CRE, we generated a mouse model, the *Hdac9*$^{\Delta Cis-/-}$ mouse that is devoid of this highly conserved non-coding region (in collaboration with Dr. Benedikt Wefers). To facilitate the development of atherosclerosis, *Hdac9*$^{\Delta Cis-/-}$ mice were crossbred into the atheroprone *Apoe*$^{-/-}$ strain and fed either with chow diet for 28 weeks or high fat diet (HFD) for 8 weeks.

First, I characterized the atherosclerotic phenotype in mice fed with chow diet for 28 weeks. To quantify the atherosclerotic plaque size in the aortic root, Oil red O staining was performed to stain the lipids accumulated inside plaques. Male *Apoe*$^{-/-}$ *Hdac9*$^{\Delta Cis-/-}$ mice developed significant larger atherosclerotic plaques in aortic root compared to their *Apoe*$^{-/-}$ littermates (Fig. 8 A and C). In contrast, female mice did not display significant differences in plaque size between the two genotypes (Fig. 8 B and D). The results indicated that deletion of the CRE showed an atherogenic effect specifically in male mice during an intermediate stage of atherogenesis. For the following *in vivo* experiments, only male littermates were used.

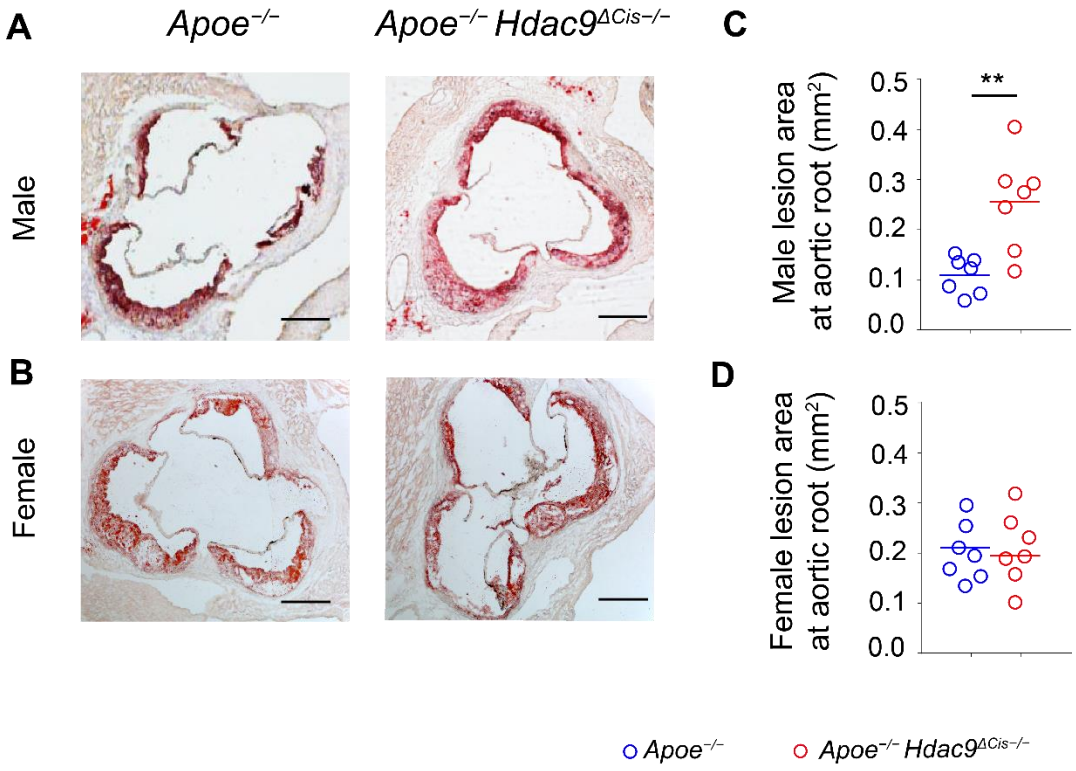

Figure 8. Male *Apoe*$^{-/-}$ *Hdac9*$^{\Delta Cis-/-}$ mice developed significant larger atherosclerotic plaques in aortic root compared to their *Apoe*$^{-/-}$ littermates.

(A and B) Shown are representative Oil red O stainings of atherosclerotic plaques in aortic root from male mice (A) and female mice (B). (C and D) Shown are corresponding atherosclerotic plaque quantifications for male mice (C) and female mice (D) in the aortic roots. Unpaired T-test was used for statistical analysis. **p ≤ 0.01; n=7 mice per cohort. Mice were fed with chow diet for 28 weeks. Scale bar, 200µm.

To further characterize the atherogenic effect of *Apoe*$^{-/-}$ *Hdac9*$^{\Delta Cis-/-}$ male mice, I quantified the plaque size across the aortic arch. Results revealed that *Apoe*$^{-/-}$ *Hdac9*$^{\Delta Cis-/-}$ male mice developed significantly larger plaque size in the aortic arch, especially at the sites of curvatures and arterial branches (Fig. 9 A and C). Furthermore, I analyzed the macrophage component inside the plaque in aortic roots, since macrophages are one of the most abundant cell types inside plaques. Immunostaining was performed using an anti-MAC2 antibody (Fig. 9 B). Quantification of MAC2^{+} plaques showed that *Apoe*$^{-/-}$ *Hdac9*$^{\Delta Cis-/-}$ exhibited a significant larger MAC2^{+} area

compared to *Apoe*$^{-/-}$ littermates (Fig. 9 D), indicating significantly more accumulation of macrophages inside atherosclerotic plaques after knocking out the CRE. This result indicated the importance of macrophages for the observed phenotype of the *Apoe*$^{-/-}$ *Hdac9*$^{\Delta Cis-/-}$ model. No difference was observed in terms of atherosclerotic plaque size in aortic arch or MAC2^{+} area inside the aortic root in female mice (data not shown).

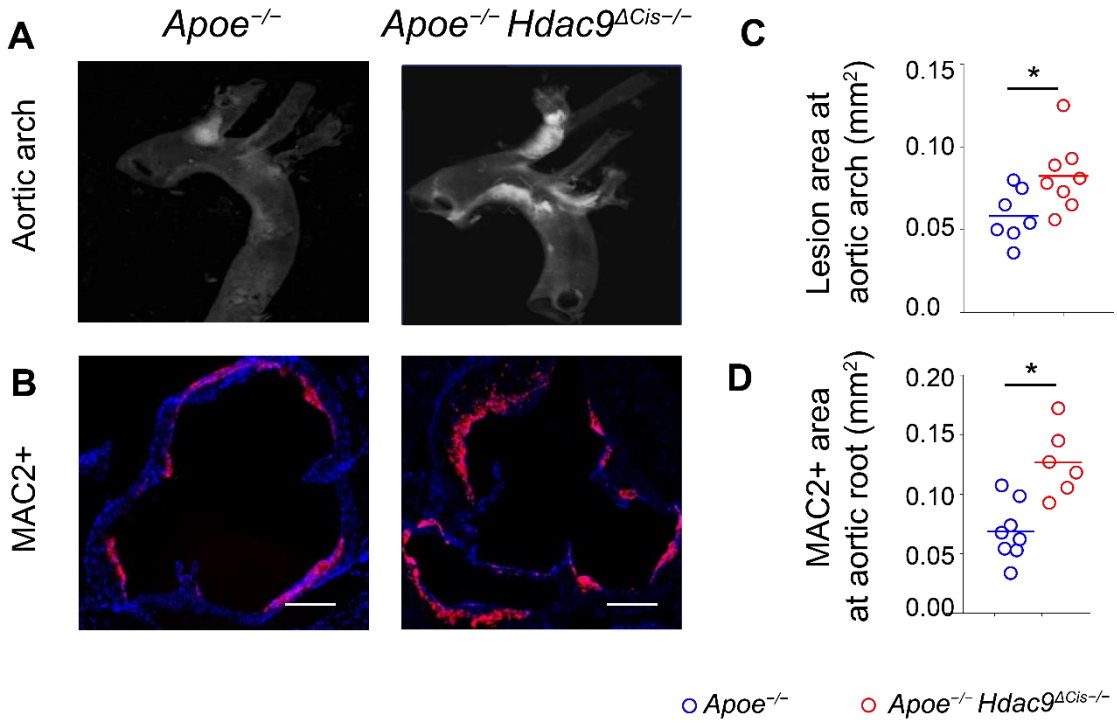

Figure 9. Male *Apoe*$^{-/-}$ *Hdac9*$^{\Delta Cis-/-}$ mice developed significantly larger atherosclerotic plaques at aortic arch and more accumulation of macrophages at aortic roots compared to their *Apoe*$^{-/-}$ littermates.

(A) Shown are representative atherosclerotic plaques at the aortic arch from male mice. (B) Shown are representative immunohistochemistry stainings of MAC2 at the aortic root from male mice. MAC2 is shown in red whereas DAPI in blue. (C, D) Shown are corresponding quantifications of (A) and (B), respectively. Unpaired T-test was used for statistical analysis. *p ≤ 0.05. N=6-8 mice per cohort. Mice were fed with chow diet for 28 weeks. Scale bar, 200µm.

5.2 *Apoe*$^{-/-}$ *Hdac9*$^{\Delta Cis-/-}$ male mice show no difference in total cholesterol levels compared to *Apoe*$^{-/-}$ littermates

Atherosclerosis is a lipid-driven chronic inflammation disorder. One study showed that HDAC9 regulated cholesterol homeostasis in *Ldlr*$^{-/-}$ mouse model (Cao et al., 2014). Knocking out HDAC9 downregulated total cholesterol level in *Ldlr*$^{-/-}$ mice. Therefore, to answer whether the exacerbation of atherosclerosis in male mice (Fig. 8 and 9) was due to the changes of cholesterol levels, total cholesterol levels from plasma were measured. However, results revealed that no significant difference of total cholesterol levels was observed in plasma between *Apoe*$^{-/-}$ *Hdac9*$^{\Delta Cis-/-}$ and *Apoe*$^{-/-}$ littermates (Fig 10).

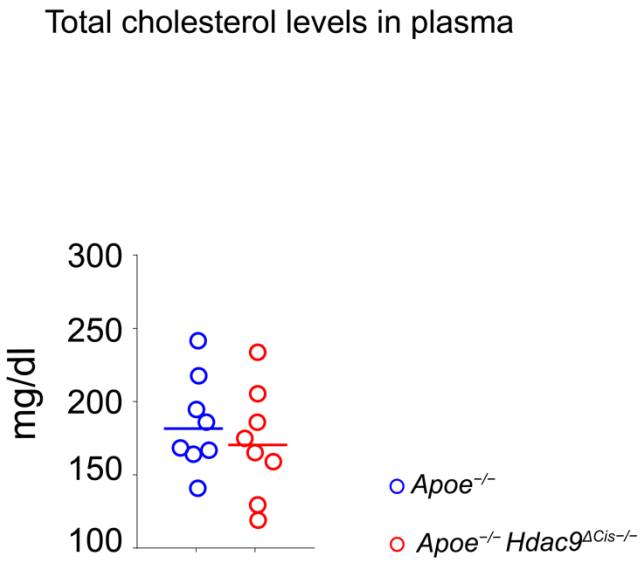

Figure 10. Male *Apoe*$^{-/-}$ *Hdac9*$^{\Delta Cis-/-}$ mice showed no difference in total cholesterol levels in plasma compared to their *Apoe*$^{-/-}$ littermates.

Shown is the quantification of total cholesterol levels in mouse plasma. Red circles represent *Apoe*$^{-/-}$ *Hdac9*$^{\Delta Cis-/-}$ mice, whereas blue circles *Apoe*$^{-/-}$. Unpaired T-test was used for statistical analysis. N=8 mice per cohort. Mice were fed with chow diet for 28 weeks.

5.3 *Apoe*$^{-/-}$ *Hdac9*$^{\Delta Cis-/-}$ male mice display a pro-inflammatory milieu with marked elevation of IL-1β, IL-6 and IL-18 in plasma compared to *Apoe*$^{-/-}$ littermates

Previous studies showed that HDAC9 and rs2107595 promoted inflammation (Cao et al., 2014; Prestel et al., 2019; Shroff et al., 2019). Therefore, I analyzed the pro-inflammatory cytokine and chemokine profile in plasma. Results showed that *Apoe*$^{-/-}$ *Hdac9*$^{\Delta Cis-/-}$ developed a more pro-inflammatory milieu with IL-1β, IL-6 and IL-18 being significantly upregulated when compared to their *Apoe*$^{-/-}$ littermates (Fig 11). Since IL-1β and IL-18 are downstream targets of the inflammasome, this result indicated that *Apoe*$^{-/-}$ *Hdac9*$^{\Delta Cis-/-}$ may have an enhanced inflammasome priming and/or activation.

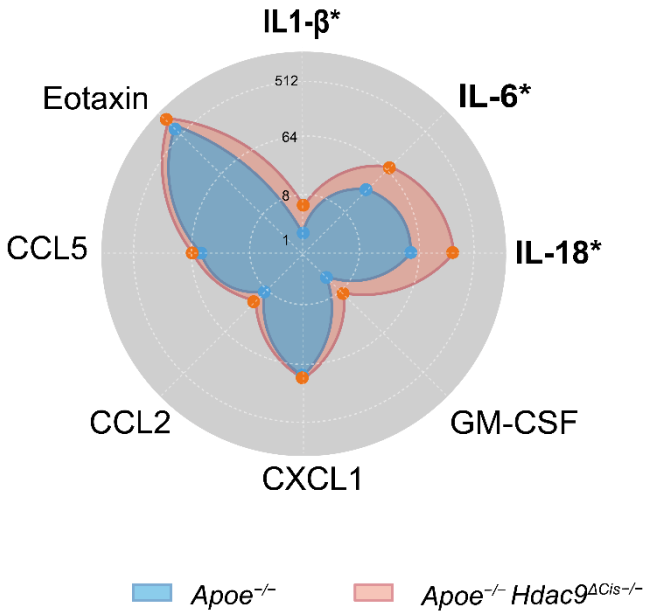

Figure 11. Male *Apoe*$^{-/-}$ *Hdac9*$^{\Delta Cis-/-}$ mice displayed marked elevation of IL-1β, IL-6 and IL-18 in plasma compared to their *Apoe*$^{-/-}$ littermates.

Shown is the chemokine and cytokine profile from mouse plasma in a spider plot. Each dot represents a data point, and each axis represents a chemokine or cytokine. Low expression value lies closer to the plot center whereas high expression further away from the center. The scale of this spider plot is log2. Two-way ANOVA was used for statistical analysis. *p ≤ 0.05. N=8 mice per cohort. Mice were fed with chow diet for 28 weeks.

5.4 *Apoe*$^{-/-}$*Hdac9*$^{\Delta Cis-/-}$ male mice contain significantly more pro-inflammatory myeloid cells in the spleen compared to *Apoe*$^{-/-}$ littermates

To further confirm the pro-inflammatory milieu in the *Apoe*$^{-/-}$ *Hdac9*$^{\Delta Cis-/}$ genotype, immune homeostasis of splenocytes was analyzed with flow cytometry (Fig. 12 A). Quantification showed that *Apoe*$^{-/-}$ *Hdac9*$^{\Delta Cis-/-}$ mice developed significantly higher percentage of pro-inflammatory Ly6G^{+} neutrophils and classical pro-inflammatory Ly6C^{hi} monocytes (Fig. 12 B), whereas the percentage of non-classical anti-inflammatory ly6C^{low} monocytes was not changed (Fig. 12 B). This result was in accord with previous chemokine and cytokine profile data (Fig. 11), confirming the pro-inflammatory milieu of *Apoe*$^{-/-}$ *Hdac9*$^{\Delta Cis-/-}$. Moreover, since Ly6G^{+} neutrophils and classical Ly6C^{hi} monocytes are originated from myeloid cells, the enrichment of those cell types indicated a myeloid-cell-specific role from *Apoe*$^{-/-}$ *Hdac9*$^{\Delta Cis-/-}$ system.

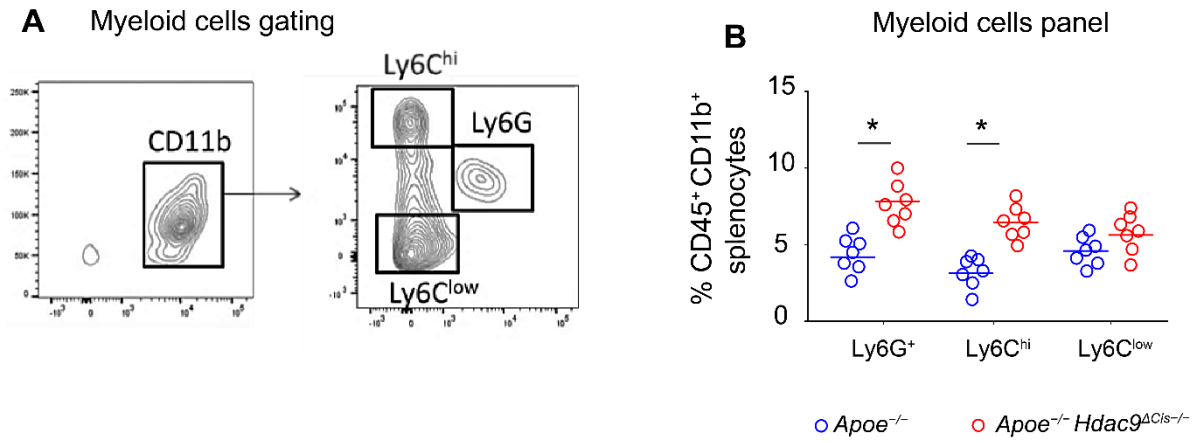

Figure 12. Male *Apoe*$^{-/-}$ *Hdac9*$^{\Delta Cis-/-}$ mice developed significantly more pro-inflammatory Ly6G^{+} neutrophils and classical pro-inflammatory Ly6C^{hi} monocytes in the spleen, whereas no differences were observed in ly6C^{low} monocytes compared to their *Apoe*$^{-/-}$ littermates.

(A) Shown is the flow cytometric gating strategy for myeloid cells panel. (B) Shown are the flow cytometric quantifications of myeloid cell subsets. Unpaired T-test was used for statistical analysis. *p ≤ 0.05. N=7 mice per cohort. Mice were fed with chow diet for 28 weeks.

5.5 *Apoe*$^{-/-}$*Hdac9*$^{\Delta Cis-/-}$ male mice show no difference in T cell numbers in the spleen compared to *Apoe*$^{-/-}$ littermates

Previous studies have delineated the role of HDAC9 in different T cell sub-types (De Zoeten et al., 2010; Tao et al., 2007; Yan et al., 2011). Therefore, I also analyzed the different T cell populations in the spleen via flow cytometry. Results revealed that the deletion of the CRE showed no effect neither for total T cells, helper T cells ($CD3^+$ $CD4^+$) nor cytotoxic T cells ($CD3^+$ $CD8^+$) in the spleen (Fig. 13), further confirming the myeloid-cell-specific role of *Apoe*$^{-/-}$ *Hdac9*$^{\Delta Cis-/-}$ model.

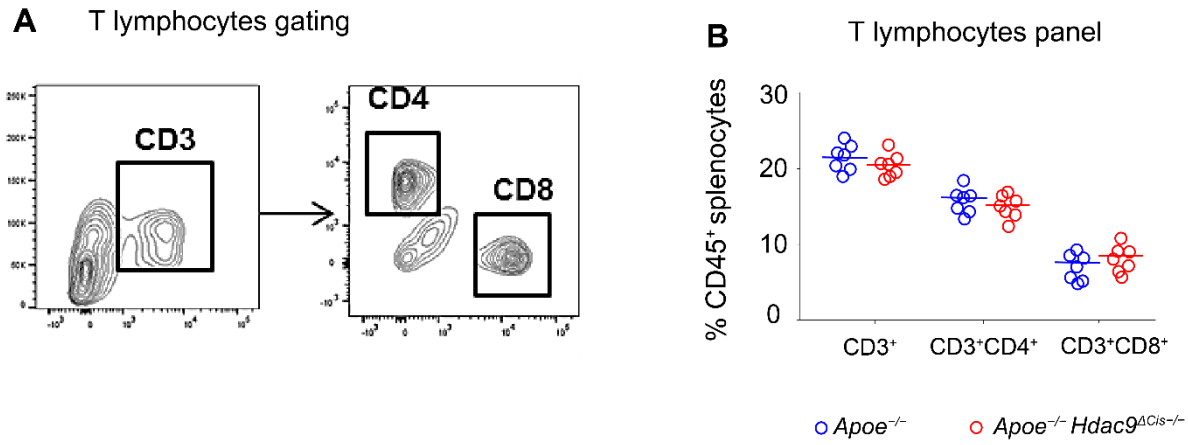

Figure 13. Male *Apoe*$^{-/-}$ *Hdac9*$^{\Delta Cis-/-}$ mice displayed no differences in T lymphocytes numbers in the spleen compared to their *Apoe*$^{-/-}$ littermate controls.

(A) Shown is the flow cytometric gating strategy for T lymphocytes panel. (B) Shown are the flow cytometric quantifications of T lymphocyte subsets. Unpaired T-test was used for statistical analysis. N=7 mice per cohort. Mice were fed with chow diet for 28 weeks.

5.6 *Apoe*$^{-/-}$ *Hdac9*$^{\Delta Cis-/-}$ male mice on HFD show mild exacerbation of atherosclerosis compared to *Apoe*$^{-/-}$ littermates

Besides analyzing mice kept on chow diet, I also characterized the atherosclerotic plaques from male mice challenged with HFD for 8 weeks starting from 8 week after birth. In line with previous findings (Fig. 8), *Apoe*$^{-/-}$ *Hdac9*$^{\Delta Cis-/-}$ male mice also developed significantly larger atherosclerotic plaques and significantly more accumulation of MAC2^{+} macrophages inside the plaque in aortic root (Fig. 14). However, the phenotype difference seemed to be milder compared to that in chow diet cohort.

Taken together, *Apoe*$^{-/-}$ *Hdac9*$^{\Delta Cis-/-}$ male mice developed exacerbated atherosclerosis both under chow diet and HFD compared to their *Apoe*$^{-/-}$ littermates. Total cholesterol levels in plasma were not changed between these two genotypes. Moreover, chemokine and cytokine profile revealed that *Apoe*$^{-/-}$ *HDAC9*$^{\Delta Cis-/-}$ developed upregulated levels of IL-1β, IL-6 and IL-18 in plasma (Fig. 11), indicating a more pro-inflammatory milieu. In support of this result, flow cytometric analysis revealed a higher percentage of pro-inflammatory Ly6G^{+} neutrophils and Ly6C^{hi} monocytes in splenocytes (Fig. 12), further confirming a pro-inflammatory phenotype when the CRE is deleted.

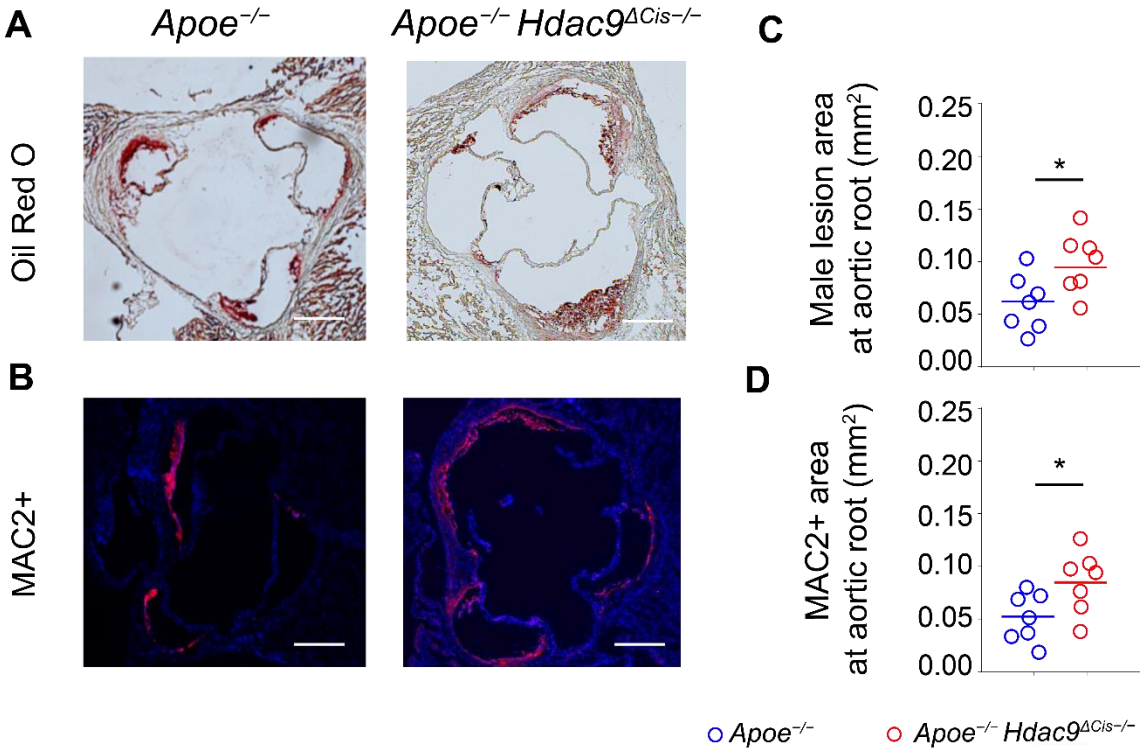

Figure 14. Male *Apoe*$^{-/-}$ *Hdac9*$^{\Delta Cis-/-}$ mice developed significantly larger atherosclerotic plaque and more accumulation of macrophages in aortic root compared to their *Apoe*$^{-/-}$ littermates when challenged with HFD.

(A) Shown are representative Oil red O staining pictures of atherosclerotic plaques at aortic root from male mice. (B) Shown are representative immunohistochemistry staining of MAC2 at aortic root from male mice. MAC2 is shown in red whereas DAPI in blue. (C, D) Shown are corresponding quantifications of (A) and (B), respectively. Unpaired T-test was used for statistical analysis. *p $\leqslant$ 0.05. N=7 mice per cohort. Mice were fed with western diet for 8 weeks from 8 weeks after birth. Scale bar, 200μm.

5.7 *Apoe*$^{-/-}$ *Hdac9*$^{\Delta Cis-/-}$ upregulate *Hdac9* in aorta compared to *Apoe*$^{-/-}$ littermate controls

Next, I tried to explore the underlying contributors to the exacerbation of the atherosclerotic development in *Apoe*$^{-/-}$ *Hdac9*$^{\Delta Cis-/-}$ mouse model (Fig. 8-15). Since the deleted region is a CRE which regulates gene expression, I speculated that the observed phenotypic difference is attributed to certain gene expression changes. Previous work from us demonstrated the regulatory function of rs2107595 in *HDAC9* expression (Azghandi et al., 2015; Prestel et al., 2019), therefore *Hdac9* gene expression might be altered after deleting the CRE encompassing the rs2107585. This leads to the first hypothesis: is the exacerbation of the atherosclerotic development due to alteration of *Hdac9* gene expression? Since CREs regulate gene expression in a cell-type-specific manner, the *Hdac9*$^{\Delta Cis-/-}$ CRE deletion model may guide us to the cell type(s) that drive the exacerbation of atherosclerosis in a HDAC9-dependent manner. Thus, I proposed following hypothesis: *Apoe*$^{-/-}$ *Hdac9*$^{\Delta Cis-/-}$ regulates *Hdac9* gene expression in candidate cell types/tissues but exerts minimal impact on *Hdac9* gene expression in other cell types/tissues. Since the deletion is located between *Hdac9* and *Twist1*, the expression of *Twist1* was also analyzed.

To test above hypothesis, first, the mRNA level of *Hdac9* and *Twist1* in different organs was analyzed from both *Apoe*$^{-/-}$ *Hdac9*$^{\Delta Cis-/-}$ and *Apoe*$^{-/-}$ via qPCR. Eight organs were dissected at the age of 14 weeks, namely: heart, aorta, skeleton muscle (next to femur), kidney, brain, thymus, spleen. Results revealed that *Hdac9* was significantly upregulated only in the aorta, whereas no significant changes were observed in other tissues (Fig. 15 A). In terms of *Hdac9* mRNA detection, two Taqman probes were purchased for detecting its two major isoforms: *Hdac9* and *Mitr*. The regulatory function of the CRE of both isoforms is approximately the same, therefore only *Hdac9*

quantification was shown in the results (data from *Mitr* expression not shown). Moreover, the deletion had minimal impact on *Twist1* expression (Fig. 15 B), indicating that the CRE specifically regulated *Hdac9* expression during the development of atherosclerosis.

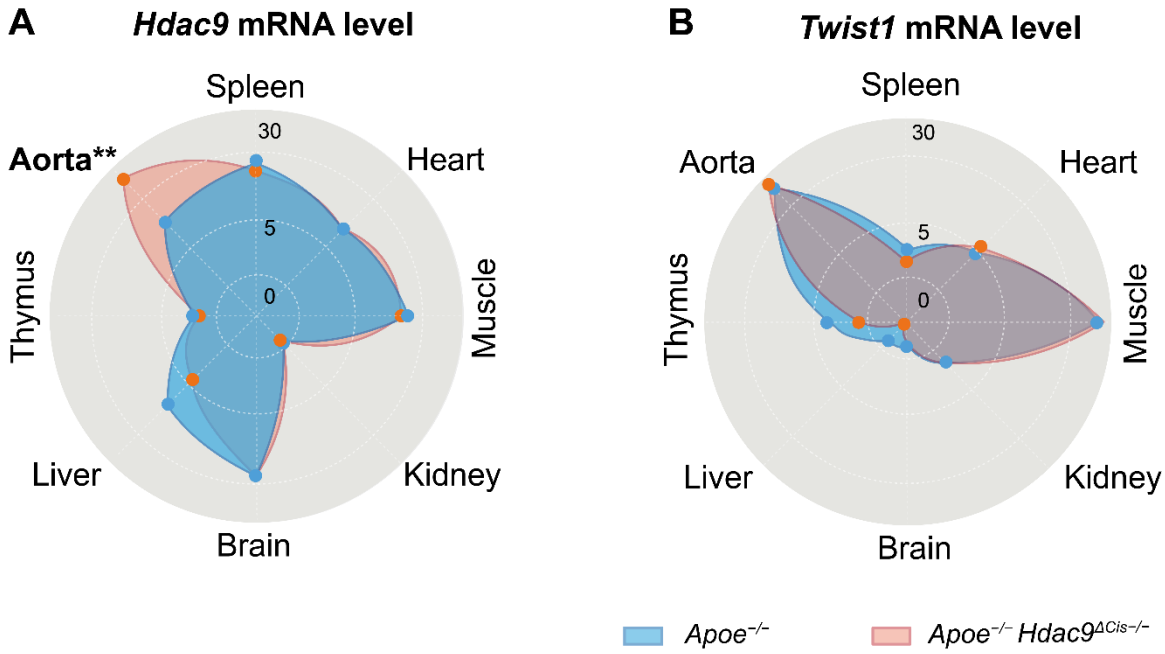

Figure 15. *Apoe*$^{-/-}$ *Hdac9*$^{\Delta Cis-/-}$ upregulates *Hdac9* in aorta but not in other tissues compared to *Apoe*$^{-/-}$ littermate controls.

(A) Shown are relative expression levels of *Hdac9* from different tissues normalized to *Hprt*. (B) Shown are relative expression levels of *Twist1* from different tissues normalized to *Hprt*. The scale of the spider plots is $\log_2$. Two-way ANOVA was used for statistical analysis. **p ≤ 0.01. N=6-10 per genotype. Mice were fed with chow diet for 14 weeks.

5.8 *Apoe*$^{-/-}$ *Hdac9*$^{\Delta Cis-/-}$ aorta displays a pro-inflammatory milieu compared with *Apoe*$^{-/-}$ littermate controls

To answer whether the CRE deletion conferred a more pro-inflammatory milieu to the aorta, the total RNA from the aorta was isolated. Gene expression of different cytokines and chemokines was analyzed via qPCR. Results showed that *Apoe*$^{-/-}$ *Hdac9*$^{\Delta Cis-/-}$ aorta entailed a more pro-inflammatory milieu with significantly higher expression of *Il1-β*, *Tnf-α*, *Ccl2*, *Il-6* and *Il-18*, but other genes such as *Icam1*, *Abcg1* and *Abca1* were not changed (Fig. 16). This result confirmed the pro-inflammatory milieu in aorta from *Apoe*$^{-/-}$ *Hdac9*$^{\Delta Cis-/-}$ mice, which was probably mediated via the upregulation of *Hdac9*.

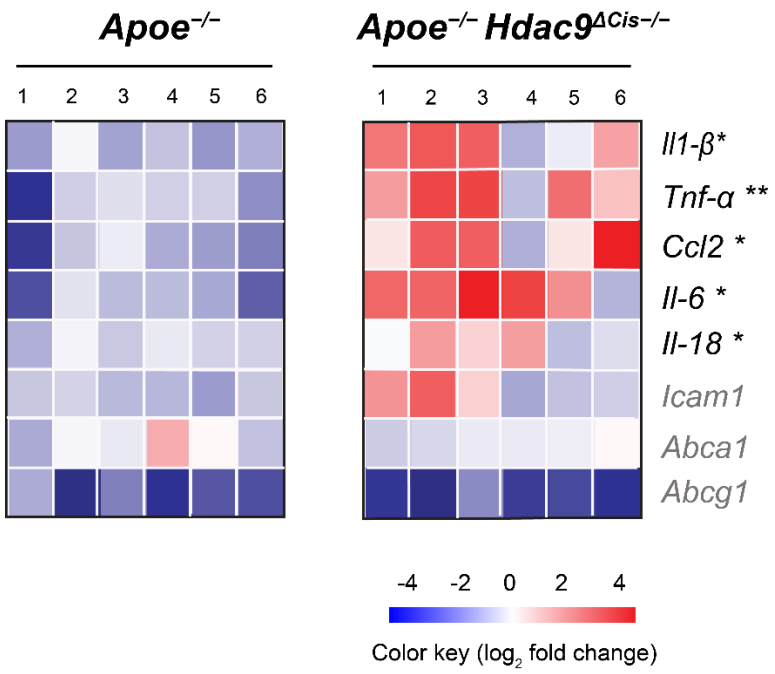

Figure 16. *Apoe*$^{-/-}$ *Hdac9*$^{\Delta Cis-/-}$ promotes a pro-inflammatory milieu in aorta compared to *Apoe*$^{-/-}$ littermate controls.

Shown is a heatmap with red representing high expression and blue low expression of different genes analyzed via qPCR. Log_2 scale was used for generating the heatmap. Unpaired T-test was used for statistical analysis. *p ≤ 0.05, **p ≤ 0.01. N=6 for each genotype.

5.9 Deletion of the CRE upregulates *Hdac9* in CD11b+ myeloid cells and inflammatory macrophages

Aorta is comprised of different cell types, especially smooth muscle cells and immune cells such as foam cells and T cells. In order to pinpoint specific cell type(s) that contribute to the drastic upregulation of *Hdac9* and pro-inflammatory milieu in the aorta, specific immune cells types especially $CD11b^+$ myeloid cell (origin of foam cells) and T cells were sorted from splenocytes for qPCR analysis. Results showed that *Apoe*$^{-/-}$ *Hdac9*$^{\Delta Cis-/-}$ in $CD11b^+$ myeloid cells (Fig. 17 A) had drastically upregulated *Hdac9* expression whereas no effect was observed in T cells (Fig. 17 B) or SMCs (primary culture from aorta) (Fig. 17 C). This result partially explained the upregulation of *Hdac9* in the whole aorta, since $CD11b^+$ myeloid cells are one of the major components in early-stage atherosclerotic plaque, but I am not excluding other cell types (e.g. endothelial cells). However, $CD11b^+$ myeloid cells are heterogeneous cell populations, including monocytes/macrophages, neutrophils and natural killer cells. Given the observation that *Apoe*$^{-/-}$ *Hdac9*$^{\Delta Cis-/-}$ plaques contain significantly more $MAC2^+$ macrophages (Fig. 9 B and D), we decided to investigate *Hdac9* transcriptional level in bone marrow derived macrophages (BMDMs) *in vitro*. Results revealed that *Hdac9* was upregulated in *Apoe*$^{-/-}$ *Hdac9*$^{\Delta Cis-/-}$ BMDMs compared to *Apoe*$^{-/-}$ without any stimuli (Fig. 17 D). Taken together, *Apoe*$^{-/-}$ *Hdac9*$^{\Delta Cis-/-}$ significantly upregulated *Hdac9* mRNA in $CD11b^+$ myeloid cells especially macrophages, but not in T cells or smooth muscle cells. Furthermore, deletion of the CRE also conferred a more pro-inflammatory milieu in the aorta.

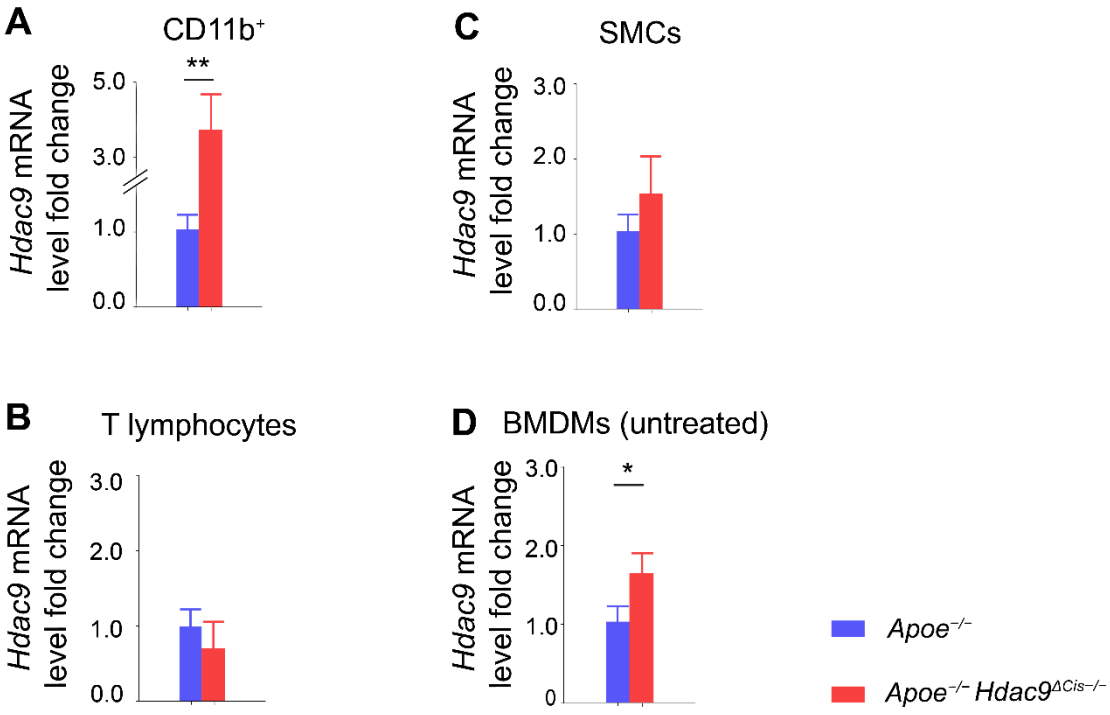

Figure 17. Deletion of the CRE upregulates *Hdac9* in CD11b+ myeloid cells and BMDMs in an atheroprone background.

(A-D) Shown are the relative *Hdac9* transcriptional levels in CD11b^{+} myeloid cells (A), T lymphocytes (B), SMCs (C) and untreated BMDMs (D). *Hprt* was used as a normalizer. Unpaired T-test was used for statistical analysis. *p ≤ 0.05, **p ≤ 0.01.

Above gene expression analysis in BMDMs was conducted in the atheroprone *Apoe*$^{-/-}$ mice. Next, I asked whether *Hdac9*$^{\Delta Cis-/-}$ in the wild-type background with normal lipid level harbors the same regulatory function on *Hdac9* gene expression in myeloid cells. To this end, different immune cell types were sorted for subsequent qPCR analysis. Results revealed that *Hdac9* was upregulated in CD11b^{+} myeloid cells after knocking out the CRE (Fig. 18 A), which was in accord with previous observation in *Apoe*$^{-/-}$ background. Moreover, no differences were observed in T cells (Fig.18 B) or smooth muscle cells (Fig. 18 C).

Previous work from us showed that the regulatory function of rs2107595 was inflammatory-specific in human macrophages (Prestel et al., 2019). To investigate whether the regulatory function of the CRE also requires a pro-inflammatory niche,

Results

BMDMs were polarized via LPS and IL4 treatment, respectively. Interestingly, *Hdac9*$^{\Delta Cis-/-}$ only displayed upregulated *Hdac9* in pro-inflammatory BMDMs but not in untreated or cells in IL4-mediated anti-inflammatory phenotype (Fig. 19).

Next, inspired by previous results (Fig. 16), the pro-inflammatory phenotype of *Hdac9*$^{\Delta Cis-/-}$ BMDMs were characterized for the expression of cytokines and chemokines. Results showed that *Hdac9*$^{\Delta Cis-/-}$ BMDMs had significantly higher upregulation of *Il1-β*, *iNos*, *Ccl2* and *Tnf-α*, suggesting a more pro-inflammatory phenotype of *Hdac9*$^{\Delta Cis-/-}$ BMDMs (Fig. 20).

Taken together, knocking out the highly conserved CRE significantly upregulated the *Hdac9* transcription level in myeloid cells, especially in macrophages (in a pro-inflammatory milieu), strongly indicating the regulatory role of the CRE in myeloid cells. Furthermore, knocking out the CRE promoted a more pro-inflammatory milieu in the aorta and BMDMs.

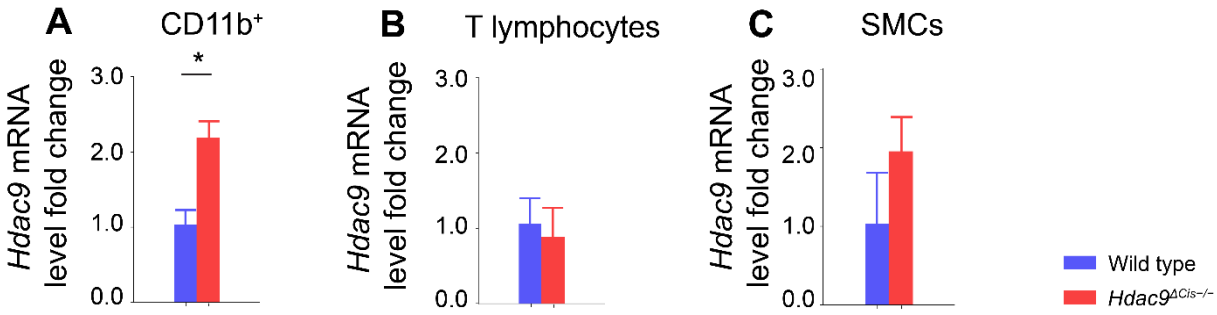

Figure 18. *Hdac9*$^{\Delta Cis-/-}$ upregulated *Hdac9* in CD11b+ myeloid cells compared to wild-type controls.

(A-C) Shown are the relative *Hdac9* transcriptional levels in CD11b^{+} myeloid cells (A), T lymphocytes (B) and SMCs (C). Unpaired T-test was used for statistical analysis. *p ≤ 0.05. N=5-7 for each genotype.

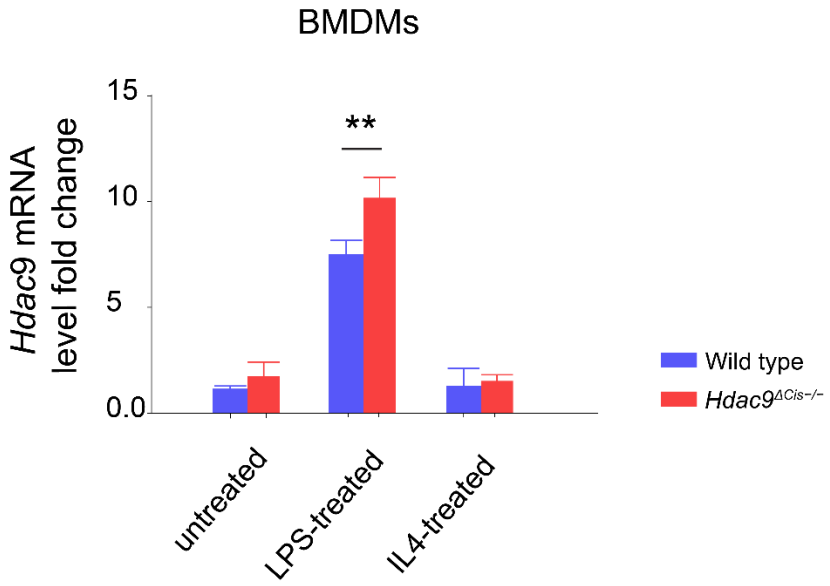

Figure 19. *Hdac9*$^{\Delta Cis-/-}$ upregulates *Hdac9* only in pro-inflammatory BMDMs.

Shown are the relative *Hdac9* transcriptional levels in differentially polarized BMDMs. Shown are the expression of different genes in LPS-treated BMDMs from the two genotypes. *Hprt* was used as a normalizer. Two-way ANOVA was used for statistical analysis. *p ≤ 0.05, **p ≤ 0.01. N=6-9 per genotype.

Figure 20. *Hdac9*$^{\Delta Cis-/-}$ displays a more pro-inflammatory phenotype in LPS-treated BMDMs with upregulation of *iNos, Ccl2, Tnf-α, Mif* and *Il1-β.*

Shown are the expression of different genes in LPS-treated BMDMs from the two genotypes. Log_2 fold changes were used for generating the heatmap with red color representing high expression and blue low expression. *Hprt* was used as a normalizer. Unpaired T-test was used for statistical analysis. *p ≤ 0.05, **p ≤ 0.01.

5.10 Bone marrow transplantation reveals the atherogenic role of *Apoe*$^{-/-}$ *Hdac9*$^{\Delta Cis-/-}$ in bone marrow cells

Previous results showed a myeloid-cell-specificity of the *Hdac9*$^{\Delta Cis-/-}$ model, therefore I was prompted to ask whether *Apoe*$^{-/-}$ *Hdac9*$^{\Delta Cis-/-}$ myeloid cells alone would be sufficient to exacerbate atherosclerosis. Since myeloid cells originate from bone marrows, therefore bone marrow transplantations (BMT) were performed in collaboration with Dr. Emiel Van der Vorst from Institute for Cardiovascular Prevention (IPEK). First, *Apoe*$^{-/-}$ recipient mice were subjected to radiation to deplete their endogenous bone marrow cells. *Apoe*$^{-/-}$ *Hdac9*$^{\Delta Cis-/-}$ and *Apoe*$^{-/-}$ littermates were used as donor mice. Their bone marrow were injected into recipient mice. After surgery, recipient mice were treated with antibiotics and then fed with HFD for 3 months before atherosclerotic phenotype was analyzed.

Results revealed that mice reconstituted with *Apoe*$^{-/-}$ *Hdac9*$^{\Delta Cis-/-}$ bone marrow developed significantly larger plaques (Fig. 21 A and C) and more accumulation of lesional MAC2^{+} macrophages (Fig. 21 B and D). This result proved the atherogenic effect of *Apoe*$^{-/-}$ *Hdac9*$^{\Delta Cis-/-}$ bone marrow cells, which is in accord with the previous phenotype difference from global knockout of CRE (Fig. 8 and 14). Notwithstanding, a potential atherogenic effect from other cell types, such as certain T-lymphocyte or B-cell sub-types, cannot be excluded, since they are also differentiated from hematopoietic cells in the bone marrow.

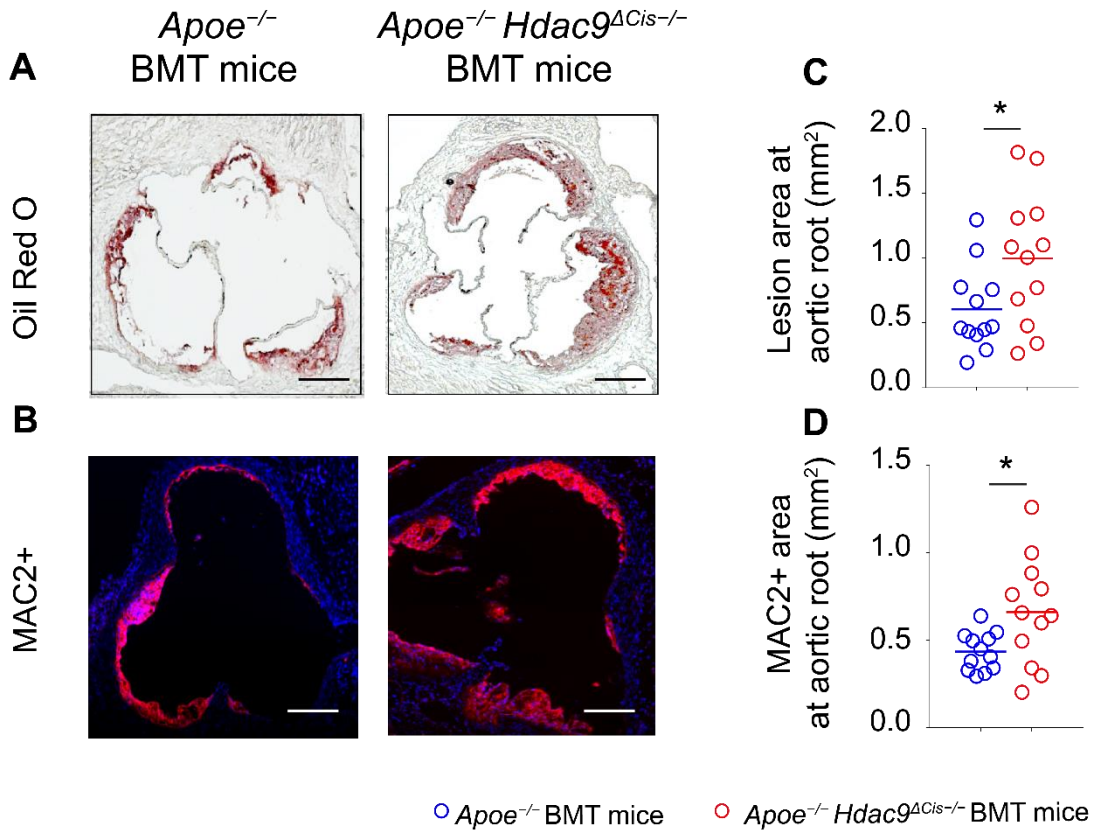

Figure 21. Male *Apoe*$^{-/-}$ *Hdac9*$^{\Delta Cis-/-}$ BMT mice develop significantly larger atherosclerotic plaque and more accumulation of macrophages at aortic root compared to their *Apoe*$^{-/-}$ BMT littermates.

(A) Shown are representative pictures of Oil Red O stained atherosclerotic plaques at the aortic root from male BMT mice. (B) Shown are representative immunohistochemistry stainings of MAC2 at the aortic root from male mice. MAC2 is shown in red whereas DAPI in blue. (C, D) Shown are corresponding quantifications of (A) and (B), respectively. *p $\leqslant$ 0.05. N=12 per group. Unpaired T-test was used for statistical analysis. Scale bar, 200μm.

5.11 *Apoe*$^{-/-}$*Hdac9*$^{\Delta Cis-/-}$ bone marrow cells do not alter total cholesterol levels in recipient mice

Furthermore, total cholesterol level of the plasma showed no difference between *Apoe*$^{-/-}$ *Hdac9*$^{\Delta Cis-/-}$ and *Apoe*$^{-/-}$ BMT mice (Fig. 22 A), and also no changes in the expression of the scavenger receptor *CD36* and cholesterol efflux transporter *Abca1* and *Abcg1* were observed in BMDMs (Fig. 22 B-D). Results indicate that *Apoe*$^{-/-}$ *Hdac9*$^{\Delta Cis-/-}$ bone marrow cells did not exacerbate atherogenesis via engulfing more lipids.

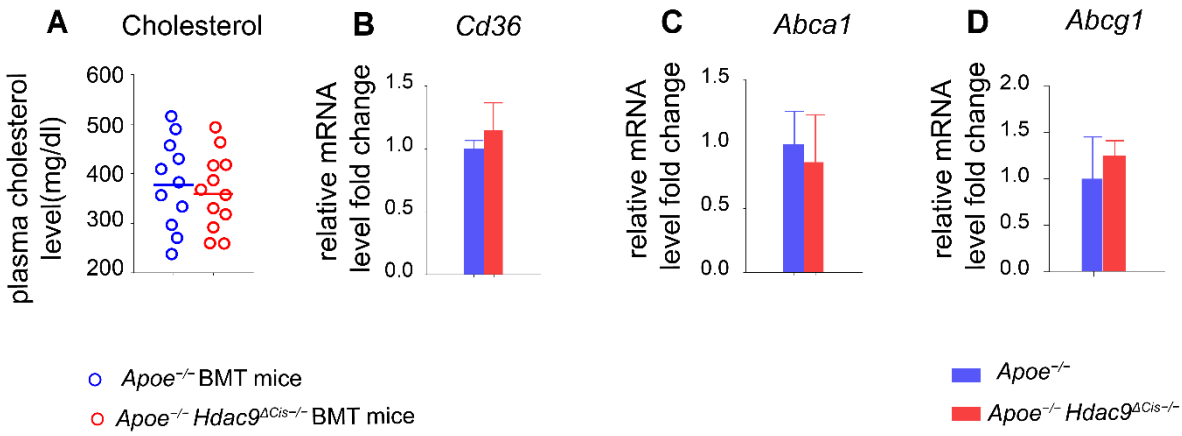

Figure 22. No difference of total cholesterol levels or the expression of *Cd36*, *Abca1* and *Abcg1* is observed between *Apoe*$^{-/-}$ *Hdac9*$^{\Delta Cis-/-}$ BMT mice and *Apoe*$^{-/-}$ BMT mice.
(A) Shown are the plasma total cholesterol level from BMT mice. (B-D) Shown are the relative expression levels of *Cd36* (B), *Abca1* (C) and *Abcg1* (D) in BMDMs normalized to *Hprt*. N=11-12 per genotype. Unpaired T-test was used for statistical analysis.

5.12 *Apoe*$^{-/-}$ *Hdac9*$^{\Delta Cis-/-}$ bone marrow cells promote more vulnerable atherosclerotic plaques in recipient mice

Since myeloid cells, and especially macrophages, are thought to secrete MMPs which digest collagen, we also analyzed the collagen percentage in BMT atherosclerotic plaques via trichrome staining. Results showed that *Apoe*$^{-/-}$ *Hdac9*$^{\Delta Cis-/-}$ BMT mice contained significantly less proportion of collagen inside plaques compared to the *Apoe*$^{-/-}$ BMT mice (Fig.23 A and B). Collagen was known to stabilize the atherosclerotic plaques, therefore more collagen content was indicative of stable plaques. However, the necrotic cores quantification showed no difference between the two groups (Fig. 23 C).

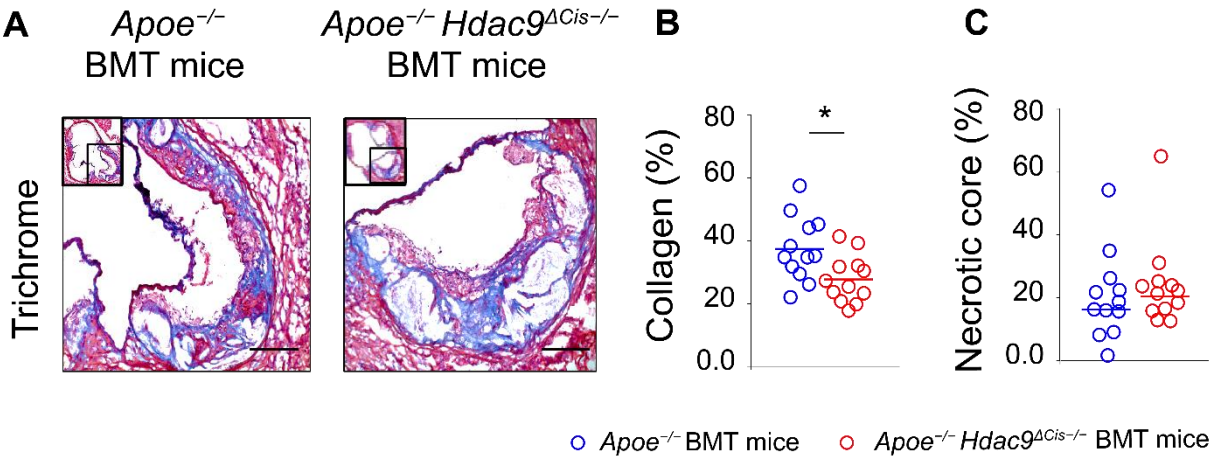

Figure 23. *Apoe*$^{-/-}$ *Hdac9*$^{\Delta Cis-/-}$ BMT mice exhibit decreased plaque collagen compared to *Apoe*$^{-/-}$ BMT controls.

(A) Shown are representative pictures of trichrome staining at aortic root. Blue represents collagen, red represents cytoplasm, black represents nuclei. (B) Shown is the quantification of collagen content (blue area) normalized to the plaque size. (C) Shown is the quantification of necrotic cores normalized to the plaque size. *p ≤ 0.05. N=12 per genotype. Unpaired T-test was used for statistical analysis. Scale bar, 100μm.

Results

Taken together, mice that feature a myeloid *Apoe*$^{-/-}$ *Hdac9*$^{\Delta Cis-/-}$ deficiency in a BMT model developed larger but more vulnerable atherosclerotic plaques compared to *Apoe*$^{-/-}$ BMT controls. This result confirmed the atherogenic role of *Apoe*$^{-/-}$ *Hdac9*$^{\Delta Cis-/-}$ myeloid cells or bone marrow cells in general.

5.13 *Apoe*$^{-/-}$ *Hdac9*$^{\Delta Cis-/-}$ mice show more cleavage of pro-caspase-1 in BMDMs

The chemokine and cytokine profiles revealed that *Apoe*$^{-/-}$ *Hdac9*$^{\Delta Cis-/-}$ mice showed significantly higher levels of IL-1β, IL-6 and IL-18 in plasma (Fig. 11). Since IL-1β and IL-18 are reported to be typical downstream effectors of the NLRP3 inflammasome (Tschopp and Schroder, 2010), I was prompted to detect inflammasome activation via quantifying pro-caspase-1 cleavage. To this end, BMDMs were primed with LPS and then activated with nigericin. Both cell lysates and supernatants were harvested for western blot analysis. Results revealed that *Apoe*$^{-/-}$ *Hdac9*$^{\Delta Cis-/-}$ BMDMs showed more cleavage of pro-caspase-1 in the supernatant compared to *Apoe*$^{-/-}$ BMDMs (Fig. 24), further confirming the inflammasome activation after deleting the CRE.

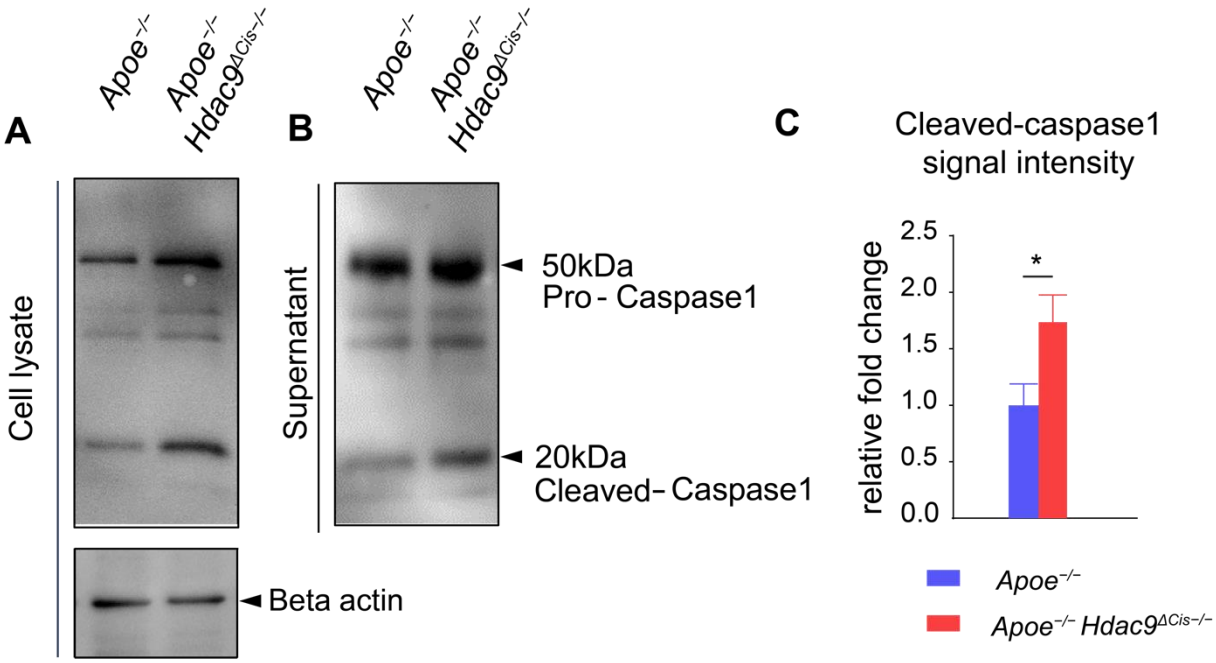

Figure 24. *Apoe*$^{-/-}$ *Hdac9*$^{\Delta Cis-/-}$ BMDMs showed more cleavage of pro-caspase-1 in the supernatant compared to *Apoe*$^{-/-}$ BMDMs.

(A, B) Shown is the western blot analysis from cell lysate (A) and supernatant (B). Membranes were probed with caspase-1 antibody which detects both pro-caspase-1 and cleaved-caspase-1. Beta Actin (ACTB) was used as a normalizer. (C) Shown is the corresponding quantification

of cleaved-caspase-1. *p ⩽ 0.05. N=7 for each genotype. Unpaired T-test was used for statistical analysis.

5.14 HDAC9 knockdown displayed less cleavage of pro-caspase-1

Since CREs were reported to regulate distal genes, we confirmed the role of HADC9 in inflammasome activation by gain-and-loss of function experiments performed in BMDMs. *Hdac9* knockdown was achieved by transfecting BMDMs with *Hdac9* specific siRNA, whereby qPCR analysis revealed a 65% depletion of *Hdac9* mRNA levels compared to BMDMs transfected with scrambled RNA (Fig. 25 A). Upon knockdown, BMDMs were treated with LPS and nigericin for inflammasome activation. Western blot analysis revealed that knockdown of *HDAC9* led to significantly less cleaved-caspase-1 compared to the scrambled RNA control (Fig. 25 B and C). This result directly showed the role of HDAC9 in inflammasome activation.

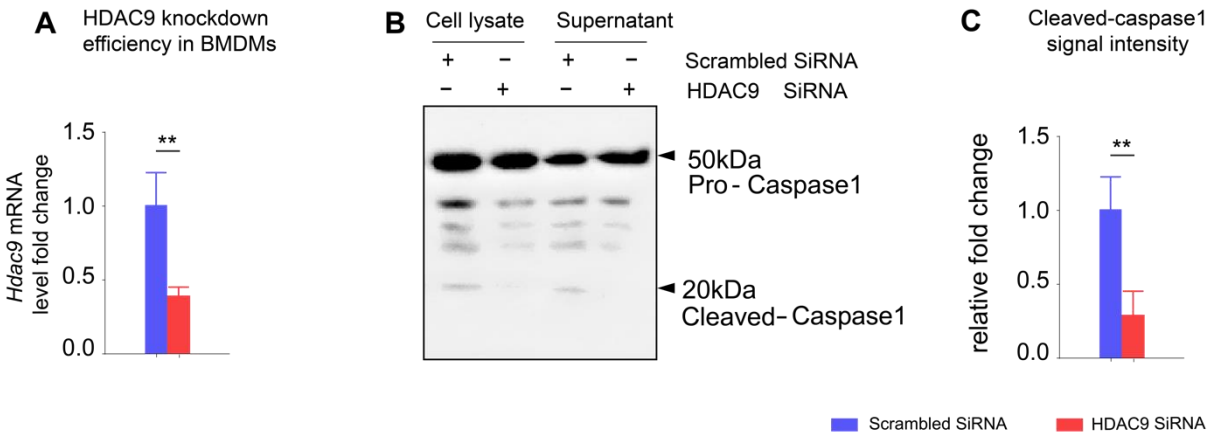

Figure 25. Knockdown of *Hdac9* in BMDMs leads to less cleavage of pro-caspase-1.
(A) Shown is the knockdown efficiency of *Hdac9* specific siRNA. Scrambled RNA was used as a control. (B) Shown is the representative Western blot revealing less cleaved caspase-1 upon *Hdac9* knockdown. (C) Shown is the quantification of 4 different independent western blot analysis. **p ⩽ 0.01. Unpaired T-test was used for statistical analysis.

5.15 Co-IP experiments showed a physical interaction between HDAC9 and NLRP3

Recently, two studies showed that HDAC6 physically interacted with NLRP3 and HDAC9 respectively, indicating the potential interaction between HDAC9 and NLRP3. Based on above results and previous data (Fig. 11), I decided to explore the potential interaction between HDAC9 and NLRP3.

Different mouse HDAC9 isoforms were cloned from BMDMs and tagged with V5 by Dr. Matthias Prestel from our lab (Fig. 26 A). Isoform1 contains the deacetylase domain, whereas isoforms 2 and 3 (MITR) are devoid of the deacetylase domain. These 3 isoforms were used to check the potential interaction between HDAC9 and NLRP3. HDAC9 isoforms were transfected together with NLRP3 in HEK293T cells. Using anti-FLAG M2 antibody, both isoforms of HDAC9 were pulled down (Fig.26 B), strongly indicating the interaction between HDAC9 and the inflammasome sensor NLRP3. Furthermore, Co-IP results revealed no interaction between the two isoforms of HDAC9 and AIM2, another inflammasome sensor (Fig. 26 C) (Kim et al., 2010), indicating the specificity between HDAC9 and NLRP3.

Taken together, HDAC9 was shown to upregulate pro-caspase-1 cleavage and physically interact with NLRP3, indicating a potential role of HDAC9 in NLRP3 inflammasome activation. However, the observed direct interaction between HDAC9 and NLRP3 is in HEK293T cells after over-expressing both of the molecules. To further confirm the endogenous interaction between HDAC9 and NLRP3, I am planning to perform co-IP in inflammasome-present cell types (e.g. macrophages).

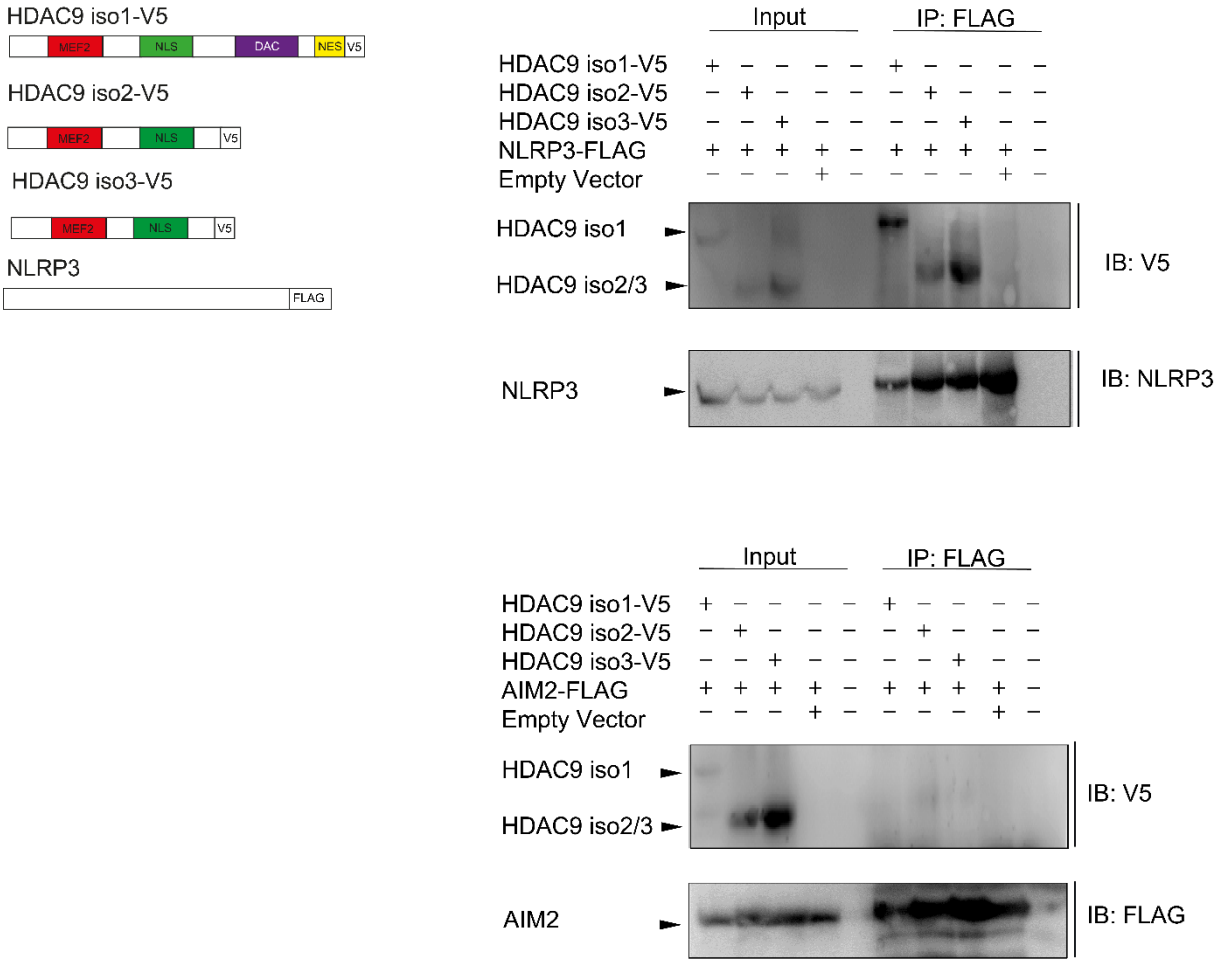

Figure 26. HDAC9 interacts with NLRP3.

(A) Shown are the illustrations of different constructs. HDAC9 different isoforms were cloned from murine BMDMs, with full-length isoform1 and shorter isoforms 2 and 3. All three HDAC9 isoforms contain MEF2 binding domain. NLS refers to nuclear localization sequence (NLS). DAC refers to deacetylase domain. HDAC9 isoforms were tagged with V5 whereas NLRP3 and AIM2 were tagged with FLAG. (B) Shown are the Co-IP results using anti-FLAG M2 antibody to pull down NLRP3 and its interaction partners. Membrane was probed with V5 antibodies to detect HDAC9 from input and IP. Same membrane was stripped and later re-probed with NLRP3 antibodies to validate the IP efficiency. (C) Shown are the Co-IP results using anti-FLAG M2 antibody to pull down AIM2 and its interaction partners. Membrane was probed with V5 antibodies to detect HDAC9 from input and IP. Same membrane was stripped and later re-probed with FLAG antibodies to detect AIM2 to validate the IP efficiency. The blot is representative of 4 different independent experiments.

6. Discussion

In this study, a novel mouse model, the *Hdac9*$^{\Delta Cis-/-}$ mouse, was generated via deleting a highly conserved CRE (around 1.1 kb) encompassing the rs2107595. Interestingly, *Hdac9*$^{\Delta Cis-/-}$ was shown to upregulate *Hdac9* in myeloid cells, in particular in pro-inflammatory macrophages, showing an expression pattern mimicking human risk allele A carriers. After crossbreeding into an atheroprone model, *Apoe*$^{-/-}$ *Hdac9*$^{\Delta Cis-/-}$ were generated and developed significantly larger atherosclerotic plaques. Chemokine and cytokine profiles showed that *Apoe*$^{-/-}$ *Hdac9*$^{\Delta Cis-/-}$ developed a pro-inflammatory milieu with upregulated levels of IL-1β, IL-6 and IL-18 in the plasma, indicating an enhanced NLRP3 inflammasome activation. Flow cytometric analysis revealed the enrichment of pro-inflammatory cell types (i.e. neutrophils, classical monocytes), further confirming the pro-inflammatory contribution of myeloid cells from *Apoe*$^{-/-}$ *Hdac9*$^{\Delta Cis-/-}$ mice. However, the atherosclerosis exacerbation was only observed in male mice. BMT experiments further confirmed the atherogenic role of *Apoe*$^{-/-}$ *Hdac9*$^{\Delta Cis-/-}$ myeloid cells. Finally, *Apoe*$^{-/-}$ *Hdac9*$^{\Delta Cis-/-}$ BMDMs showed more cleavage of pro-caspase-1. Gain-and-loss of function also confirmed the role of HDAC9 in pro-caspase-1 cleavage in BMDMs. To tap into the molecular mechanism, co-IP results revealed the potential physical interaction between HDAC9 and NLRP3.

6.1 Novelty of the *Hdac9*$^{\Delta Cis-/-}$ mouse model

Most studies on CRE function were performed only *in vitro*. Recently, a study showed that rs9349379 is associated with vascular diseases. Interestingly, this SNP is located in a CRE with enhancer signatures in an aorta-specific fashion, suggesting a regulatory function in vasculature cell types (e.g. endothelial cells). CRISPR-Cas9-based editing in human induced pluripotent stem cells (iPSCs)-derived endothelial cells showed that

rs9349379 distally regulated the expression of endothelin-1 (*EDN1* (Gupta et al., 2017). Indeed, human iPSCs have offered unprecedented opportunities to study human diseases (Choi et al., 2009). Via harnessing the pluripotency of iPSCs, they may be differentiated into a monolayer of any cell type of interest *in vitro*. However, there are several limitations of using iPSCs to model human disease. First, iPSCs lose the complexity of pathological etiologies. Atherosclerosis is orchestrated by different cell types, therefore differentiating into a specific cell type may not recapitulate disease mechanism and a monolayer cell system is far away from recapitulating the *in vivo* environment. The *HDAC9*$^{\Delta Cis-/-}$ mouse model overcomes this limitation. This model offers spatiotemporal information on the regulatory function of the CRE while maintaining the transcriptional fidelity during atherogenesis. Moreover, our mouse model offers insights into changes in cellular compositions inside spleens and atherosclerotic plaques. Second, atherosclerosis is lipid-triggered disease. The iPSCs system is not recapitulating the changes in lipid metabolism during atheroprogression. Whereas mice models give straightforward information of the lipid profile from different ages, diets and genders. Therefore, establishing an animal model mirroring human disease progression, may overcome the limitation from cell-culture-based approaches. To this end, we designed and generated the *HDAC9*$^{\Delta Cis-/-}$ mouse model. An interesting point of the *HDAC9*$^{\Delta Cis-/-}$ mouse model is that it entails a short deletion of 1.1 kb comprising a CRE. Most of other CRE mouse models harbor much larger deletions. For example, one recent study showed that deletion of a 20-kb-long enhancer resulted in the downregulation of *Pitx2c*, mitigating the atrial fibrillation (AF) predisposition (Zhang et al., 2019). Another recent study identified a 640-kb non-coding region as a face-specific CRE. Deletion of this CRE in mice resulted in mild upregulation of MyC, thereby altering facial morphogenesis (Uslu et al., 2014). Compared to those 2 recent

studies, the 1.1 kb deletion size from our *Hdac9*$^{\Delta Cis-/-}$ mouse model is quite specific, indicating a strong regulatory potency from our CRE as a crucial regulator for atherosclerotic development.

6.2 *Hdac9*$^{\Delta Cis-/-}$ mice show an upregulation of *HDAC9* in a cell- and tissue-specific manner

Deletion of the CRE upregulated *Hdac9* in myeloid cells. The lead SNP rs2107595 was shown to regulate *HDAC9* transcription (Prestel et al., 2019). Mechanistically, the E2F3/Rb-complex was shown to bind to rs2107595, thereby regulating *HDAC9* transcription. Interestingly, the deleted CRE contains several E2F3 binding motifs, pointing also to a role of E2F3 *in vivo*. Moreover, E2F family members were reported as ultimate transcriptional effector governing myeloid cell development (Trikha et al., 2011), indicating a myeloid-specific regulatory role of the conserved CRE at the *Hdac9* locus. Indeed, qPCR analysis revealed that both *Hdac9*$^{\Delta Cis-/-}$ and *Apoe*$^{-/-}$ *Hdac9*$^{\Delta Cis-/-}$ showed upregulation of *Hdac9* in myeloid cells, especially in BMDMs. This result is in accord with our previous finding that rs2107595 upregulated *HDAC9* in human myeloid-cell-derived PBMCs (Azghandi et al., 2015).

Upregulation of *Hdac9* was seen predominantly in pro-inflammatory macrophages. *Hdac9*$^{\Delta Cis-/-}$ showed upregulation of *Hdac9* only in LPS-treated BMDMs. No difference was observed in untreated or IL-4-treated BMDMs. These results indicated that the regulatory function of the CRE is only active in a pro-inflammatory milieu in differentiated macrophages. In support of this data, it was previously shown that in human blood-derived macrophages risk allele A carriers showed elevated *HDAC9* levels only upon pro-inflammatory treatment of TNFα and IFNγ (Prestel et al., 2019), further supporting the concept of a pro-inflammatory-niche specificity of the CRE. Indeed, macrophages CREs were reported to change chromatin landscape upon pro-

inflammatory stimuli (Ghisletti and Natoli, 2013). For example, in pro-inflammatory macrophages, NF- κB was reported to bind to active enhancers whereas STAT6 was shown to occupy other enhancer regions in anti-inflammatory macrophages (Ghisletti et al., 2010; Szanto et al., 2010). Those findings explained the upregulation of *Hdac9* only in pro-inflammatory macrophages upon knocking out the CRE in *Hdac9*$^{\Delta Cis-/-}$ mouse model. Interestingly, my results showed that *Apoe*$^{-/-}$ *Hdac9*$^{\Delta Cis-/-}$ upregulated *Hdac9* without any external stimuli. This is probably due to the altered lipid homeostasis upon the depletion of Apoe, a glycoprotein, thought to clear atherogenic lipoproteins (Hofker et al., 1998). In macrophages, Apoe facilitates the lipid remnants efflux and transports them to liver for excretion. Therefore, knocking out Apoe blocks the lipid efflux and the resulting accumulated lipid remnants could polarize macrophages into a pro-inflammatory phenotype. This is evidenced by one study (Baitsch et al., 2011) showing over-expressing Apoe in mouse macrophages upregulated M2 markers (e.g. arginase-1) and downregulated M1 markers (e.g. interleukin-12). Therefore, compared to wild type, *Apoe*$^{-/-}$ macrophages already harbor an innate pro-inflammatory milieu without any exogenous stimuli (e.g. LPS). This may explain the upregulation in untreated *Apoe*$^{-/-}$ *Hdac9*$^{\Delta Cis-/-}$ macrophages.

Apoe$^{-/-}$ *Hdac9*$^{\Delta Cis-/-}$ showed upregulation of *Hdac9* specifically in the aorta. Accumulative evidence showed that under chow diet for 14 weeks, *Apoe*$^{-/-}$ mice start to form atherosclerotic fatty streaks which is full of lipid-laden foam cells, whereas wild type mice can hardly develop fatty streaks (Nakashima et al., 1994). Early-stage atherosclerotic plaques were thought to entail a pro-inflammatory milieu. Since the regulatory function of our CRE responded in a pro-inflammatory-phenotype-specific manner, it makes sense of the upregulation of *Hdac9* in aortas during early-stage atherosclerosis.

Apoe$^{-/-}$ *Hdac9*$^{\Delta Cis-/-}$ mice showed an enrichment of pro-inflammatory myeloid cell subsets from the spleen. My results reveal that *Apoe*$^{-/-}$ *Hdac9*$^{\Delta Cis-/-}$ mice were skewed into a more pro-inflammatory immune homeostasis, evidenced by enrichment of pro-inflammatory Ly6G^{+} neutrophils and LyC6^{hi} classical monocytes from the spleen. However, no difference was observed in regard to T cell compositions, further indicating the cell-type-specific regulatory function of the CRE. Interestingly, our group found that the *Hdac9* deficiency mouse model (deletion of exon 4 and 5) showed a decreased pro-inflammatory Ly6G^{+} neutrophils and LyC6^{hi} classical monocytes from the spleen (not published). These data are complementary to my findings, since *Apoe*$^{-/-}$ *Hdac9*$^{\Delta Cis-/-}$ was shown to upregulate *Hdac9* expression. The role of HDAC9 in enhancing the innate immunity and myeloid cell proliferation has been evidence by previous studies (Cao et al., 2014; Li et al., 2016; Lu et al., 2018). Interestingly, *Hdac9* and *Nlrp3* were found to be upregulated in granulocyte-monocyte progenitors (GMPs) from *Ldlr−/−* mice fed with western diet, indicating the role of HDAC9 in monocyte differentiation and proliferation (Christ et al., 2018).

6.3 *Apoe*$^{-/-}$ *Hdac9*$^{\Delta Cis-/-}$ mice show exacerbation of atherosclerosis

Atherosclerotic plaque quantification shows the athero-protective role of the CRE. Under chow diet for 28 weeks, *Apoe*$^{-/-}$ *Hdac9*$^{\Delta Cis-/-}$ mice developed significantly larger plaques. Our previous results showed that knocking out HDAC9 in *Apoe*$^{-/-}$ background significantly reduced atherosclerotic plaque size when mice kept on chow diet for 28 weeks (Azghandi et al., 2015). Furthermore, it was shown that *Hdac9* deficiency in Ldlr$^{-/-}$ background also attenuated atherosclerosis (Cao et al., 2014). These two findings underscored the atherogenic role of HDAC9. Since the deletion of the CRE

resulted in upregulation of *Hdac9*, *Apoe*$^{-/-}$ *Hdac9*$^{\Delta Cis-/-}$ was expected to develop more atherosclerotic plaques.

However, the phenotypic difference was only observed in male mice. HDAC9 was shown to play a gender-specific role in some diseases. For example, HDAC9 was reported to regulate hypertension-induced chronic kidney diseases with a sex difference (Bourgeois et al., 2017). Another report showed that HDAC9 suppresses the expression of Estrogen Receptor, thereby establishing the sex difference in cardioprotection (van Rooij et al., 2010). However, no difference in plaque size from female might be also due to the untapped role of HDAC9 in advanced stage of atherosclerosis. My data showed that after 28 weeks of chow diet, female mice developed larger atherosclerotic plaques compared to male mice, indicating an intermediate or even advanced stage of atherosclerosis. Since previous studies only showed that HDAC9 and rs2107595 played a role predominantly in early stage of atherosclerosis (Azghandi et al., 2015; Franceschini et al., 2018; Markus et al., 2013) , the atherogenic role of HDAC9 in intermediate or advanced stages is not known yet. Bone marrow transplantation experimental results showed that *Apoe*$^{-/-}$ *Hdac9*$^{\Delta Cis-/-}$ haemopoietic stem cells were sufficient to exacerbate atherogenesis. Gene expression analysis showed that knocking out the CRE significantly upregulated *Hdac9* in myeloid cells, especially in macrophages. Since most of the macrophages come from the bone marrow cells, therefore I was prompted to perform the BMT experiments. Besides the increase in plaque size in BMT mice, trichrome staining also revealed that *Apoe*$^{-/-}$ *Hdac9*$^{\Delta Cis-/-}$ haemopoietic stem cells led to more vulnerable plaques evidenced by less collagen content. This result echoes with previous GWAS, since rs2107595 was associated with atherosclerotic stroke due to vulnerable plaques (Malik et al., 2018). The robustness of our data was also corroborated by *Hdac9*$^{-/-}$ (deletion of *Hdac9* exon

4 and 5) BMT model which developed a more stable plaque from my colleague (data not published). However, to further verify plaque stability, SMCs number need to be determined because of their contributions to plaque stability (MacLeod et al., 1994; Schwartz et al., 2000a).

Atherosclerotic plaque rupture and thrombotic events are partially mediated by MMPs, which are a family of matrix-erosion proteases produced majorly from myeloid cells (Brauer, 2006). Among them, *MMP12* was reported to digest extracellular matrix and lead to atherosclerotic plaque rupture (Johnson et al., 2005; Luttun et al., 2004; Newby, 2007; Prescott et al., 1999). Similar to *HDAC9*, *MMP12* was also identified to be associated with large artery stroke (Traylor et al., 2014), adverse prognosis for cardiovascular disease (Scholtes et al., 2012) and late stage atherosclerotic plaque instability (Morgan et al., 2004). Most importantly, one study (Oksala et al., 2017) showed that in advanced human carotid plaque samples, HDAC9 *and* MMP12 were found synergistically expressed in M4 macrophages. The link between *HDAC9* and other MMPs have not yet been established in regard to atherosclerotic plaque stability. All the evidence indicated that elevation of *Hdac9* in myeloid cells may lead to upregulation of *Mmp12* in the *Hdac9*$^{\Delta Cis-/-}$ model, explaining the plaque vulnerability in BMT mice.

6.4 *The Hdac9*$^{\Delta Cis-/-}$ genotype promotes a pro-inflammatory milieu in atherogenic *Apoe*$^{-/-}$ background

Deletion of the CRE promoted a pro-inflammatory milieu. *Apoe*$^{-/-}$ *Hdac9*$^{\Delta Cis-/-}$ mice showed an upregulation of IL1-β, IL-6 and IL-18 in the plasma, suggesting a role of HDAC9 in promoting pro-inflammatory response. Moreover, in this study, I have shown that aortas of *Apoe*$^{-/-}$ *Hdac9*$^{\Delta Cis-/-}$ mice entailed a more pro-inflammatory milieu. To exclude the potential pro-inflammatory effect of *Apoe* deficiency, I have also shown

that *Hdac9*$^{\Delta Cis-/-}$ BMDMs contained an enhanced pro-inflammatory response to LPS. Several lines of evidence support my findings. Cao and others have shown that *Ldlr*$^{-/-}$ *Hdac9*$^{\Delta Cis-/-}$ macrophages were skewed into a more anti-inflammatory phenotype (Cao et al., 2014). They showed that *Hdac9* deficiency decreased IL1-β and IL-6 secretion and increased M2 markers (e.g. IL-10) mRNA levels in peritoneal macrophages, indicating that *Hdac9* deficiency desensitized the pro-inflammatory response in macrophages. Another study showed that *Hdac9* deficiency downregulated *Il1-β*, *Il-6*, *Il-18* and *iNos* transcriptional level in the brain and BV2 microglial cells (Lu et al., 2018). Mechanistically, they demonstrated that *Hdac9* deficiency was associated with decreased phosphorylation of IκBα, NF-kB and mitogen-activated protein kinases (MAPKs). Other studies showed the pro-inflammatory role of HDAC9 in ECs (Han et al., 2016; Shi et al., 2016) and T cells (Beier et al., 2012; Tao et al., 2007).

IL1-β is known to be a crucial extracellular pro-inflammatory mediator in cardiovascular diseases (Libby, 2017). Once being produced, IL1-β is released into circulation to activate and amplify pro-inflammatory response. For example, IL1-β was shown to activate human ECs, thereby upregulating the expression of adhesion molecules ICAM-1 and VCAM-1 (Bevilacqua et al., 1985). IL1-β was also reported to induce the proliferation and migration of SMCs (De et al., 1993; Massberg et al., 2003). Recent Canakinumab Anti-Inflammatory Thrombosis Outcome Study (CANTOS) further confirmed the role of IL1-β in atherosclerosis development (Merhi-Soussi et al., 2005; Shimokawa et al., 1996). Moreover, IL1-β was shown to produce IL-6 (Akira et al., 1990; Loppnow and Libby, 1990), which explains our cytokine profile readout. The major producers of IL1-β are myeloid cells (Fatkhullina et al., 2016). Since IL1-β and IL-18 are typical downstream effectors of inflammasome, I decided to explore the role of HDAC9 in NLRP3 inflammasome.

6.5 The role of HDAC9 in NLRP3 inflammasome priming and activation

To further confirm that inflammasome activation was due to upregulation of *Hdac9* instead of other random distal gene(s), HDAC9 gain- and loss-of-function experiments were performed in BMDMs by over-expressing and knocking down HDAC9. Two different isoforms (full-length HDAC9 and MITR) showed no difference in cleaving pro-caspase-1, indicating the importance of *HDAC9* N-terminal. Furthermore, we saw interaction between HDAC9 (full-length HDAC9 and MITR) and NLRP3, upon ectopic expression in HEK293T cells. Taken together, this study showed that HDAC9 plays a role in inflammasome priming and activation. So far, this is the first report to demonstrate that HDAC9 plays a role in inflammasome activation.

Several reports have indirectly supported my finding. HDAC6 was reported to inhibit the NLRP3 inflammasome activation via directly interacting with NLRP3 (Hwang et al., 2015). Mechanistically, they showed that the suppressive role of HDAC6 was not due to its deacetylase activity but by interacting with NLRP3 through the ubiquitination domain of HDAC6. Ubiquitination of NLRP3 is a prerequisite of inflammasome activation (Py et al., 2013a). Hypothetically, HDAC6 could sequester ubiquitinated NLRP3 to from an aggresome thereby inhibiting the inflammasome assembly (Hwang et al., 2015). Another study show that HDAC6 interacted with HDAC9 through its second deacetylase domain in neuronal cells (Salian-Mehta et al., 2015), which prompted me to hypothesize the interaction between HDAC9 and NLRP3. Indeed, I saw a robust interaction between HDAC9 and NLRP3 (but not with AIM2) after over-expressing them into HEK293T cells. However, HEK cells lack endogenous ASC, Caspase-1 and other inflammasome components, therefore the inflammasome is not assembled in HEK cell. Thus, the observed HDAC9 and NLRP3 interaction in HEK

cells might not reflect the interaction in macrophages or other cell types exhibiting inflammasome function. To further confirm the role of HDAC9 in NLRP3 inflammasome activation, experiments need to be performed in inflammasome relevant cell types, such as BMDMs. Furthermore, the co-IP was performed after transfecting HDAC9 and NLRP3, which did not pull down the endogenous HDAC9 in HEK cells. The reason we constructed HDAC9-V5 plasmids is that there is no HDAC9-specific antibody so far. Also, NLRP3 inflammasome is assembled from many different proteins (e.g. ASC), which makes this complex biochemically 'sticky'. Via over-expressing simply NLRP3 in HEK cells, we can avoid the unspecific binding between HDAC9 and inflammasome as a whole. This is due to the fact that over-expressing NLRP3 only in HEK cells does not trigger the assembly.

6.6 Hypothesis for the molecular mechanism underlying the role of HDAC9 in NLRP3 inflammasome activation

Possible biochemical mechanisms for the role of HDAC9 in inflammasome activation are still lacking. Based on literature and my current data, I would propose two hypotheses.

Hypothesis 1: HDAC9 may confer a post-translational modification to NLRP3 via direct interaction. There are several lines of evidence supporting this hypothesis. Frist, a growing body of evidence has shown that in order to successfully assemble inflammasome, NLRP3 is subject to post-translational modification, such as phosphorylation (Spalinger et al., 2016) and ubiquitination (Py et al., 2013b). For instance, Protein Tyrosine Phosphatase Non-Receptor 22 (PTPN22) has been reported to positively regulate NLRP3 inflammasome via dephosphorylating Y861 residue (Diaz-Gallo et al., 2011). Another report showed that S295 phosphorylation was reported to inhibit NLRP3 inflammasome activation via Protein Kinase A (PKA)

(Guo et al., 2016). In regard to ubiquitination, K48 and K63 are known to negatively regulate NLRP3 inflammasome function (Han et al., 2015; Kawashima et al., 2017; Py et al., 2013b; Yan et al., 2015). For example, deubiquitinase BRCC3 activated NLRP3 inflammasome through directly interacting with NLRP3 (Py et al., 2013b). G5, a BRCC3 inhibitor, impaired the inflammasome assembly by polyubiquitinating at K63 and K48 of NLRP3. Collectively, post-translational modifications of NLRP3 are essential for inflammasome activation. Since HDAC9 interacts with other molecules including HDAC3, I hypothesized that HDAC9 together with its interaction partners may confer NLRP3 phosphorylation, ubiquitination and potentially other PTMs (e.g. acetylation). Another line of evidence leading to this hypothesis is that HDAC9 was reported to deacytelase TBK1 via a direct interaction, which resulted in an enhanced kinase activity (Li et al., 2016). Third line of evidence is that the cross-talk between acetylation and phosphorylation has been highlighted in various studies (van Noort et al., 2012). For instance, phosphorylation of Ser15 and Ser46 of tumor suppressor P53 is prerequisite for p53 acetylation (Hofmann et al., 2002; Sakaguchi et al., 1998). Moreover, others have found that trichostatin A (TSA), a HDAC inhibitor, increased phosphorylation of different kinases such as: protein tyrosine kinase 2 (PTK2), mitogen-activated protein kinase 3 (MAPK3; ERK1), and muscle pyruvate kinase (Bryson and White, 2015). Therefore, I hypothesized that HDAC9 may interact with certain kinases and phosphatases, thereby affecting their kinase activity, which subsequently regulates NLRP3 inflammasome activation.

Hypothesis 2: HDAC9 may regulate ER (endoplasmic reticulum) stress and in turn activate NLRP3 inflammasome via regulating the ROS production. Several lines of information have encouraged me to conceive this hypothesis. Firstly, ROS production has been proven as a stimulus for inflammasome, which has been described in

introduction part. Secondly, some HDACs are thought to play a role in ROS production. For example, previous studies reported that in breast cancer cells and human monocytes, various HDACi, including TSA, resulted in an enhanced ROS production (Rehman et al., 2014; Sun et al., 2014). Thirdly, our transcriptome sequencing data indicated this directionality (data not shown). Ingenuity Pathway Analysis (IPA) of our sequencing data revealed that HDAC9 might regulate the ER stress pathways. ER stress has been documented as a hallmark during the progression of atherosclerosis, especially in advanced stages (Tabas, 2010). The prolonged ER stress in atherosclerotic plaque may result in enhanced ROS production and inflammatory response (Hotamisligil, 2010; Zeeshan et al., 2016). Specifically, our transcriptomic sequencing data revealed some significantly regulated genes, such as *Atf4* and *Chop*. *Chop* deficiency has been reported to reduce atherosclerotic plaque size both in *Ldlr*$^{-/-}$ and *Apoe*$^{-/-}$ mouse models (Thorp et al., 2009). Interestingly, *Chop* has been shown to correlate with the activity of caspase-1 (Lebeaupin et al., 2015). All the evidence indicate that HDAC9 might regulate inflammasome activation via ER stress genes (e.g. *Chop*).

7. List of abbreviations

ATLOS	Arterial tertiary lymphoid organs
AD	Alzheimer’s disease
CAMKII	Ca2+/calmodulin-dependent protein kinase ii
CTBP	C-terminal-binding protein
CHIP	Chromatin immunoprecipitation
CRES	Cis-regulatory elements
CREB	Cyclic amp-responsive element-binding protein
DAMPS	Damage-associated molecular patterns
DC	Dendritic cell
DHSS	Dnase I hypersensitive sites
DMSO	Dimethyl sulfoxide
EDTA	Ethylenediaminetetraacetic acid
FBS	Fetal bovine serum
FSC	Forward scattered
GM-CSF	Granulocyte/macrophage colony-stimulating factor
GR	Glucocorticoid receptor
H	Hours
HATS	Histone acetyl transferases
H3K4ME1	Histone h3 lysine 4 monomethylation
H3K27AC	Histone h3 lysine 27 acetylation
H3K27ME3	Histone h3 lysine 27 trimethylation
HBSS	Hank‘s balanced salt solution
HDACS	Histone deacetylases
H&E	Hematoxylin and eosin staining
HRP	Horseradish peroxidase
HSC	Hematopoietic stem cell
HSPC	Hematopoietic stem and progenitor cell
ICAM-1	Intercellular adhesion molecule-1
IFN-Γ	Interferon- γ
IL	Interleukin
I.P.	Intraperitoneal
LAS	Large artery atherosclerotic stroke

List of abbreviations

LC-MS	Liquid chromatography–mass spectrometry
LDL	Low-density lipoprotein
LDLR	Low density lipoprotein (ldl) receptor
LPS	Lipopolysaccharide
MITR	Mef2 interacting transcriptional repressor
MIN	Minutes
ML	Milliliter
MMP	Matrix metalloproteinase
NFKB	Nuclear factor-kappa-b
NSCLC	Non-small cell lung cancer
OXLDL	Oxidized LDL
PAMP	Pathogen-associated molecular pattern
PBS	Phosphate-buffered saline
PCR	Polymerase chain reaction
PDGF	Platelet derived growth factor
PKD1	Protein kinase d
PFA	Paraformaldehyd
PRC2	Polycomb repressor complex 2
PTMS	Post translational modifications
PWAS	Proteome-wide analysis of disease-associated snps
ROS	Reactive oxygen species
RT	Room temperature
S	Seconds
SCFAC	Short chain fatty acid
SEM	Standard error of mean
SMCS	Smooth muscle cells
TLR	Toll like receptor
TNF- A	Tumor necrosis factor-α
VCAM1	Vascular cell adhesion molecule-1
VSMCS	Vascular smooth muscle cells

8. Acknowledgement

Firstly, I need to thank my parents for nurturing me with an inquisitive and analytical mind, which enabled me to overcome adversaries and difficulties during these years. Secondly, I would like to thank Prof. Dichgans for giving me the opportunity to work here at ISD. It is a privilege to work in this state-of-the-art institute. Also, being assigned to this project motivated me to acquire different techniques and knowledge in several different topics including atherosclerosis, immunology, genetics and epigenetics. Specifically, he helped me to polish my presentation skills and encourage me to come up with my own scientific ideas for my project. Next, I need to thank Prof. Bernhagen for guiding and supporting me through the doctoral work. The valuable suggestion from Prof. Bernhagen have been instrumental for this project. Another very important person for this project is my daily supervisor Dr. Prestel who gave a lot of input in terms of molecular and biochemical part of this project. Besides work, Dr. Prestel also helped with my accommodation in Munich, which made my personal life here much easier compared to other foreign students. In addition, my colleague Dr. Asare also offered suggestions especially in terms of atherosclerotic *in vivo* experiments. There are many other people, I am extremely grateful to, such as Prof. Dr. Lauduner, Dr. Omar El Bounkari, Dr. Stephan Roth, Dr. Farida Hellal, Dr. Mary Susan Lopez, Melanie Schneider, Natalie Ziech, Babara Linder and other colleagues for helping with my doctoral work in various different ways.

9. Reference

Abbott, R.D., Curb, J.D., Rodriguez, B.L., Masaki, K.H., Popper, J.S., Ross, G.W., and Petrovitch, H. (2003). Age-related changes in risk factor effects on the incidence of thromboembolic and hemorrhagic stroke. Journal of clinical epidemiology *56*, 479-486.
Adams, H.P., Jr., Bendixen, B.H., Kappelle, L.J., Biller, J., Love, B.B., Gordon, D.L., and Marsh, E.E., 3rd (1993). Classification of subtype of acute ischemic stroke. Definitions for use in a multicenter clinical trial. TOAST. Trial of Org 10172 in Acute Stroke Treatment. Stroke *24*, 35-41.
Agarwal, A., Banerjee, A., and Banerjee, U.C. (2011). Xanthine oxidoreductase: a journey from purine metabolism to cardiovascular excitation-contraction coupling. Crit Rev Biotechnol *31*, 264-280.
Akinyemi, R., Tiwari, H.K., Arnett, D.K., Ovbiagele, B., Irvin, M.R., Wahab, K., Sarfo, F., Srinivasasainagendra, V., Adeoye, A., Perry, R.T.*, et al.* (2018). APOL1, CDKN2A/CDKN2B, and HDAC9 polymorphisms and small vessel ischemic stroke. Acta neurologica Scandinavica *137*, 133-141.
Akira, S., Hirano, T., Taga, T., and Kishimoto, T. (1990). Biology of multifunctional cytokines: IL 6 and related molecules (IL 1 and TNF). The FASEB journal *4*, 2860-2867.
Alchini, R., Sato, H., Matsumoto, N., Shimogori, T., Sugo, N., and Yamamoto, N. (2017). Nucleocytoplasmic Shuttling of Histone Deacetylase 9 Controls Activity-Dependent Thalamocortical Axon Branching. Scientific reports *7*, 6024.
Anderson, R.H. (2000). Clinical anatomy of the aortic root. Heart *84*, 670-673.
Averill, L.E., Meagher, R.C., and Gerrity, R.G. (1989). Enhanced monocyte progenitor cell proliferation in bone marrow of hyperlipemic swine. Am J Pathol *135*, 369-377.
Azghandi, S., Prell, C., van der Laan, S.W., Schneider, M., Malik, R., Berer, K., Gerdes, N., Pasterkamp, G., Weber, C., Haffner, C.*, et al.* (2015). Deficiency of the stroke relevant HDAC9 gene attenuates atherosclerosis in accord with allele-specific effects at 7p21.1. Stroke *46*, 197-202.
Backs, J., Backs, T., Bezprozvannaya, S., McKinsey, T.A., and Olson, E.N. (2008). Histone deacetylase 5 acquires calcium/calmodulin-dependent kinase II responsiveness by oligomerization with histone deacetylase 4. Mol Cell Biol *28*, 3437-3445.
Backs, J., Song, K., Bezprozvannaya, S., Chang, S., and Olson, E.N. (2006). CaM kinase II selectively signals to histone deacetylase 4 during cardiomyocyte hypertrophy. J Clin Invest *116*, 1853-1864.
Baitsch, D., Bock, H.H., Engel, T., Telgmann, R., Muller-Tidow, C., Varga, G., Bot, M., Herz, J., Robenek, H., von Eckardstein, A.*, et al.* (2011). Apolipoprotein E induces antiinflammatory phenotype in macrophages. Arterioscler Thromb Vasc Biol *31*, 1160-1168.
Bannister, A.J., and Kouzarides, T. (2011). Regulation of chromatin by histone modifications. Cell Res *21*, 381-395.
Bauernfeind, F., Bartok, E., Rieger, A., Franchi, L., Nunez, G., and Hornung, V. (2011). Cutting edge: reactive oxygen species inhibitors block priming, but not activation, of the NLRP3 inflammasome. J Immunol *187*, 613-617.
Beier, U.H., Wang, L., Han, R., Akimova, T., Liu, Y., and Hancock, W.W. (2012). Histone deacetylases 6 and 9 and sirtuin-1 control Foxp3+ regulatory T cell function through shared and isoform-specific mechanisms. Sci Signal *5*, ra45-ra45.

Reference

Bevan, S., Traylor, M., Adib-Samii, P., Malik, R., Paul, N.L., Jackson, C., Farrall, M., Rothwell, P.M., Sudlow, C., Dichgans, M.*, et al.* (2012). Genetic heritability of ischemic stroke and the contribution of previously reported candidate gene and genomewide associations. Stroke *43*, 3161-3167.

Bevilacqua, M.P., Pober, J.S., Wheeler, M.E., Cotran, R.S., and Gimbrone, M.A., Jr. (1985). Interleukin-1 activation of vascular endothelium. Effects on procoagulant activity and leukocyte adhesion. Am J Pathol *121*, 394-403.

Boehme, A.K., Esenwa, C., and Elkind, M.S. (2017). Stroke Risk Factors, Genetics, and Prevention. Circ Res *120*, 472-495.

Boucher, D., Monteleone, M., Coll, R.C., Chen, K.W., Ross, C.M., Teo, J.L., Gomez, G.A., Holley, C.L., Bierschenk, D., Stacey, K.J.*, et al.* (2018). Caspase-1 self-cleavage is an intrinsic mechanism to terminate inflammasome activity. J Exp Med *215*, 827-840.

Bourgeois, C.T., Satou, R., and Prieto, M.C. (2017). HDAC9 is an epigenetic repressor of kidney angiotensinogen establishing a sex difference. Biology of sex differences *8*, 18.

Boyle, A.P., Davis, S., Shulha, H.P., Meltzer, P., Margulies, E.H., Weng, Z., Furey, T.S., and Crawford, G.E. (2008). High-resolution mapping and characterization of open chromatin across the genome. Cell *132*, 311-322.

Brainin, M., and Heiss, W.-D. (2019). Textbook of stroke medicine (Cambridge University Press).

Brass, L.M., Isaacsohn, J.L., Merikangas, K.R., and Robinette, C.D. (1992). A study of twins and stroke. Stroke *23*, 221-223.

Brauer, P. (2006). MMPs--role in cardiovascular development and disease. Frontiers in bioscience: a journal and virtual library *11*, 447-478.

Brown, D.I., and Griendling, K.K. (2009). Nox proteins in signal transduction. Free Radic Biol Med *47*, 1239-1253.

Bryson, B.D., and White, F.M. (2015). Quantitative Profiling of Lysine Acetylation Reveals Dynamic Crosstalk between Receptor Tyrosine Kinases and Lysine Acetylation. PLoS One *10*, e0126242.

Cao, Q., Rong, S., Repa, J.J., Clair, R.S., Parks, J.S., and Mishra, N. (2014). Histone deacetylase 9 represses cholesterol efflux and alternatively activated macrophages in atherosclerosis development. Arteriosclerosis, thrombosis, and vascular biology *34*, 1871-1879.

Carta, S., Penco, F., Lavieri, R., Martini, A., Dinarello, C.A., Gattorno, M., and Rubartelli, A. (2015). Cell stress increases ATP release in NLRP3 inflammasome-mediated autoinflammatory diseases, resulting in cytokine imbalance. Proc Natl Acad Sci U S A *112*, 2835-2840.

Chen, J., Zhang, Z., Wang, N., Guo, M., Chi, X., Pan, Y., Jiang, J., Niu, J., Ksimu, S., Li, J.Z.*, et al.* (2017). Role of HDAC9-FoxO1 Axis in the Transcriptional Program Associated with Hepatic Gluconeogenesis. Scientific reports *7*, 6102.

Chinetti-Gbaguidi, G., Colin, S., and Staels, B. (2015). Macrophage subsets in atherosclerosis. Nature Reviews Cardiology *12*, 10.

Chinnadurai, G. (2002). CtBP, an unconventional transcriptional corepressor in development and oncogenesis. Mol Cell *9*, 213-224.

Choi, K.D., Yu, J., Smuga-Otto, K., Salvagiotto, G., Rehrauer, W., Vodyanik, M., Thomson, J., and Slukvin, I. (2009). Hematopoietic and endothelial differentiation of human induced pluripotent stem cells. Stem cells (Dayton, Ohio) *27*, 559-567.

Reference

Choudhary, C., Kumar, C., Gnad, F., Nielsen, M.L., Rehman, M., Walther, T.C., Olsen, J.V., and Mann, M. (2009). Lysine acetylation targets protein complexes and co-regulates major cellular functions. Science *325*, 834-840.

Christ, A., Gunther, P., Lauterbach, M.A.R., Duewell, P., Biswas, D., Pelka, K., Scholz, C.J., Oosting, M., Haendler, K., Bassler, K.*, et al.* (2018). Western Diet Triggers NLRP3-Dependent Innate Immune Reprogramming. Cell *172*, 162-175 e114.

Chung, J., Zhang, X., Allen, M., Wang, X., Ma, Y., Beecham, G., Montine, T.J., Younkin, S.G., Dickson, D.W., Golde, T.E.*, et al.* (2018). Genome-wide pleiotropy analysis of neuropathological traits related to Alzheimer's disease. Alzheimer's research & therapy *10*, 22.

Cochain, C., Vafadarnejad, E., Arampatzi, P., Pelisek, J., Winkels, H., Ley, K., Wolf, D., Saliba, A.E., and Zernecke, A. (2018). Single-Cell RNA-Seq Reveals the Transcriptional Landscape and Heterogeneity of Aortic Macrophages in Murine Atherosclerosis. Circ Res *122*, 1661-1674.

Combadiere, C., Potteaux, S., Rodero, M., Simon, T., Pezard, A., Esposito, B., Merval, R., Proudfoot, A., Tedgui, A., and Mallat, Z. (2008). Combined inhibition of CCL2, CX3CR1, and CCR5 abrogates Ly6C(hi) and Ly6C(lo) monocytosis and almost abolishes atherosclerosis in hypercholesterolemic mice. Circulation *117*, 1649-1657.

Cybulsky, M.I., Lichtman, A.H., Hajra, L., and Iiyama, K. (1999). Leukocyte adhesion molecules in atherogenesis. Clinica chimica acta *286*, 207-218.

DALYs, G.B.D., and Collaborators, H. (2018). Global, regional, and national disability-adjusted life-years (DALYs) for 359 diseases and injuries and healthy life expectancy (HALE) for 195 countries and territories, 1990-2017: a systematic analysis for the Global Burden of Disease Study 2017. Lancet *392*, 1859-1922.

Dang, W., Steffen, K.K., Perry, R., Dorsey, J.A., Johnson, F.B., Shilatifard, A., Kaeberlein, M., Kennedy, B.K., and Berger, S.L. (2009). Histone H4 lysine 16 acetylation regulates cellular lifespan. Nature *459*, 802-807.

Davies, M.J., Gordon, J., Gearing, A., Pigott, R., Woolf, N., Katz, D., and Kyriakopoulos, A. (1993). The expression of the adhesion molecules ICAM-1, VCAM-1, PECAM, and E-selectin in human atherosclerosis. The Journal of pathology *171*, 223-229.

Davis, C.A., Hitz, B.C., Sloan, C.A., Chan, E.T., Davidson, J.M., Gabdank, I., Hilton, J.A., Jain, K., Baymuradov, U.K., Narayanan, A.K.*, et al.* (2018). The Encyclopedia of DNA elements (ENCODE): data portal update. Nucleic Acids Res *46*, D794-D801.

De, S., Zelazny, E., Souhrada, J., and Souhrada, M. (1993). Interleukin-1 β stimulates the proliferation of cultured airway smooth muscle cells via platelet-derived growth factor. American journal of respiratory cell and molecular biology *9*, 645-651.

De Zoeten, E.F., Wang, L., Sai, H., Dillmann, W.H., and Hancock, W.W. (2010). Inhibition of HDAC9 increases T regulatory cell function and prevents colitis in mice. Gastroenterology *138*, 583-594.

Di Giorgio, E., Franforte, E., Cefalu, S., Rossi, S., Dei Tos, A.P., Brenca, M., Polano, M., Maestro, R., Paluvai, H., Picco, R.*, et al.* (2017). The co-existence of transcriptional activator and transcriptional repressor MEF2 complexes influences tumor aggressiveness. PLoS genetics *13*, e1006752.

Diaz-Gallo, L.M., Espino-Paisan, L., Fransen, K., Gomez-Garcia, M., van Sommeren, S., Cardena, C., Rodrigo, L., Mendoza, J.L., Taxonera, C., Nieto, A.*, et al.* (2011). Differential association of two PTPN22 coding variants with Crohn's disease and ulcerative colitis. Inflamm Bowel Dis *17*, 2287-2294.

Reference

Domingo-Fernández, R., Coll, R.C., Kearney, J., Breit, S., and O'Neill, L.A. (2017). The intracellular chloride channel proteins CLIC1 and CLIC4 induce IL-1β transcription and activate the NLRP3 inflammasome. Journal of Biological Chemistry *292*, 12077-12087.

Duan, L., Wei, L., Tian, Y., Zhang, Z., Hu, P., Wei, Q., Liu, S., Zhang, J., Wang, Y., Li, D.*, et al.* (2018). Novel Susceptibility Loci for Moyamoya Disease Revealed by a Genome-Wide Association Study. Stroke *49*, 11-18.

Duewell, P., Kono, H., Rayner, K.J., Sirois, C.M., Vladimer, G., Bauernfeind, F.G., Abela, G.S., Franchi, L., Nunez, G., Schnurr, M.*, et al.* (2010). NLRP3 inflammasomes are required for atherogenesis and activated by cholesterol crystals. Nature *464*, 1357-1361.

Erbay, E., Babaev, V.R., Mayers, J.R., Makowski, L., Charles, K.N., Snitow, M.E., Fazio, S., Wiest, M.M., Watkins, S.M., and Linton, M.F. (2009). Reducing endoplasmic reticulum stress through a macrophage lipid chaperone alleviates atherosclerosis. Nature medicine *15*, 1383.

Falcone, G.J., Malik, R., Dichgans, M., and Rosand, J. (2014). Current concepts and clinical applications of stroke genetics. Lancet Neurol *13*, 405-418.

Fatkhullina, A.R., Peshkova, I.O., and Koltsova, E.K. (2016). The Role of Cytokines in the Development of Atherosclerosis. Biochemistry (Mosc) *81*, 1358-1370.

Febbraio, M., Hajjar, D.P., and Silverstein, R.L. (2001). CD36: a class B scavenger receptor involved in angiogenesis, atherosclerosis, inflammation, and lipid metabolism. The Journal of clinical investigation *108*, 785-791.

Feng, Y., Schouteden, S., Geenens, R., Van Duppen, V., Herijgers, P., Holvoet, P., Van Veldhoven, P.P., and Verfaillie, C.M. (2012). Hematopoietic stem/progenitor cell proliferation and differentiation is differentially regulated by high-density and low-density lipoproteins in mice. PloS one *7*, e47286.

Fischer, A., Sananbenesi, F., Mungenast, A., and Tsai, L.-H. (2010). Targeting the correct HDAC (s) to treat cognitive disorders. Trends in pharmacological sciences *31*, 605-617.

Fischle, W., Dequiedt, F., Hendzel, M.J., Guenther, M.G., Lazar, M.A., Voelter, W., and Verdin, E. (2002). Enzymatic activity associated with class II HDACs is dependent on a multiprotein complex containing HDAC3 and SMRT/N-CoR. Molecular cell *9*, 45-57.

Fischle, W., Emiliani, S., Hendzel, M.J., Nagase, T., Nomura, N., Voelter, W., and Verdin, E. (1999). A new family of human histone deacetylases related to Saccharomyces cerevisiae HDA1p. J Biol Chem *274*, 11713-11720.

Flossmann, E., Schulz, U.G., and Rothwell, P.M. (2004). Systematic review of methods and results of studies of the genetic epidemiology of ischemic stroke. Stroke *35*, 212-227.

Franceschini, N., Giambartolomei, C., de Vries, P.S., Finan, C., Bis, J.C., Huntley, R.P., Lovering, R.C., Tajuddin, S.M., Winkler, T.W., Graff, M.*, et al.* (2018). GWAS and colocalization analyses implicate carotid intima-media thickness and carotid plaque loci in cardiovascular outcomes. Nat Commun *9*, 5141.

Fung, T.T., Rexrode, K.M., Mantzoros, C.S., Manson, J.E., Willett, W.C., and Hu, F.B. (2009). Mediterranean diet and incidence and mortality of coronary heart disease and stroke in women. Circulation *119*, 1093.

Fustinoni, O., and Biller, J. (2000). Ethnicity and stroke: beware of the fallacies (Am Heart Assoc).

Galkina, E., and Ley, K. (2009). Immune and inflammatory mechanisms of atherosclerosis. Annual review of immunology *27*.

Geer, J.C., McGill Jr, H.C., and Strong, J.P. (1961). The fine structure of human atherosclerotic lesions. The American journal of pathology *38*, 263.

Reference

Ghisletti, S., Barozzi, I., Mietton, F., Polletti, S., De Santa, F., Venturini, E., Gregory, L., Lonie, L., Chew, A., and Wei, C.-L. (2010). Identification and characterization of enhancers controlling the inflammatory gene expression program in macrophages. Immunity *32*, 317-328.

Ghisletti, S., and Natoli, G. (2013). Deciphering cis-regulatory control in inflammatory cells. Philos Trans R Soc Lond B Biol Sci *368*, 20120370.

Gill, J.S., Zezulka, A.V., Shipley, M.J., Gill, S.K., and Beevers, D.G. (1986). Stroke and alcohol consumption. New England Journal of Medicine *315*, 1041-1046.

Gimbrone, M.A., Jr., and Garcia-Cardena, G. (2016). Endothelial Cell Dysfunction and the Pathobiology of Atherosclerosis. Circ Res *118*, 620-636.

Giral, H., Landmesser, U., and Kratzer, A. (2018). Into the Wild: GWAS Exploration of Non-coding RNAs. Front Cardiovasc Med *5*, 181.

Gong, Y.N., Wang, X., Wang, J., Yang, Z., Li, S., Yang, J., Liu, L., Lei, X., and Shao, F. (2010). Chemical probing reveals insights into the signaling mechanism of inflammasome activation. Cell Res *20*, 1289-1305.

Gorelick, P.B. (2019). The global burden of stroke: persistent and disabling. Lancet Neurol *18*, 417-418.

Green, J.P., Yu, S., Martín-Sánchez, F., Pelegrin, P., Lopez-Castejon, G., Lawrence, C.B., and Brough, D. (2018). Chloride regulates dynamic NLRP3-dependent ASC oligomerization and inflammasome priming. Proceedings of the National Academy of Sciences *115*, E9371-E9380.

Grozinger, C.M., Hassig, C.A., and Schreiber, S.L. (1999). Three proteins define a class of human histone deacetylases related to yeast Hda1p. Proc Natl Acad Sci U S A *96*, 4868-4873.

Grozinger, C.M., and Schreiber, S.L. (2000). Regulation of histone deacetylase 4 and 5 and transcriptional activity by 14-3-3-dependent cellular localization. Proceedings of the National Academy of Sciences *97*, 7835-7840.

Guo, C., Xie, S., Chi, Z., Zhang, J., Liu, Y., Zhang, L., Zheng, M., Zhang, X., Xia, D., Ke, Y.*, et al.* (2016). Bile Acids Control Inflammation and Metabolic Disorder through Inhibition of NLRP3 Inflammasome. Immunity *45*, 944.

Gupta, R.M., Hadaya, J., Trehan, A., Zekavat, S.M., Roselli, C., Klarin, D., Emdin, C.A., Hilvering, C.R.E., Bianchi, V., Mueller, C*., et al.* (2017). A Genetic Variant Associated with Five Vascular Diseases Is a Distal Regulator of Endothelin-1 Gene Expression. Cell *170*, 522-533 e515.

Haberland, M., Arnold, M.A., McAnally, J., Phan, D., Kim, Y., and Olson, E.N. (2007). Regulation of HDAC9 gene expression by MEF2 establishes a negative-feedback loop in the transcriptional circuitry of muscle differentiation. Mol Cell Biol *27*, 518-525.

Hajra, L., Evans, A.I., Chen, M., Hyduk, S.J., Collins, T., and Cybulsky, M.I. (2000). The NF-κB signal transduction pathway in aortic endothelial cells is primed for activation in regions predisposed to atherosclerotic lesion formation. Proceedings of the National Academy of Sciences *97*, 9052-9057.

Han, S., Lear, T.B., Jerome, J.A., Rajbhandari, S., Snavely, C.A., Gulick, D.L., Gibson, K.F., Zou, C., Chen, B.B., and Mallampalli, R.K. (2015). Lipopolysaccharide Primes the NALP3 Inflammasome by Inhibiting Its Ubiquitination and Degradation Mediated by the SCFFBXL2 E3 Ligase. J Biol Chem *290*, 18124-18133.

Han, X., Han, X., Wang, Z., Shen, J., and Dong, Q. (2016). HDAC9 regulates ox-LDL-induced endothelial cell apoptosis by participating in inflammatory reactions. Front Biosci (Landmark Ed) *21*, 907-917.

Reference

Hardy, J., and Singleton, A. (2009). Genomewide association studies and human disease. N Engl J Med *360*, 1759-1768.

He, Y., Zeng, M.Y., Yang, D., Motro, B., and Nunez, G. (2016). NEK7 is an essential mediator of NLRP3 activation downstream of potassium efflux. Nature *530*, 354-357.

Heintzman, N.D., Stuart, R.K., Hon, G., Fu, Y., Ching, C.W., Hawkins, R.D., Barrera, L.O., Van Calcar, S., Qu, C., Ching, K.A*., et al.* (2007). Distinct and predictive chromatin signatures of transcriptional promoters and enhancers in the human genome. Nat Genet *39*, 311-318.

Hofker, M.H., van Vlijmen, B.J., and Havekes, L.M. (1998). Transgenic mouse models to study the role of APOE in hyperlipidemia and atherosclerosis. Atherosclerosis *137*, 1-11.

Hofmann, T.G., Moller, A., Sirma, H., Zentgraf, H., Taya, Y., Droge, W., Will, H., and Schmitz, M.L. (2002). Regulation of p53 activity by its interaction with homeodomain-interacting protein kinase-2. Nat Cell Biol *4*, 1-10.

Hotamisligil, G.S. (2010). Endoplasmic reticulum stress and atherosclerosis. Nat Med *16*, 396-399.

Hu, Y., Sun, L., Tao, S., Dai, M., Wang, Y., Li, Y., and Wu, J. (2019). Clinical significance of HDAC9 in hepatocellular carcinoma. Cell Mol Biol (Noisy-le-grand) *65*, 23-28.

Huang, Y., Jian, W., Zhao, J., and Wang, G. (2018). Overexpression of HDAC9 is associated with poor prognosis and tumor progression of breast cancer in Chinese females. OncoTargets and therapy *11*, 2177-2184.

Hwang, I., Lee, E., Jeon, S.A., and Yu, J.W. (2015). Histone deacetylase 6 negatively regulates NLRP3 inflammasome activation. Biochem Biophys Res Commun *467*, 973-978.

Jerrard-Dunne, P., Cloud, G., Hassan, A., and Markus, H.S. (2003). Evaluating the genetic component of ischemic stroke subtypes: a family history study. Stroke *34*, 1364-1369.

Jin, C., and Flavell, R.A. (2010). Molecular mechanism of NLRP3 inflammasome activation. Journal of clinical immunology *30*, 628-631.

Jo, E.-K., Kim, J.K., Shin, D.-M., and Sasakawa, C. (2016). Molecular mechanisms regulating NLRP3 inflammasome activation. Cellular & molecular immunology *13*, 148.

Johnson, J.L., George, S.J., Newby, A.C., and Jackson, C.L. (2005). Divergent effects of matrix metalloproteinases 3, 7, 9, and 12 on atherosclerotic plaque stability in mouse brachiocephalic arteries. Proceedings of the National Academy of Sciences *102*, 15575-15580.

Jonasson, L., Holm, J., Skalli, O., Bondjers, G., and Hansson, G.K. (1986). Regional accumulations of T cells, macrophages, and smooth muscle cells in the human atherosclerotic plaque. Arteriosclerosis *6*, 131-138.

Kawashima, A., Karasawa, T., Tago, K., Kimura, H., Kamata, R., Usui-Kawanishi, F., Watanabe, S., Ohta, S., Funakoshi-Tago, M., Yanagisawa, K*., et al.* (2017). ARIH2 Ubiquitinates NLRP3 and Negatively Regulates NLRP3 Inflammasome Activation in Macrophages. J Immunol *199*, 3614-3622.

Kim, K., Shim, D., Lee, J.S., Zaitsev, K., Williams, J.W., Kim, K.W., Jang, M.Y., Seok Jang, H., Yun, T.J., Lee, S.H*., et al.* (2018). Transcriptome Analysis Reveals Nonfoamy Rather Than Foamy Plaque Macrophages Are Proinflammatory in Atherosclerotic Murine Models. Circ Res *123*, 1127-1142.

Kim, S., Bauernfeind, F., Ablasser, A., Hartmann, G., Fitzgerald, K.A., Latz, E., and Hornung, V. (2010). Listeria monocytogenes is sensed by the NLRP3 and AIM2 inflammasome. European journal of immunology *40*, 1545-1551.

Ko, K.A., Fujiwara, K., Krishnan, S., and Abe, J.I. (2017). En Face Preparation of Mouse Blood Vessels. J Vis Exp.

Reference

Konstantinov, I.E., Mejevoi, N., and Anichkov, N.M. (2006). Nikolai N. Anichkov and his theory of atherosclerosis. Tex Heart Inst J *33*, 417-423.

Lansdell, T.A., Fisher, C., Simmonds, K., Reeves, M.J., Woo, D., Dorrance, A.M., and Demel, S.L. (2019). Rs10230207 genotype confers changes in HDAC9 and TWIST1, but not FERD3L in lymphoblasts from patients with intracranial aneurysm. Neurogenetics *20*, 83-89.

Lebeaupin, C., Proics, E., de Bieville, C.H., Rousseau, D., Bonnafous, S., Patouraux, S., Adam, G., Lavallard, V.J., Rovere, C., Le Thuc, O.*, et al.* (2015). ER stress induces NLRP3 inflammasome activation and hepatocyte death. Cell Death Dis *6*, e1879.

Lee, C.D., Folsom, A.R., and Blair, S.N. (2003). Physical activity and stroke risk: a meta-analysis. Stroke *34*, 2475-2481.

Lee, G.-S., Subramanian, N., Kim, A.I., Aksentijevich, I., Goldbach-Mansky, R., Sacks, D.B., Germain, R.N., Kastner, D.L., and Chae, J.J. (2012). The calcium-sensing receptor regulates the NLRP3 inflammasome through Ca 2+ and cAMP. Nature *492*, 123.

Legube, G., and Trouche, D. (2003). Regulating histone acetyltransferases and deacetylases. EMBO reports *4*, 944-947.

Li, B., Hu, C., Liu, J., Liao, X., Xun, J., Xiao, M., and Yan, J. (2019). Associations among Genetic Variants and Intracranial Aneurysm in a Chinese Population. Yonsei Med J *60*, 651-658.

Li, X., Zhang, Q., Ding, Y., Liu, Y., Zhao, D., Zhao, K., Shen, Q., Liu, X., Zhu, X., Li, N.*, et al.* (2016). Methyltransferase Dnmt3a upregulates HDAC9 to deacetylate the kinase TBK1 for activation of antiviral innate immunity. Nat Immunol *17*, 806-815.

Libby, P. (2017). Interleukin-1 beta as a target for atherosclerosis therapy: biological basis of CANTOS and beyond. Journal of the American College of Cardiology *70*, 2278-2289.

Libby, P., Aikawa, M., and Jain, M. (2006). Vascular endothelium and atherosclerosis. In The vascular endothelium II (Springer), pp. 285-306.

Libby, P., Ridker, P.M., and Hansson, G.K. (2011). Progress and challenges in translating the biology of atherosclerosis. Nature *473*, 317-325.

Lin, J.D., Nishi, H., Poles, J., Niu, X., McCauley, C., Rahman, K., Brown, E.J., Yeung, S.T., Vozhilla, N., Weinstock, A.*, et al.* (2019). Single-cell analysis of fate-mapped macrophages reveals heterogeneity, including stem-like properties, during atherosclerosis progression and regression. JCI Insight *4*.

Lino Cardenas, C.L., Kessinger, C.W., Cheng, Y., MacDonald, C., MacGillivray, T., Ghoshhajra, B., Huleihel, L., Nuri, S., Yeri, A.S., Jaffer, F.A.*, et al.* (2018). An HDAC9-MALAT1-BRG1 complex mediates smooth muscle dysfunction in thoracic aortic aneurysm. Nat Commun *9*, 1009.

Lino Cardenas, C.L., Kessinger, C.W., Chou, E.L., Ghoshhajra, B., Yeri, A.S., Das, S., Weintraub, N.L., Malhotra, R., Jaffer, F.A., and Lindsay, M.E. (2019). HDAC9 complex inhibition improves smooth muscle-dependent stenotic vascular disease. JCI insight *4*.

Little, G.H., Bai, Y., Williams, T., and Poizat, C. (2007). Nuclear calcium/calmodulin-dependent protein kinase IIdelta preferentially transmits signals to histone deacetylase 4 in cardiac cells. J Biol Chem *282*, 7219-7231.

Liu, C.L., Wang, Y., Liao, M., Wemmelund, H., Ren, J., Fernandes, C., Zhou, Y., Sukhova, G.K., Lindholt, J.S., Johnsen, S.P.*, et al.* (2016). Allergic Lung Inflammation Aggravates Angiotensin II-Induced Abdominal Aortic Aneurysms in Mice. Arterioscler Thromb Vasc Biol *36*, 69-77.

Loppnow, H., and Libby, P. (1990). Proliferating or interleukin 1-activated human vascular smooth muscle cells secrete copious interleukin 6. J Clin Invest *85*, 731-738.

Reference

Lu, S., Li, H., Li, K., and Fan, X.D. (2018). HDAC9 promotes brain ischemic injury by provoking IkappaBalpha/NF-kappaB and MAPKs signaling pathways. Biochem Biophys Res Commun *503*, 1322-1329.

Luttun, A., Lutgens, E., Manderveld, A., Maris, K., Collen, D., Carmeliet, P., and Moons, L. (2004). Loss of matrix metalloproteinase-9 or matrix metalloproteinase-12 protects apolipoprotein E–deficient mice against atherosclerotic media destruction but differentially affects plaque growth. Circulation *109*, 1408-1414.

Ma, Z., Liu, D., Di, S., Zhang, Z., Li, W., Zhang, J., Xu, L., Guo, K., Zhu, Y., Li, X.*, et al.* (2019). Histone deacetylase 9 downregulation decreases tumor growth and promotes apoptosis in non-small cell lung cancer after melatonin treatment. J Pineal Res *67*, e12587.

MacLeod, D.C., Strauss, B.H., de Jong, M., Escaned, J., Umans, V.A., van Suylen, R.-J., Verkerk, A., de Feyter, P.J., and Serruys, P.W. (1994). Proliferation and extracellular matrix synthesis of smooth muscle cells cultured from human coronary atherosclerotic and restenotic lesions. Journal of the American College of Cardiology *23*, 59-65.

Malek, A.M., Alper, S.L., and Izumo, S. (1999). Hemodynamic shear stress and its role in atherosclerosis. Jama *282*, 2035-2042.

Malik, R., Chauhan, G., Traylor, M., Sargurupremraj, M., Okada, Y., Mishra, A., Rutten-Jacobs, L., Giese, A.K., van der Laan, S.W., Gretarsdottir, S.*, et al.* (2018). Multiancestry genome-wide association study of 520,000 subjects identifies 32 loci associated with stroke and stroke subtypes. Nat Genet *50*, 524-537.

Malik, R., and Dichgans, M. (2018). Challenges and opportunities in stroke genetics. Cardiovasc Res *114*, 1226-1240.

Mariathasan, S., Weiss, D.S., Newton, K., McBride, J., O'Rourke, K., Roose-Girma, M., Lee, W.P., Weinrauch, Y., Monack, D.M., and Dixit, V.M. (2006). Cryopyrin activates the inflammasome in response to toxins and ATP. Nature *440*, 228-232.

Markus, H.S. (2011). Stroke genetics. Hum Mol Genet *20*, R124-131.

Markus, H.S., Makela, K.M., Bevan, S., Raitoharju, E., Oksala, N., Bis, J.C., O'Donnell, C., Hainsworth, A., and Lehtimaki, T. (2013). Evidence HDAC9 genetic variant associated with ischemic stroke increases risk via promoting carotid atherosclerosis. Stroke *44*, 1220-1225.

Massberg, S., Vogt, F., Dickfeld, T., Brand, K., Page, S., and Gawaz, M. (2003). Activated platelets trigger an inflammatory response and enhance migration of aortic smooth muscle cells. Thrombosis research *110*, 187-194.

Masumoto, H., Hawke, D., Kobayashi, R., and Verreault, A. (2005). A role for cell-cycle-regulated histone H3 lysine 56 acetylation in the DNA damage response. Nature *436*, 294-298.

Matsukura, M., Ozaki, K., Takahashi, A., Onouchi, Y., Morizono, T., Komai, H., Shigematsu, H., Kudo, T., Inoue, Y., Kimura, H.*, et al.* (2015). Genome-Wide Association Study of Peripheral Arterial Disease in a Japanese Population. PloS one *10*, e0139262.

Menu, P., Pellegrin, M., Aubert, J., Bouzourene, K., Tardivel, A., Mazzolai, L., and Tschopp, J. (2011). Atherosclerosis in ApoE-deficient mice progresses independently of the NLRP3 inflammasome. Cell death & disease *2*, e137.

Merhi-Soussi, F., Kwak, B.R., Magne, D., Chadjichristos, C., Berti, M., Pelli, G., James, R.W., Mach, F., and Gabay, C. (2005). Interleukin-1 plays a major role in vascular inflammation and atherosclerosis in male apolipoprotein E-knockout mice. Cardiovasc Res *66*, 583-593.

Meyer, J.S., Rogers, R.L., Mortel, K.F., and Judd, B.W. (1987). Hyperlipidemia is a risk factor for decreased cerebral perfusion and stroke. Archives of neurology *44*, 418-422.

Reference

Mohanta, S.K., Yin, C., Peng, L., Srikakulapu, P., Bontha, V., Hu, D., Weih, F., Weber, C., Gerdes, N., and Habenicht, A.J. (2014). Artery tertiary lymphoid organs contribute to innate and adaptive immune responses in advanced mouse atherosclerosis. Circ Res *114*, 1772-1787.

Morgan, A.R., Rerkasem, K., Gallagher, P.J., Zhang, B., Morris, G.E., Calder, P.C., Grimble, R.F., Eriksson, P., McPheat, W.L., and Shearman, C.P. (2004). Differences in matrix metalloproteinase-1 and matrix metalloproteinase-12 transcript levels among carotid atherosclerotic plaques with different histopathological characteristics. Stroke *35*, 1310-1315.

Muñoz-Planillo, R., Kuffa, P., Martínez-Colón, G., Smith, B.L., Rajendiran, T.M., and Núñez, G. (2013). K+ efflux is the common trigger of NLRP3 inflammasome activation by bacterial toxins and particulate matter. Immunity *38*, 1142-1153.

Murakami, T., Ockinger, J., Yu, J., Byles, V., McColl, A., Hofer, A.M., and Horng, T. (2012). Critical role for calcium mobilization in activation of the NLRP3 inflammasome. Proceedings of the National Academy of Sciences *109*, 11282-11287.

Murphy, A.J., Akhtari, M., Tolani, S., Pagler, T., Bijl, N., Kuo, C.-L., Wang, M., Sanson, M., Abramowicz, S., and Welch, C. (2011). ApoE regulates hematopoietic stem cell proliferation, monocytosis, and monocyte accumulation in atherosclerotic lesions in mice. The Journal of clinical investigation *121*, 4138-4149.

Nakashima, Y., Plump, A.S., Raines, E.W., Breslow, J.L., and Ross, R. (1994). ApoE-deficient mice develop lesions of all phases of atherosclerosis throughout the arterial tree. Arterioscler Thromb *14*, 133-140.

Nelson, C.P., Goel, A., Butterworth, A.S., Kanoni, S., Webb, T.R., Marouli, E., Zeng, L., Ntalla, I., Lai, F.Y., Hopewell, J.C.*, et al.* (2017). Association analyses based on false discovery rate implicate new loci for coronary artery disease. Nature genetics *49*, 1385-1391.

Newby, A.C. (2007). Metalloproteinases and vulnerable atherosclerotic plaques. Trends in cardiovascular medicine *17*, 253-258.

Nikkari, S.T., Järveläinen, H., Wight, T.N., Ferguson, M., and Clowes, A.W. (1994). Smooth muscle cell expression of extracellular matrix genes after arterial injury. The American journal of pathology *144*, 1348.

Oksala, N.K.J., Seppala, I., Rahikainen, R., Makela, K.M., Raitoharju, E., Illig, T., Klopp, N., Kholova, I., Laaksonen, R., Karhunen, P.J.*, et al.* (2017). Synergistic Expression of Histone Deacetylase 9 and Matrix Metalloproteinase 12 in M4 Macrophages in Advanced Carotid Plaques. European journal of vascular and endovascular surgery : the official journal of the European Society for Vascular Surgery *53*, 632-640.

Orford, J.L., Selwyn, A.P., Ganz, P., Popma, J.J., and Rogers, C. (2000). The comparative pathobiology of atherosclerosis and restenosis. The American journal of cardiology *86*, 6H-11H.

Paauw, N.D., Lely, A.T., Joles, J.A., Franx, A., Nikkels, P.G., Mokry, M., and van Rijn, B.B. (2018). H3K27 acetylation and gene expression analysis reveals differences in placental chromatin activity in fetal growth restriction. Clin Epigenetics *10*, 85.

Paletta-Silva, R., Rocco-Machado, N., and Meyer-Fernandes, J.R. (2013). NADPH oxidase biology and the regulation of tyrosine kinase receptor signaling and cancer drug cytotoxicity. Int J Mol Sci *14*, 3683-3704.

Parra, M., and Verdin, E. (2010). Regulatory signal transduction pathways for class IIa histone deacetylases. Curr Opin Pharmacol *10*, 454-460.

Reference

Patnala, R., Clements, J., and Batra, J. (2013). Candidate gene association studies: a comprehensive guide to useful in silico tools. BMC Genet *14*, 39.

Petrie, K., Guidez, F., Howell, L., Healy, L., Waxman, S., Greaves, M., and Zelent, A. (2003). The histone deacetylase 9 gene encodes multiple protein isoforms. The Journal of biological chemistry *278*, 16059-16072.

Petrilli, V., Papin, S., Dostert, C., Mayor, A., Martinon, F., and Tschopp, J. (2007). Activation of the NALP3 inflammasome is triggered by low intracellular potassium concentration. Cell death and differentiation *14*, 1583.

Pober, J.S., and Cotran, R.S. (1990). Cytokines and endothelial cell biology. Physiol Rev *70*, 427-451.

Prescott, M.F., Sawyer, W.K., VON LINDEN-REED, J., Jeune, M., Chou, M., Caplan, S.L., and Jeng, A.Y. (1999). Effect of matrix metalloproteinase inhibition on progression of atherosclerosis and aneurysm in LDL receptor-deficient mice overexpressing MMP-3, MMP-12, and MMP-13 and on restenosis in rats after balloon injury. Annals of the New York Academy of Sciences *878*, 179-190.

Prestel, M., Prell-Schicker, C., Webb, T., Malik, R., Lindner, B., Ziesch, N., Rex-Haffner, M., Roh, S., Viturawong, T., Lehm, M.*, et al.* (2019). The Atherosclerosis Risk Variant rs2107595 Mediates Allele-Specific Transcriptional Regulation of HDAC9 via E2F3 and Rb1. Stroke *50*, 2651-2660.

Py, B.F., Kim, M.-S., Vakifahmetoglu-Norberg, H., and Yuan, J. (2013a). Deubiquitination of NLRP3 by BRCC3 critically regulates inflammasome activity. Molecular cell *49*, 331-338.

Py, B.F., Kim, M.S., Vakifahmetoglu-Norberg, H., and Yuan, J. (2013b). Deubiquitination of NLRP3 by BRCC3 critically regulates inflammasome activity. Mol Cell *49*, 331-338.

Rehman, M.U., Jawaid, P., Yoshihisa, Y., Li, P., Zhao, Q.L., Narita, K., Katoh, T., Kondo, T., and Shimizu, T. (2014). Spiruchostatin A and B, novel histone deacetylase inhibitors, induce apoptosis through reactive oxygen species-mitochondria pathway in human lymphoma U937 cells. Chem Biol Interact *221*, 24-34.

Roadmap Epigenomics, C., Kundaje, A., Meuleman, W., Ernst, J., Bilenky, M., Yen, A., Heravi-Moussavi, A., Kheradpour, P., Zhang, Z., Wang, J.*, et al.* (2015). Integrative analysis of 111 reference human epigenomes. Nature *518*, 317-330.

Ross, R. (1999). Atherosclerosis--an inflammatory disease. N Engl J Med *340*, 115-126.

Rudijanto, A. (2007). The role of vascular smooth muscle cells on the pathogenesis of atherosclerosis. Acta Med Indones *39*, 86-93.

Sakaguchi, K., Herrera, J.E., Saito, S., Miki, T., Bustin, M., Vassilev, A., Anderson, C.W., and Appella, E. (1998). DNA damage activates p53 through a phosphorylation-acetylation cascade. Genes Dev *12*, 2831-2841.

Salgado, E., Bian, X., Feng, A., Shim, H., and Liang, Z. (2018). HDAC9 overexpression confers invasive and angiogenic potential to triple negative breast cancer cells via modulating microRNA-206. Biochem Biophys Res Commun *503*, 1087-1091.

Salian-Mehta, S., Xu, M., McKinsey, T.A., Tobet, S., and Wierman, M.E. (2015). Novel Interaction of Class IIb Histone Deacetylase 6 (HDAC6) with Class IIa HDAC9 Controls Gonadotropin Releasing Hormone (GnRH) Neuronal Cell Survival and Movement. J Biol Chem *290*, 14045-14056.

Sanford, J.A., O'Neill, A.M., Zouboulis, C.C., and Gallo, R.L. (2019). Short-Chain Fatty Acids from Cutibacterium acnes Activate Both a Canonical and Epigenetic Inflammatory Response in Human Sebocytes. J Immunol *202*, 1767-1776.

Reference

Santos-Rosa, H., Schneider, R., Bannister, A.J., Sherriff, J., Bernstein, B.E., Emre, N.C., Schreiber, S.L., Mellor, J., and Kouzarides, T. (2002). Active genes are tri-methylated at K4 of histone H3. Nature *419*, 407-411.

Sata, M., Saiura, A., Kunisato, A., Tojo, A., Okada, S., Tokuhisa, T., Hirai, H., Makuuchi, M., Hirata, Y., and Nagai, R. (2002). Hematopoietic stem cells differentiate into vascular cells that participate in the pathogenesis of atherosclerosis. Nature medicine *8*, 403.

Schiffrin, E.L. (2002). Beyond blood pressure: the endothelium and atherosclerosis progression (Oxford University Press).

Schiopu, A., and Cotoi, O.S. (2013). S100A8 and S100A9: DAMPs at the crossroads between innate immunity, traditional risk factors, and cardiovascular disease. Mediators of inflammation *2013*.

Schober, A., Bernhagen, J., and Weber, C. (2008). Chemokine-like functions of MIF in atherosclerosis. J Mol Med (Berl) *86*, 761-770.

Scholtes, V.P., Johnson, J.L., Jenkins, N., Sala-Newby, G.B., de Vries, J.P.P., de Borst, G.J., de Kleijn, D.P., Moll, F.L., Pasterkamp, G., and Newby, A.C. (2012). Carotid Atherosclerotic Plaque Matrix Metalloproteinase-12–Positive Macrophage Subpopulation Predicts Adverse Outcome After Endarterectomy. Journal of the American Heart Association *1*, e001040.

Schwartz, S.M., Virmani, R., and Rosenfeld, M.E. (2000a). The good smooth muscle cells in atherosclerosis. Curr Atheroscler Rep *2*, 422-429.

Schwartz, S.M., Virmani, R., and Rosenfeld, M.E. (2000b). The good smooth muscle cells in atherosclerosis. Current atherosclerosis reports *2*, 422-429.

Shi, W., Wei, X., Wang, Z., Han, H., Fu, Y., Liu, J., Zhang, Y., Guo, J., Dong, C., and Zhou, D. (2016). HDAC 9 exacerbates endothelial injury in cerebral ischaemia/reperfusion injury. Journal of cellular and molecular medicine *20*, 1139-1149.

Shimada, K., Crother, T.R., Karlin, J., Dagvadorj, J., Chiba, N., Chen, S., Ramanujan, V.K., Wolf, A.J., Vergnes, L., Ojcius, D.M.*, et al.* (2012). Oxidized mitochondrial DNA activates the NLRP3 inflammasome during apoptosis. Immunity *36*, 401-414.

Shimbo, H., Oyoshi, T., and Kurosawa, K. (2018). Contiguous gene deletion neighboring TWIST1 identified in a patient with Saethre-Chotzen syndrome associated with neurodevelopmental delay: Possible contribution of HDAC9. Congenital anomalies *58*, 33-35.

Shimokawa, H., Ito, A., Fukumoto, Y., Kadokami, T., Nakaike, R., Sakata, M., Takayanagi, T., Egashira, K., and Takeshita, A. (1996). Chronic treatment with interleukin-1 beta induces coronary intimal lesions and vasospastic responses in pigs in vivo. The role of platelet-derived growth factor. J Clin Invest *97*, 769-776.

Shlyueva, D., Stampfel, G., and Stark, A. (2014). Transcriptional enhancers: from properties to genome-wide predictions. Nat Rev Genet *15*, 272-286.

Shroff, N., Ander, B.P., Zhan, X., Stamova, B., Liu, D., Hull, H., Hamade, F.R., Dykstra-Aiello, C., Ng, K., Sharp, F.R.*, et al.* (2019). HDAC9 Polymorphism Alters Blood Gene Expression in Patients with Large Vessel Atherosclerotic Stroke. Transl Stroke Res *10*, 19-25.

Song, N., Liu, Z.S., Xue, W., Bai, Z.F., Wang, Q.Y., Dai, J., Liu, X., Huang, Y.J., Cai, H., Zhan, X.Y.*, et al.* (2017). NLRP3 Phosphorylation Is an Essential Priming Event for Inflammasome Activation. Mol Cell *68*, 185-197 e186.

Spalinger, M.R., Kasper, S., Gottier, C., Lang, S., Atrott, K., Vavricka, S.R., Scharl, S., Raselli, T., Frey-Wagner, I., Gutte, P.M.*, et al.* (2016). NLRP3 tyrosine phosphorylation is controlled by protein tyrosine phosphatase PTPN22. J Clin Invest *126*, 4388.

Reference

Spracklen, C.N., Karaderi, T., Yaghootkar, H., Schurmann, C., Fine, R.S., Kutalik, Z., Preuss, M.H., Lu, Y., Wittemans, L.B.L., Adair, L.S*., et al.* (2019). Exome-Derived Adiponectin-Associated Variants Implicate Obesity and Lipid Biology. Am J Hum Genet *105*, 15-28.

Sun, S., Han, Y., Liu, J., Fang, Y., Tian, Y., Zhou, J., Ma, D., and Wu, P. (2014). Trichostatin A targets the mitochondrial respiratory chain, increasing mitochondrial reactive oxygen species production to trigger apoptosis in human breast cancer cells. PLoS One *9*, e91610.

Suzuki, H., Kurihara, Y., Takeya, M., Kamada, N., Kataoka, M., Jishage, K., Ueda, O., Sakaguchi, H., Higashi, T., and Suzuki, T. (1997). A role for macrophage scavenger receptors in atherosclerosis and susceptibility to infection. Nature *386*, 292.

Swanson, K.V., Deng, M., and Ting, J.P. (2019). The NLRP3 inflammasome: molecular activation and regulation to therapeutics. Nat Rev Immunol *19*, 477-489.

Swirski, F.K., Libby, P., Aikawa, E., Alcaide, P., Luscinskas, F.W., Weissleder, R., and Pittet, M.J. (2007). Ly-6Chi monocytes dominate hypercholesterolemia-associated monocytosis and give rise to macrophages in atheromata. J Clin Invest *117*, 195-205.

Szanto, A., Balint, B.L., Nagy, Z.S., Barta, E., Dezso, B., Pap, A., Szeles, L., Poliska, S., Oros, M., and Evans, R.M. (2010). STAT6 transcription factor is a facilitator of the nuclear receptor PPARγ-regulated gene expression in macrophages and dendritic cells. Immunity *33*, 699-712.

Szmitko, P.E., Wang, C.-H., Weisel, R.D., de Almeida, J.R., Anderson, T.J., and Verma, S. (2003). New markers of inflammation and endothelial cell activation: Part I. Circulation *108*, 1917-1923.

Tabas, I. (2010). The role of endoplasmic reticulum stress in the progression of atherosclerosis. Circ Res *107*, 839-850.

Tacke, F., Alvarez, D., Kaplan, T.J., Jakubzick, C., Spanbroek, R., Llodra, J., Garin, A., Liu, J., Mack, M., van Rooijen, N*., et al.* (2007). Monocyte subsets differentially employ CCR2, CCR5, and CX3CR1 to accumulate within atherosclerotic plaques. J Clin Invest *117*, 185-194.

Tang, T., Lang, X., Xu, C., Wang, X., Gong, T., Yang, Y., Cui, J., Bai, L., Wang, J., and Jiang, W. (2017). CLICs-dependent chloride efflux is an essential and proximal upstream event for NLRP3 inflammasome activation. Nature communications *8*, 202.

Tao, R., De Zoeten, E.F., Özkaynak, E., Chen, C., Wang, L., Porrett, P.M., Li, B., Turka, L.A., Olson, E.N., and Greene, M.I. (2007). Deacetylase inhibition promotes the generation and function of regulatory T cells. Nature medicine *13*, 1299.

Thierry-Mieg, D., and Thierry-Mieg, J. (2006). AceView: a comprehensive cDNA-supported gene and transcripts annotation. Genome Biol *7 Suppl 1*, S12 11-14.

Thorp, E., Li, G., Seimon, T.A., Kuriakose, G., Ron, D., and Tabas, I. (2009). Reduced apoptosis and plaque necrosis in advanced atherosclerotic lesions of Apoe−/− and Ldlr−/− mice lacking CHOP. Cell metabolism *9*, 474-481.

Traylor, M., Mäkelä, K.-M., Kilarski, L.L., Holliday, E.G., Devan, W.J., Nalls, M.A., Wiggins, K.L., Zhao, W., Cheng, Y.-C., and Achterberg, S. (2014). A novel MMP12 locus is associated with large artery atherosclerotic stroke using a genome-wide age-at-onset informed approach. PLoS genetics *10*, e1004469.

Trikha, P., Sharma, N., Opavsky, R., Reyes, A., Pena, C., Ostrowski, M.C., Roussel, M.F., and Leone, G. (2011). E2f1-3 are critical for myeloid development. J Biol Chem *286*, 4783-4795.

Tsai, J.-C., Perrella, M.A., Yoshizumi, M., Hsieh, C.-M., Haber, E., Schlegel, R., and Lee, M.-E. (1994). Promotion of vascular smooth muscle cell growth by homocysteine: a link to atherosclerosis. Proceedings of the National Academy of Sciences *91*, 6369-6373.

Tschopp, J., and Schroder, K. (2010). NLRP3 inflammasome activation: The convergence of multiple signalling pathways on ROS production? Nature reviews immunology *10*, 210.

Reference

Uslu, V.V., Petretich, M., Ruf, S., Langenfeld, K., Fonseca, N.A., Marioni, J.C., and Spitz, F. (2014). Long-range enhancers regulating Myc expression are required for normal facial morphogenesis. Nat Genet *46*, 753-758.

van der Vorst, E.P., Doring, Y., and Weber, C. (2015). Chemokines and their receptors in Atherosclerosis. J Mol Med (Berl) *93*, 963-971.

van Noort, V., Seebacher, J., Bader, S., Mohammed, S., Vonkova, I., Betts, M.J., Kühner, S., Kumar, R., Maier, T., and O'Flaherty, M. (2012). Cross-talk between phosphorylation and lysine acetylation in a genome-reduced bacterium. Molecular systems biology *8*.

van Rooij, E., Fielitz, J., Sutherland, L.B., Thijssen, V.L., Crijns, H.J., Dimaio, M.J., Shelton, J., De Windt, L.J., Hill, J.A., and Olson, E.N. (2010). Myocyte enhancer factor 2 and class II histone deacetylases control a gender-specific pathway of cardioprotection mediated by the estrogen receptor. Circ Res *106*, 155-165.

VanderLaan, P.A., Reardon, C.A., and Getz, G.S. (2004). Site specificity of atherosclerosis: site-selective responses to atherosclerotic modulators. Arterioscler Thromb Vasc Biol *24*, 12-22.

Vega, R.B., Harrison, B.C., Meadows, E., Roberts, C.R., Papst, P.J., Olson, E.N., and McKinsey, T.A. (2004). Protein kinases C and D mediate agonist-dependent cardiac hypertrophy through nuclear export of histone deacetylase 5. Mol Cell Biol *24*, 8374-8385.

Verdel, A., and Khochbin, S. (1999). Identification of a new family of higher eukaryotic histone deacetylases. Coordinate expression of differentiation-dependent chromatin modifiers. J Biol Chem *274*, 2440-2445.

Verdin, E., Dequiedt, F., and Kasler, H.G. (2003). Class II histone deacetylases: versatile regulators. TRENDS in Genetics *19*, 286-293.

Wang, A.H., Bertos, N.R., Vezmar, M., Pelletier, N., Crosato, M., Heng, H.H., Th'ng, J., Han, J., and Yang, X.J. (1999). HDAC4, a human histone deacetylase related to yeast HDA1, is a transcriptional corepressor. Mol Cell Biol *19*, 7816-7827.

Wang, X.-b., Han, Y.-d., Sabina, S., Cui, N.-h., Zhang, S., Liu, Z.-j., Li, C., and Zheng, F. (2016). HDAC9 variant Rs2107595 modifies susceptibility to coronary artery disease and the severity of coronary atherosclerosis in a Chinese Han population. PloS one *11*, e0160449.

Wang, X., Collins, H.L., Ranalletta, M., Fuki, I.V., Billheimer, J.T., Rothblat, G.H., Tall, A.R., and Rader, D.J. (2007). Macrophage ABCA1 and ABCG1, but not SR-BI, promote macrophage reverse cholesterol transport in vivo. The Journal of clinical investigation *117*, 2216-2224.

Wefers, B., Bashir, S., Rossius, J., Wurst, W., and Kuhn, R. (2017). Gene editing in mouse zygotes using the CRISPR/Cas9 system. Methods *121-122*, 55-67.

Wen, H., Gris, D., Lei, Y., Jha, S., Zhang, L., Huang, M.T., Brickey, W.J., and Ting, J.P. (2011). Fatty acid-induced NLRP3-ASC inflammasome activation interferes with insulin signaling. Nat Immunol *12*, 408-415.

Wolf, P.A., D'Agostino, R.B., Kannel, W.B., Bonita, R., and Belanger, A.J. (1988). Cigarette smoking as a risk factor for stroke: the Framingham Study. Jama *259*, 1025-1029.

Wyller, T. (1999). Stroke and gender. The journal of gender-specific medicine: JGSM: the official journal of the Partnership for Women's Health at Columbia *2*, 41-45.

Xie, D., Zhu, J., Liu, Q., Li, J., Song, M., Wang, K., Zhou, Q., Jia, Y., and Li, T. (2019). Dysregulation of HDAC9 Represses Trophoblast Cell Migration and Invasion Through TIMP3 Activation in Preeclampsia. Am J Hypertens *32*, 515-523.

Xu, G., Li, N., Zhang, Y., Zhang, J., Xu, R., and Wu, Y. (2019). MicroRNA-383-5p inhibits the progression of gastric carcinoma via targeting HDAC9 expression. Braz J Med Biol Res *52*, e8341.

Reference

Yan, K., Cao, Q., Reilly, C.M., Young, N.L., Garcia, B.A., and Mishra, N. (2011). Histone deacetylase 9 deficiency protects against effector T cell-mediated systemic autoimmunity. Journal of Biological Chemistry *286*, 28833-28843.
Yan, Y., Jiang, W., Liu, L., Wang, X., Ding, C., Tian, Z., and Zhou, R. (2015). Dopamine controls systemic inflammation through inhibition of NLRP3 inflammasome. Cell *160*, 62-73.
Yang, X.J., and Seto, E. (2008). The Rpd3/Hda1 family of lysine deacetylases: from bacteria and yeast to mice and men. Nat Rev Mol Cell Biol *9*, 206-218.
Yaron, J., Gangaraju, S., Rao, M., Kong, X., Zhang, L., Su, F., Tian, Y., Glenn, H., and Meldrum, D. (2015). K+ regulates Ca 2+ to drive inflammasome signaling: dynamic visualization of ion flux in live cells. Cell death & disease *6*, e1954.
Zeeshan, H.M., Lee, G.H., Kim, H.R., and Chae, H.J. (2016). Endoplasmic Reticulum Stress and Associated ROS. Int J Mol Sci *17*, 327.
Zhang, C.L., McKinsey, T.A., Chang, S., Antos, C.L., Hill, J.A., and Olson, E.N. (2002). Class II histone deacetylases act as signal-responsive repressors of cardiac hypertrophy. Cell *110*, 479-488.
Zhang, C.L., McKinsey, T.A., and Olson, E.N. (2001). The transcriptional corepressor MITR is a signal-responsive inhibitor of myogenesis. Proc Natl Acad Sci U S A *98*, 7354-7359.
Zhang, M., Hill, M.C., Kadow, Z.A., Suh, J.H., Tucker, N.R., Hall, A.W., Tran, T.T., Swinton, P.S., Leach, J.P., Margulies, K.B.*, et al.* (2019). Long-range Pitx2c enhancer-promoter interactions prevent predisposition to atrial fibrillation. Proc Natl Acad Sci U S A.
Zhao, Y.X., Wang, Y.S., Cai, Q.Q., Wang, J.Q., and Yao, W.T. (2015). Up-regulation of HDAC9 promotes cell proliferation through suppressing p53 transcription in osteosarcoma. International journal of clinical and experimental medicine *8*, 11818-11823.
Zhou, R., Yazdi, A.S., Menu, P., and Tschopp, J. (2011). A role for mitochondria in NLRP3 inflammasome activation. Nature *469*, 221-225.
Zhou, X., Marks, P.A., Rifkind, R.A., and Richon, V.M. (2001). Cloning and characterization of a histone deacetylase, HDAC9. Proc Natl Acad Sci U S A *98*, 10572-10577.
Zhou, X., Richon, V.M., Rifkind, R.A., and Marks, P.A. (2000). Identification of a transcriptional repressor related to the noncatalytic domain of histone deacetylases 4 and 5. Proc Natl Acad Sci U S A *97*, 1056-1061.